

The Chemical Compositions of Non-Variable Red and Blue Field Horizontal Branch Stars

Bi-Qing For¹ and Christopher Sneden

Department of Astronomy, University of Texas, Austin, TX 78712, USA

ABSTRACT

We present a new detailed abundance study of field red horizontal branch (RHB) and blue horizontal branch (BHB) non-variable stars. High resolution and high S/N echelle spectra of 11 RHB and 12 BHB were obtained with the McDonald 2.7 m telescope, and the RHB sample was augmented by reanalysis of spectra of 25 stars from a recent survey. We derived stellar atmospheric parameters based on spectroscopic constraints, and computed relative abundance ratios for 24 species of 19 elements. The species include Si II and Ca II, which have not been previously studied in RHB and BHB ($T_{\text{eff}} < 9000$ K) stars. The abundance ratios are generally consistent with those of similar-metallicity field stars in different evolutionary stages. We estimated the masses of the RHB and BHB stars by comparing their $T_{\text{eff}} - \log g$ positions with HB model evolutionary tracks. The mass distribution suggests that our program stars possess masses of $\sim 0.5 M_{\odot}$. Finally, we compared the temperature distributions of field RHB and BHB stars with field RR Lyraes in the metallicity range $-0.8 \gtrsim [\text{Fe}/\text{H}] \gtrsim -2.5$. This yielded effective temperatures estimates of 5900 K and 7400 K for the red and blue edges of the RR Lyrae instability strip.

Subject headings: stars:abundances – stars: horizontal-branch

1. Introduction

Horizontal branch (HB) stars are evolved objects that are fusing helium in their cores (Hoyle & Schwarzschild 1955). As low-mass main sequence stars age, they first ascend the

¹biqing@astro.as.utexas.edu

red giant branch (RGB), undergo internal helium-flash (losing some of their mass somewhere along the RGB), and finally take up residence on the HB while they complete their helium consumption. The helium core mass is relatively constant in all types of HB stars ($\sim 0.5 M_{\odot}$), but they have a large hydrogen envelope mass range.

HB stars are commonly found in globular clusters (GCs), as well as in field disk and halo populations of our Milky Way. They exhibit a range of photometric colors (or temperatures) which is known as the HB morphology. The distribution can be divided into several groups:

- Red horizontal branch (RHB) stars, which are all HBs cooler than the instability strip (IS).
- RR Lyraes (RR Lyr), named after their prototype. These are variable stars with intermediate temperature and color, located in the IS.
- Blue horizontal branch (BHB) stars, which are hotter than the RR Lyr IS. Their temperatures ranges from 8000–20,000 K, which is also subdivided into HBA ($T_{\text{eff}} < 10,000$ K) and HBB stars ($T_{\text{eff}} > 10,000$ K) (Möhler 2004). This division corresponds roughly to A and B spectral type. In this paper, we analyze only HBA stars, referring to them collectively as BHB stars.
- Extreme horizontal branch (EHB) stars, which are hotter extension of HB (20,000–40,000 K). These stars often lie below the main sequence in the Hertzsprung-Russell diagram, and thus they are also referred to as hot subdwarfs (see review by Heber 2009).

The assignment of a star to a particular HB group is based on color (or temperature), but the physical cause that determines the position could be affected by multiple parameters. Metallicity, also referred to as the first parameter, was suggested by Sandage & Wallerstein (1960) to explain the HB morphology as seen in the GCs. Metal-rich clusters have mostly RHB stars and metal-poor clusters have mostly BHB and/or EHB stars.

However, this is not the full story of the HB morphology. Globular clusters that possess similar metallicity often exhibit different HB types. For example, compare the color-magnitude diagrams of M3 vs M13 (see Rosenberg et al. 2000), which clearly indicates that HB morphology is influenced by other parameter(s).

The early study of Searle & Zinn (1978) suggested that the cluster age could be the second parameter, but later investigation by, e.g, Peterson et al. (1995) and Behr (2003a) argued that stellar rotation could also be a significant contributor. Alternative explanations, such as CNO abundance (Rood & Seitzer 1981), mixing and helium abundance (Sweigart

1997), central concentration of the cluster (Fusi Pecci et al. 1993), and Na–O anticorrelation (Gratton et al. 2007) also have been proposed. Lee et al. (1994) demonstrated that various second parameters can produce different HB morphologies. To what extent these potential second parameters influence the variety of observed HB distributions in GCs remains an open question.

Chemical abundance studies of GCs provide ideal laboratories for testing predictions of stellar evolution and nucleosynthesis. Horizontal branch stars are particularly useful for probing several aspects of post-main sequence evolution because they are sensitive to the composition and structure of main sequence stars prior to the exhaustion of their hydrogen fuel (Behr 2003b). Unfortunately, HBs in GCs and stellar streams are faint and as such, hard to observe at high spectral resolution. On the other hand, field horizontal branch (FHB) stars are significantly brighter than cluster stars, and could be useful in many aspects. For example, FHB stars have been used as tracers of Galactic structure (see Wilhelm et al. 1996; Altmann 2000). In addition, field RR Lyrae stars (easy to identify from their variability) yield important information on stellar evolution and pulsation. Their absolute magnitudes and metallicities provide powerful constraints on synthetic HB models (see Cassisi et al. 2004; Demarque et al. 2000).

While FHB kinematics have been widely used to study Galactic structure, their chemical compositions have received scant attention. There are only a handful of detailed abundance studies of FHB stars to date (see Adelman & Hill 1987; Adelman & Philip 1990; Lambert et al. 1996). Behr (2003b) conducted a rotational velocity study of FHB stars, with only the derivation of Mg abundances for all HB stars. He performed a more extensive chemical abundance study for BHB stars in GCs (Behr 2003a). A recent large survey of FHB stars was carried out by Preston et al. (2006a), but their sample was limited to very metal-poor RHB stars ($[\text{Fe}/\text{H}] < -2$) that were selected from the HK objective-prism survey. Their primary objectives were to investigate any abundance anomalies in these stars, and to derive the fundamental T_{eff} red edge of the metal-poor RR Lyr IS. They concluded that: (a) FRHB stars generally possess normal enhancements of α -elements; (b) there is a $[\text{Si}/\text{Fe}]$ dependence on T_{eff} which is unrelated to nucleosynthesis issues; (c) $[\text{Mn}/\text{Fe}]$ is subsolar; and (d) the n -capture elements have large star-to-star relative abundance scatter. They also derived the temperature of the red edge of the metal-poor RR Lyr IS, by interfacing the temperature distributions of field metal-poor RHB and RR Lyr stars with stars of similar metallicities in globular clusters.

In this paper, we present the first detailed abundance study of field RHB and BHB stars that spans an effective temperature range of 4000 K. We explore possible abundance anomalies and their implications on HB evolution. This work potentially can provide a

different point of views toward understanding HB morphology, and results should aid in application of HB chemical compositions to stellar stream investigations. §2 describes the target selection and interstellar reddening. The observations and reduction are given in §3. In §4 and 5, we present the line list compilation, equivalent width measurements and analysis methods. The results of individual elemental abundances and evolutionary states of HB stars are given in §6 and §7. We discuss the implication of several elemental abundances of our HB samples in §8. Lastly, we summarize the results of this work in §9.

2. Target Selection and Reddening

The observed targets for this program were selected from Behr (2003b). That paper contains a compilation of known FHB stars that he used for his rotational velocity study. We selected the FHB stars that have $V < 11$, $[\text{Fe}/\text{H}] \leq -1.2$ and $T_{\text{eff}} < 9000$ K. The temperature restriction was chosen to avoid abundance anomalies due to gravitational settling and diffusion processes that are observed in the hotter BHB stars (e.g, Behr 2003a). RR Lyr stars were deliberately excluded in this program; a companion study of their chemical compositions will be presented in paper II.

We also included metal-poor field red horizontal branch (MPFRHB) stars studied by Preston et al. (2006a) in our program. We did not re-observe the MPFRHB stars, but we analyzed them in a manner consistent with that of the newly observed targets. We refer the reader to the description of target selection and observational details in Preston et al. (2006a). Table 1 gives basic information for our program stars.

Reddening estimates $E(B - V)$ of individual stars were obtained from the NASA/IPAC Extragalactic Database² (NED) extinction calculator. This technique is based on the *Infrared Astronomical Satellite* (IRAS) and *Diffuse Infrared Background Experiment* (DIRBE) measurements of dust IR emission maps of Schlegel et al. (1998) (hereafter SFD). We chose this method in preference to the older Burstein & Heiles (1982) maps, which are based on H I 21-cm column density and galaxy counts, because the H I maps suffer from the general problem of saturation in the 21-cm line in high extinction regions and have lower spatial resolution than the SFD maps.

Some uncertainties in $E(B - V)$ values estimated from the SFD maps might arise from missing cold dust emission that is not detected by IRAS. In fact, $E(B - V)$ values determined from SFD are probably systematically larger by ~ 0.02 mag as compared to

² <http://nedwww.ipac.caltech.edu/forms/calculator.html>

those of Burstein & Heiles (1982) (e.g., see comments in Meléndez et al. 2006 and references therein). Burstein & Heiles (1982) maps are not error free. In fact, their maps contain systematic effect that arises from fluctuations in galaxy count and variation in gas-to-dust ratio. To be consistent and to reduce the degree of systematic effect in our analysis, we only adopted extinctions from SFD maps. To correct these systematic effects of SFD maps, we used a 10 % correction factor as suggested by Meléndez et al.:

$$cE(B - V) = 0.9E(B - V) - 0.01, \quad (1)$$

where $cE(B - V)$ is the corrected $E(B - V)$. We employed the corrected $E(B - V)$ for calculating the photometric T_{eff} , which we used to compare with our independent spectroscopic T_{eff} values. The details will be given in §5.1.

3. Observations and Reductions

The observations were made with the McDonald 2.7 m Smith telescope, using the “2dcoudé” cross-dispersed echelle spectrograph. We used this instrument with a 1.2” slit and in its “cs23-e2” configuration; it gives a 2-pixel resolving power of $R \equiv \lambda/\Delta\lambda \sim 60,000$ with spectra projected onto a Tektronix 2048 × 2048 CCD chip with no binning. The total wavelength range is $\sim 3700 - 8200 \text{ \AA}$ with complete spectral coverage for $\lambda < 5900 \text{ \AA}$, and with gaps in coverage increasing toward the red. We usually integrated on the target stars for 1.5 hr, yielding S/N per resolution element of ~ 70 near 4000 \AA , ~ 140 near 5000 \AA , and ~ 240 near 7000 \AA . The typical seeing for our observing runs varied from 1.5” to 2.2”. Our observations in 2007–2008 were taken in conjunction with another project, for which we positioned the grating so that more red portion of the spectrum was projected onto the CCD. This resulted in sacrificing some useful blue-spectral echelle orders, which meant that there were fewer lines available for analysis. Optimal spectral coverage was obtained for observing run in 2009.

ThAr comparison lamp exposures were taken at the beginning and the end of each night. We also took the spectra of hot, rapidly rotating, relatively featureless stars throughout the night at different airmasses. These spectra were used to aid in removing telluric features from the spectra of our program stars. Table 2 summarizes the observations and stars that are listed but lack sufficient numbers of detected Fe I & Fe II lines for stellar parameter estimations were excluded from abundance analysis.

We performed reductions of the spectra with the IRAF³ ECHELLE package. The raw

³The Image Reduction and Analysis Facility, a general purpose software package for astronomical data, is

data were bias, flat-field, and scattered-light corrected, then extracted to one-dimensional spectra and wavelength-calibrated in standard fashion. The wavelength calibration arc identification was based on the line list in the IRAF package data file (thar.dat) and the Th-Ar wavelength table for the 2dcoudé spectrograph (Allende Prieto 2001). The individual wavelength-corrected spectra were then average combined into a single spectrum.

Subsequently, we used the SPECTRE⁴ (Fitzpatrick & Sneden 1987) code to normalize the spectra and to remove cosmic rays contamination from the spectral lines. Figure 1 shows typical normalized spectra of RHB and BHB stars. Several of the hotter BHB stars exhibit significant rotational broadening.

4. Line List and Equivalent Width Measurements

We compiled an input line list of various elements from previous studies on HB stars (i.e., Preston et al. 2006a,b; Hubrig et al. 2009; Khalack et al. 2007, 2008; Clementini et al. 1995 & Lambert et al. 1996). Species such as Si II and Ca II have been included in past HBB studies, but to our knowledge this is the first use of these species for RHB and BHB analysis. Excitation potentials (E.P.) and laboratory oscillator strengths ($\log gf$) are extracted from various sources, which we cite in Table 3.

For each star, we measured the equivalent widths (EWs) of unblended atomic absorption lines interactively with SPECTRE. We either adopted the EW value given by fitting a Gaussian to the line profile or by integrating over the relative absorption across a line profile. If a particular line was contaminated by cosmic rays or had an obviously distorted profile (especially lines in BHB stars can be blended with nearby lines due to rotational broadening), we excluded it. Very strong lines on the damping portion of the curve-of-growth (defined as those with reduced widths $\log RW \equiv \log EW/\lambda \gtrsim -4.0$) are relatively insensitive to abundance, and thus were not measured here. After initial trials, we also excluded very weak lines ($EW < 5 \text{ m}\text{\AA}$) because the EW measurement errors were too large. Since our program stars have a wide range of T_{eff} and metallicity, the number of lines measured varied considerably. The lines used for each star, along with species, E.P., $\log gf$, its associated references, and measured EWs are listed in Table 3.

We may compare our EW measurements of stars with existing previous studies. Only a

written and supported by the IRAF programming group of the National Optical Astronomy Observatories (NOAO) in Tucson, AZ.

⁴An interactive spectrum measurement package, available at <http://verdi.as.utexas.edu/spectre.html>

few high-resolution, detailed chemical abundance investigations of field BHB stars have been conducted to date. The only published iron EW measurements are from Adelman & Hill (1987) and Adelman & Philip (1990), which were measured on coudé spectrograms recorded with photographic plates. Figure 2 & 3 show the comparison of Fe I & Fe II EW measurements in four stars. The literature data for the cooler (CS 22951–077) and hotter (CS 22941–027) MPFRHB stars are from Preston et al. (2006a) and those for the two BHB stars (HD 161817 & HD 109995) are from Adelman & Hill (1987). Taking the EW measurements difference between Preston et al. (2006a), Adelman & Hill (1987) and this study (as shown in Figures 2 & 3), we find: for CS 22951–077, $\Delta\text{EW} = 1.3 \pm 0.3 \text{ m}\text{\AA}$, $\sigma = 2.7 \text{ m}\text{\AA}$, 82 lines; for CS 22941–027, $\Delta\text{EW} = 1.0 \pm 0.4 \text{ m}\text{\AA}$, $\sigma = 2.7 \text{ m}\text{\AA}$, 37 lines; for HD 161817, $\Delta\text{EW} = -2.3 \pm 0.8 \text{ m}\text{\AA}$, $\sigma = 4.4 \text{ m}\text{\AA}$, 32 lines; and for HD 109995, $\Delta\text{EW} = -2.4 \pm 1.3 \text{ m}\text{\AA}$, $\sigma = 5.3 \text{ m}\text{\AA}$, 16 lines. We only compute the EW difference of lines with $\text{EW} < 75 \text{ m}\text{\AA}$ in BHB stars because the larger EW difference in strong lines of HD 161817 is probably due to the different measurement techniques of the two studies. In our case, strong lines were treated by either fitting the damping wing or integrating over the line profile. Since the deviations (ΔEW) are small, we conclude that our EW measurements are in excellent agreement with others.

5. Analysis

Our analysis is based on equivalent width matching and spectrum synthesis. Both methods require a stellar atmosphere model that is characterized by four parameters: effective temperature (T_{eff}), surface gravity ($\log g$), metallicity ($[M/H]$) and microturbulence (v_t). We constructed models by interpolation⁵ in Kurucz’s non-convective-overshooting atmosphere model grid (Castelli et al. 1997). The elemental abundances were derived using the current version of the local thermodynamic equilibrium (LTE) spectral line synthesis code MOOG⁶ (Snedden 1973). With the exception of iron ($\log_{\epsilon}(\text{Fe}) = 7.52$), this code adopted the solar and meteoritic abundances of Anders & Grevesse (1989). The details on determining the stellar parameters and methodologies are given in the following subsections.

⁵ The interpolation code was kindly provided by Andrew McWilliam and Inese Ivans.

⁶ Available at <http://verdi.as.utexas.edu/moog.html>.

5.1. Stellar Parameters

An initial stellar atmosphere model was created based on the stellar parameters of Preston et al. (2006a) and Behr (2003b). Final model atmosphere parameters were determined by iteration, through spectroscopic constraints: (1) for T_{eff} , that the abundances of individual Fe I lines show no trend with E.P.; (2) for v_t , that the abundances of individual Fe I lines show no trend with reduced width ($\log RW$); (3) for $\log g$, that ionization equilibrium be achieved between the abundances derived from the Fe I and Fe II species; and (4) for metallicity $[M/H]$, that its value is consistent with the $[Fe/H]$ determination. In the case of $[Fe/H] < -2.5$, we adopted $[M/H] = -2.5$ for the stellar atmosphere model due to no available models in our grid below this metallicity. Table 4 presents the derived stellar atmosphere model parameters and Fe metallicities of our program stars.

The standard spectroscopic constraints method has drawbacks. In particular, “spectroscopic” gravities derived from ionization balance may be lower than “trigonometric” gravities derived from stellar parallaxes (π) or “evolutionary” gravities inferred from HR-diagram positions (see e.g., Allende Prieto et al. 1999). Such mismatches may arise from statistical equilibria that are not well described by LTE. These so-called NLTE effects are mainly due to the additional ionization of neutral-species beyond collisions by UV photons. The problem can increase with decreasing metallicity due to smaller UV line opacities in metal-poor stars. Discrepancies in derived $[Fe\ I/H]$ and $[Fe\ II/H]$ are the result: Fe I lines yield lower abundances than do Fe II lines, which are then “corrected” by decreasing assumed gravities in LTE analysis (Thévenin & Idiart 1999). A full discussion of NLTE effects is beyond the scope of this paper. In the following section, we consider the effects of $\log g$ uncertainties on our derived abundances.

We have compared our spectroscopic T_{eff} ’s to those based purely on photometry. We computed photometric temperatures using the metallicity-dependent T_{eff} -color formula of giants developed by Alonso et al. (1999). These relationships are based on the infrared flux method (IRFM) (Blackwell & Shallis 1977). We employed only $V - K$ colors for this exercise. In contrast to $B - V$ colors, where blue continua are severely affected by line blanketing, $V - K$ colors are largely insensitive to the choice of metallicity and gravity.

The $(V - K)$ values of our stars, as listed in Table 1, are based on V_{Johnson} and 2MASS J and K_s magnitudes. The calibration curve of Alonso et al. (1999) is based on $(V - K)_{\text{TCS}}$. Therefore, several color transformations were required. We converted these colors to the TCS system in two ways. First, we simply shifted the 2MASS K_s magnitudes to the K_{TCS} ⁷

⁷ K_{TCS} is the broad-band K magnitude in the photometric system developed for the Observatorio del

using Eq. 5(c) of Ramírez & Meléndez (2005): $K_{TCS} = K_{2MASS} - 0.014 + 0.027(J - K)_{2MASS}$. The V_{TCS} magnitudes are essentially equal to $V_{Johnson}$, thus the K transformation should be sufficient to convert our $V - K$ values to $(V - K)_{TCS}$. Second, a better method is to shift $(V_{Johnson} - K_s)$ into $(V - K)_{TCS}$ by two corrections as described in Johnson et al. (2005); we computed the $(V - K)_{TCS}$ using their Eq. 6: $(V - K)_{TCS} = 0.050 + 0.993(V_{Johnson} - K_s)$. For each of these conversion attempts, we then applied extinction corrections to the colors, adopting an extinction ratio of $k = E(V - K)/E(B - V)$, where $k = 2.74$ for $(V - K)_{TCS}$ (Ramírez & Meléndez 2005). Photometric T_{eff} were subsequently calculated using polynomial relation described in Eq. 8 of Alonso et al. (1999). There are two BHB stars that possess $V - K$ colors that are smaller than $V - K$ range (< 0.2) of this equation's calibration. For these stars we simply assumed that the polynomial fit could be extrapolated to $V - K \simeq 0$.

We compared the calculated photometric T_{eff} of both methods and found that the difference is small ($\Delta T_{eff} = 54 \pm 1$ K, $\sigma = 6$ K, $N_{star} = 34$) for RHB stars and somewhat larger ($\Delta T_{eff} = 109 \pm 3$ K, $\sigma = 11$ K, $N_{star} = 11$) for BHB stars. The larger difference for BHB stars is most likely due to the color- T_{eff} transformation, because it is based mostly on cooler stars. The error of calculated photometric T_{eff} depends on the slope of the polynomial fit, $\Delta T_{eff}/\Delta X$, where ΔX is a function of extinction ratio (k) and error in reddening ($\Delta E(B - V)$). The error is represented by 17 K per 0.01 mag for $V - K < 2.2$ (Alonso et al. 1999).

We show the comparison of the calculated photometric T_{eff} values that are adopted from the first color-transformation method to the derived spectroscopic T_{eff} values in Figure 4. Taking the difference (our spectroscopic T_{eff} minus photometric T_{eff}), we show that both T_{eff} values of both RHB ($\Delta T_{eff} = -73 \pm 30$ K, $\sigma = 177$ K, $N_{star} = 34$) and BHB stars ($\Delta T_{eff} = 59 \pm 91$ K, $\sigma = 300$ K, $N_{star} = 11$) are in good agreement.

Ideally our spectroscopic gravities should be compared with trigonometric or physical gravities, but such an exercise is not possible here. Our stars have no reliable parallax data from *Hipparcos* (Perryman et al. 1997); they are too distant. Most stars selected from the Behr (2003a) catalog have large errors in their parallaxes, and no parallaxes have been reported for stars selected from Preston et al. (2006a).

Teide (Tenerife) 1.5m telescope (Alonso et al. 1994).

5.2. Parameter Uncertainties

To estimate the effects of uncertainties in our spectroscopically-based T_{eff} on derived abundances, we varied the assumed T_{eff} 's of HD 119516 (RHB) and HD 161817 (BHB). For HD 119516, raising T_{eff} by 150 K from the derived 5400 K produced an unacceptably large trend of derived $\log \epsilon(\text{Fe})$ with excitation potential. For the BHB star, HD 161817, T_{eff} can be raised to 200 K before the trend of $\log \epsilon(\text{Fe})$ with E.P. becomes too large. Repeating these trials for other stars suggested that 150 K and 200 K are typical uncertainties for the RHB and BHB stars, respectively. The difference between the two groups is due to the lesser number of available Fe I lines in BHB spectra, which causes larger error in T_{eff} derivation.

We estimated v_t uncertainties in a similar manner, assessing the trends of Fe I abundances with $\log(\text{RW})$. This yielded v_t errors of 0.2 km s⁻¹ and 0.3 km s⁻¹ for RHB and BHB stars, respectively. Finally, (assuming that $\log g$ based on the neutral/ion ionization balance of Fe abundance is correct) from the dependence Fe II abundances with $\log g$, we estimated the error of $\log g$ to be 2σ of Fe II abundance error. The mean error of $\log g$ to be ~ 0.16 dex. We adopted the internal error (σ) of Fe I abundances as the model [M/H] error.

5.3. Comparisons with Previous Studies

We compared our derived $\log g$ and T_{eff} values with those of Preston et al. (2006a) and Behr (2003b), as shown in Figures 5 & 6. Behr (2003b) derived these quantities by comparing the synthetic photometric color and the observed color over a grid of $T_{\text{eff}} - \log g$ values. Preston et al. (2006a) employed the same method as we do, i.e., from spectroscopic constraints, but they used both Fe and Ti abundances for determining $\log g$ from ionization-balance considerations. We decided here not to use Ti in the $\log g$ estimation, because the Ti I $\log gf$ values from the NIST atomic transition database⁸ are of relatively high uncertainty and there are not many measurable Ti I lines ($N < 6$) in most cases for our RHB stars. Using small number of lines would cause larger error in $\log g$ estimation and could yield systematic error (see below). Additionally, we have no detections of Ti I lines in our BHB sample. Therefore to be consistent in our RHB and BHB star analyses, we decided to only use Fe I and Fe II abundances in estimations of $\log g$.

Our T_{eff} 's for RHB stars are $\Delta T_{\text{eff}}(\text{Preston-us}) = 59 \pm 20$ K ($\sigma = 100$ K, $N = 25$) and $\Delta T_{\text{eff}}(\text{Behr-us}) = 154 \pm 40$ K ($\sigma = 134$ K, $N = 11$), which are in good agreement. Comparison of BHB stars can only be made with Behr. Our T_{eff} values generally agree with

⁸National Institute of Standards and Technology (NIST): <http://www.nist.gov/physlab/data/asd.cfm> .

his, $\Delta T_{\text{eff}}(\text{Behr-us}) = -152 \pm 43 \text{ K}$ ($\sigma = 134 \text{ K}$, $N = 10$) except for HD 8376 and possibly HD 93329. Our derived RHB $\log g$ values are systematically lower ($\Delta \log g$ (Preston–us) = $0.41 \pm 0.06 \text{ dex}$, $\sigma = 0.3 \text{ dex}$, $N = 25$) than those of Preston et al., which is due to different derivation methods. To demonstrate such systematic effect, we performed tests using both Fe and Ti lines. Abundances of neutral species of Titanium is generally larger than ionized species by 0.12–0.2 dex. As such, this requires a larger $\log g$, which is 0.2–0.5 dex, to achieve the ionization equilibrium for Ti.

Our derived $\log g$ values show no correlation with Behr’s, and we note significant deviations for HD 8376, HD 6461 and HD 6229. For HD 6461 our derived $[\text{Fe I}/\text{H}]$ is +0.6 dex higher than Behr’s, which in turn forces a larger $\log g$ to achieve the ionization equilibrium. Our T_{eff} for HD 8376 is about 500 K larger than Behr’s estimate, which forces a much larger $\log g$ value in our analysis. We do not have an explanation for the $\log g$ deviation of HD 6229.

5.4. Microturbulence vs Effective Temperature

We plot our v_t values against T_{eff} in Figure 7, where the correlations (dashed lines) were derived by fitting linear least squares regression lines to the RHB and BHB data. The clear positive correlation of microturbulent velocity with temperature in RHB stars has been found by others (see Preston et al. 2006a and references therein). It is possible that the BHB stars have an anti-correlation between these two quantities. The star-to-star scatter is large, but if we exclude HD 8376⁹, the anti-correlation remains. We have extended the dashed lines beyond their intersection in the figure; comparison of these lines with the RR Lyr data indicates that there is no v_t correlation with T_{eff} in this domain. This issue will be revisited in paper II.

These trends in derived v_t with T_{eff} undoubtedly are related to the envelope/atmosphere instabilities of RR Lyr stars. The evolutionary track of a HB star indicates that it evolves from the hot end, crosses the RR Lyr IS into the cool HB region, before ascending to the AGB. As an HB star evolves toward the RR Lyr IS blue edge, its atmosphere begins to be unstable, which results in increasing line widths that we model as increasing microturbulence. And as the HB star evolves away from the RR Lyr IS red edge, the line widths decrease as the stability is regained. We caution here that our microturbulence values are simple compensations for complex physical changes that are occurring in HB stars near the

⁹ Our derived v_t for HD 8376 is rather uncertain because no v_t choice can eliminate the trend of $\log \epsilon(\text{Fe})$ with $\log(\text{EW}/\lambda)$ for this star. This is the only program star for which we have trouble in finding an acceptable v_t value.

instability strip, and thus should be interpreted with caution.

6. Chemical Abundances

With the model atmosphere parameters listed in Table 4, we derived the abundances of most elements from their EW measurements. In the cases of Ca II, Mn I, Ni II, Sr II, Zr II, Ba II, La II, and Eu II, the detectable transitions are complex: they are either partially blended, or have significant hyperfine and/or isotopic substructure, or all of these things. We employed spectrum synthesis to determine abundances for these species. That is, for each line we computed theoretical spectra of a wavelength region within $\pm 10\text{\AA}$ of the line for a variety of assumed abundances, then broadened the computed spectrum with Gaussian line profile (or a combination of Gaussian plus rotational velocity line profile), and finally compared these spectra to the observed ones. The assumed abundances were changed iteratively to obtain acceptable synthetic/observed spectrum matches. For stars with detectable rotational line broadening, we began with the $v\sin i$ estimates of Behr (2003b) and derived the final $v\sin i$ based on the fit to observed line profile. Our final numbers were always in good agreement ($\Delta v\sin i \simeq 1 - 2 \text{ km s}^{-1}$) with initial values. The damping constant of Barklem & O’Mara (1998) was adopted whenever possible in both EW analyses and spectrum syntheses method.

We present the derived abundances ratio $[X/\text{Fe}]$ in Tables 5–8, and plot these as functions of metallicity in Figure 8–10 and T_{eff} in Figures 11–13. Non-LTE corrections have been applied to the data on these figures and tables wherever applicable. The mean $[X/\text{Fe}]$ values of RHB and BHB stars are summarized in Table 9. In the following subsections we comment on individual elements.

The total error in the abundances is a combination of internal error (line-to-line scatter), and external errors (induced by stellar model atmosphere parameter uncertainties). The line-to-line scatter is given by the abundance standard deviation (σ) from individual spectral lines. To estimate the errors caused by model parameter uncertainties, we performed numerical experiments for four stars, in which we varied the model parameter errors as estimated in §5.2. These stars are CS 22898–043 (very metal-poor), HD 25532 (moderately metal-poor), HD 93329 (BHB) and BD+18° 2890 (RHB). They were selected because they are representative of our whole sample. The results of $[X/\text{Fe}]$ sensitivity to different stellar model atmosphere parameter variations are shown in Table 10 & 11. In most cases $\Delta[X/\text{Fe}] \lesssim 0.05$ in response to changes in $\log g$, $[M/H]$ and v_t . On the other hand, varying T_{eff} by 150 K has a larger effect on the abundance ratios of cool, metal-poor RHB star BD+18° 2890, especially on the neutral species. The overall average variations in $[X/\text{Fe}]$ are small, $\simeq 0.05$. Thus, in general external error from stellar model atmosphere parameters do not greatly influence

the derived abundance ratios. For abundances derived from one spectral line, we adopted an error of 0.2 dex, judging from the statistical source of error (ie., sensitivity of $\Delta[X/Fe]$ with stellar parameters error, uncertainties in measuring the EW or matching a synthetic spectrum etc).

6.1. The Light Alpha Elements: Magnesium, Calcium and Titanium

It has been known for decades that metal-poor stars are generally overabundant in α -elements (e.g., Wallerstein et al. 1963). Our HB stars show standard enhancements in these elements, with neutral species $\langle [Mg,Ca,Si,Ti/Fe] \rangle \simeq +0.3$ (see Figure 8).

Two RHB stars, BD+18° 2890 and CS 22883–037, exhibit relatively low $[Mg/Fe]$, but not in other α -elements. Only a single Mg I line was analyzed in both of these cases, which resulted in larger abundance uncertainties. Caution is advised in interpreting the Mg abundances of BD+18° 2890 and CS 22883–037.

The Calcium abundances of BHB stars have a larger scatter than the RHB stars. There is also an offset, ~ 0.3 dex of mean $[Ca/Fe]$ of RHB and BHB stars. We investigated this offset by synthesizing the Ca II 3933Å K-line of BHB stars. This line is rarely used in abundance analyses, as it is extremely strong in cool stars. In our case, the K-line could be analyzed in BHB stars, in which the line is not very strong and uncontaminated in most cases. There are weak interstellar contamination for HD 2857 and BD+25° 2602. However, it does not affect our abundances derivation, which is based on a Gaussian line profile fitting to the line. The abundances in BHB stars for Ca I and Ca II are approximately consistent with each other. The presence of the BHB/RHB offset is currently unknown. We also note that there is an unexplained trend of decreasing $[Ca/Fe]$ with increasing T_{eff} for BHB stars (see Figure 11). Investigation of larger sample of BHB stars might resolve this puzzle.

There are no Ti I lines detectable in our BHB stars. Additionally, our $\log gf$ values for the Ti I lines are taken from the NIST compilation, but their estimated uncertainties are large. In the RHB stars, Ti I lines are visible, but not many measurable lines. The analysis yields a trend of increasing $[Ti\ I/Fe]$ with increasing T_{eff} (see Figure 11). This trend is opposite the sense of Si (discussed below) and has been noted by others (see Lai et al. 2008 and references therein). The abundance ratios derived from Ti II, unlike those of the other α -elements, do not decline as the metallicity increases. The mean value is flat, with small scatter, across the entire metallicity range. The Ti II-based titanium abundances should be trustworthy as many Ti II lines were used to determine the abundances.

6.2. The Alpha Element Silicon: A Special Case

Substantial dependence of $[\text{Si I}/\text{Fe}]$ with temperature has been found in previous studies of metal-poor field stars (see Cayrel et al. 2004, Cohen et al. 2004, Preston et al. 2006a, Sneden & Lawler 2008 & Lai et al. 2008). This effect seems to depend entirely on T_{eff} ; there is no apparent trend with $\log g$. To address this puzzle, Shi et al. (2009) investigated NLTE effects in warm metal-poor stars. They showed that the Si I 3905.53 Å lines and Si II 6347 Å, 6371 Å lines exhibit significant NLTE departures in warm metal-poor stars. Their study was limited to a sample of metal-poor dwarfs and a single cool giant. Observationally however, warmer FRHB stars ($6000 \text{ K} \lesssim T_{\text{eff}} \lesssim 6400 \text{ K}$) have similar Si abundances to those of metal-poor main sequence turnoff stars, $[\text{Si}/\text{Fe}] \simeq 0$ (see Figure 10 of Preston et al. or Figure 8 of Sneden & Lawler), in spite of their large gravity differences ($\langle \Delta \log g \rangle \sim 2$). Thus, the effect seems to be most dependent on T_{eff} , so we assume that the predicted NLTE effects for main sequence stars will also affect our low gravity, metal-poor, warm RHB and BHB stars. Taking the offsets of +0.1 dex and –0.1 dex to the Si I and Si II abundances from these lines, as suggested by Shi et al., we corrected the abundances of these two species in our program stars with $T_{\text{eff}} \geq 6000 \text{ K}$. Note that there is a large star-to-star scatter for RHB and BHB stars even after this adjustment (see Figure 11). This suggests, in agreement with the conclusions of Shi et al., that addition of an offset is inadequate to produce abundance consistency for this species.

The Si I abundances of all the BHB stars and the CS stars, with the exception of CS 22940–070, were exclusively derived from the 3905.53 Å line. As always, the reader is cautioned about the abundances derived from a single line. The blue-spectral region of hot stars are not overcrowded with lines, so blending is not an issue in this case. For cool stars, 3905.53 Å might be blended with a weak CH transition (Cohen et al. 2004) which would become stronger with decreasing temperature. However, Preston et al. (2006a) argue that the CH contamination in metal-poor RHB stars is very weak, and will not seriously affect the derived Si abundance. The line is thus essentially unblended and weak enough for abundance determinations in all BHB stars, and in RHB stars with $T_{\text{eff}} \geq 5400 \text{ K}$ and $[\text{Fe}/\text{H}] \leq -2$.¹⁰ Lines of Si I in the red-spectral region ($> 5600 \text{ Å}$) were used to derive abundances for the rest of the RHB stars. There are eight stars that we used at least four lines for determining the abundances. For these stars, we derived $\langle [\text{Si I}/\text{Fe}] \rangle = +0.42$, which is consistent with the mean of typical α -enhancement in metal-poor stars.

In Figure 14, we summarize the Si I abundances found in large-sample studies and the

¹⁰ We could not determine a Si abundance for HD 119516 because our spectrum of the 3905 Å line was corrupted by cosmic rays.

spectral regions that were used to derive the Si I abundances. All investigators agree on the declining trend of $[\text{Si I}/\text{Fe}]$ with increasing T_{eff} among cooler metal-poor stars, and we have shown that the abundances reach a (low) plateau in BHB stars. Resolution of this unsatisfactory situation is beyond the scope of this study.

An important check on the Si abundances is provided by our detection of Si II, which has mainly been studied in stars with $T_{\text{eff}} > 10,000$ K. Only a handful of dwarfs have reported Si II abundances (see Stephens & Boesgaard 2002), and no prior investigation has been done for RHB stars. In general, Si II lines are very weak for RHB stars, only becoming strong ($\text{EW} > 30$ mÅ) in BHB stars. We caution that weak lines and 1–3 Si II lines were used for deriving the Si II abundances.

In Figure 15, we illustrate the mixture of lines that have been used to derive Si II abundances for both RHB and BHB stars. The scatter of $[\text{Si II}/\text{Fe}]$ is large but the mean abundances agree with the general α -enhancement indicated by Mg and Ca for our HB stars. We find unusually large Si II abundances for CS 22955–174 and CS 22937–072. However, they show normal enhancement in Si I (i.e., +0.3 and +0.5 dex, respectively). Unfortunately, in both cases, only 1–2 Si I or Si II lines were used to derive their abundances, so these abnormally large abundances should be viewed with caution.

6.3. Light Odd-Z Elements Sodium and Aluminum

For sodium abundances, we used mainly the Na I resonance D-lines (5889.9 Å, 5895.9 Å). Only a few of the cooler RHB stars have detectable, albeit weak, higher excitation Na I lines (the 5682.6 Å, 5688.2 Å and the 6154.2 Å, 6160.7 Å doublets). We visually inspected the D-line spectral region to search for ISM contamination of the stellar lines. Any suspected line blending resulted in dropping the D-line measures for a star. The derived $[\text{Na}/\text{Fe}]$ values exhibit a large star-to-star scatter (see Figure 8). We warn the reader that the Na I D-lines are relatively strong in the RHB stars as compared to the BHB stars. Unfortunately, there are only two BHB stars in our samples that have measurable, clean D-lines. Therefore, we could not make direct comparison with the star-to-star scatters in BHB and RHB stars. Nevertheless, the large variations derived here are consistent with those seen in previous field metal-poor star studies (see Pilachowski et al. 1996; Venn et al. 2004 and references therein).

Aluminum is underabundant in RHB stars, $\langle[\text{Al}/\text{Fe}]\rangle \simeq -0.64$, and overabundant in BHB stars, $\langle[\text{Al}/\text{Fe}]\rangle \simeq +0.36$ (see Figure 8). There are only two Al I lines, the resonance transitions 3944 Å and 3961 Å in the blue spectral region, which we can employ for this study.

The 3944 Å line can be contaminated by CH transition (Arpigny & Magain 1983). However, it is not an issue in our very warm BHB stars and it is even undetectable in our metal-poor RHB stars. Additionally, the 3961 Å line can only be a reliable abundance indicator in metal-poor stars, as it is affected by the strong wing of Ca II H and H_ε features in higher metallicity stars (Snedden & Lawler 2008). Higher excitation Al lines in the red spectral region, e.g., the 6696 Å, 6698 Å pair, generally result in higher [Al/Fe] (see discussion of Francois 1984). The discrepancy of [Al/Fe] between the transitions of red and the blue spectral region is currently not completely understood. Unfortunately we could not detect the red Al I lines in our stars.

As noted by others, Na D lines and the Al I red and blue resonance spectral region can be significantly altered from NLTE effects. These corrections are important for warm, metal-poor turnoff stars with $T_{\text{eff}} \gtrsim 6000$ K (Baumueller et al. 1998). The suggested NLTE corrections are -0.5 dex for Na (Baumueller et al. 1998) and $+0.65$ dex for Al (Baumueller & Gehren 1997). Since the majority of our RHB stars are below this T_{eff} we only applied NLTE corrections of suggested values to Na and Al abundance ratios of our BHB stars.

6.4. The iron-peak elements: Scandium through Zinc

Scandium lines can have substantial hyperfine substructure. We synthesized a few Sc II lines with their full substructure, and found that the abundances derived from synthesis do not differ by more than 0.05 dex from those derived by the single-line EW method. Thus, we used the EW method for deriving all final Sc II abundances. A study by Cohen et al. (2004) showed that there are discrepancies of [Sc II/Fe] among different evolutionary groups of metal-poor stars, in which they are generally enhanced in main sequence stars while RGB stars exhibit deficiencies. Our results are more in accord with those of main-sequence stars, $\langle [\text{Sc II/Fe}] \rangle \simeq +0.13$ (see Figure 9).

Our vanadium abundances come exclusively from V II lines, which were detectable in both RHB and BHB stars. We find no trends of [V/Fe] with either [Fe/H] or T_{eff} .

Chromium abundances derived from Cr I transitions generally yield smaller abundances than those from Cr II lines in metal-poor stars (e.g, Preston et al. 2006a, Sobeck et al. 2007, and references therein). Ideally, we would have preferred to use recent laboratory transition probabilities for both Cr I (Sobeck et al. 2007) and Cr II (Nilsson et al. 2006) for our study. However, there are no Cr II lines studied by Nilsson et al. (2006) that are routinely detectable

in our spectra. Therefore, we employed the transition probabilities of detectable Cr I and Cr II lines from Sobeck et al. (2007) and NIST, respectively. The offset between Cr I & Cr II remains (see Figure 9). The trend of increasing Cr II with decreasing metallicity is due to large line detection/measurement uncertainty; only 1–2 lines were used in relatively metal-poor, RHB stars. This offset is also present in the detailed Cr transition probability study of Sobeck et al. (2007). Ionization imbalance or non-LTE effect could be the cause.

A trend of increasing $[\text{Cr I/Fe}]$ with increasing $T_{\text{eff}} < 7000 \text{ K}$ has also been found for RHB stars (see Figure 12). This is first pointed out by Lai et al. (2008) (see their Figure 21). Clearly no such trend is apparent in our BHB stars.

Manganese abundances of field and halo metal-poor dwarf and giant stars have been shown to be substantially underabundant (see, e.g, Sobeck et al. 2006, Lai et al. 2008, and references therein). Our analysis yields $\langle [\text{Mn/Fe}] \rangle \simeq -0.35$. The general trend of increasing $[\text{Mn/Fe}]$ with at higher $[\text{Fe/H}]$ metallicities in our HB sample is in agreement with those and other previous studies. We refer the reader to review the extensive discussion of Sobeck et al. (2006) regarding the production of Mn.

We derived nickel abundances via spectrum synthesis of the Ni II 4067 Å line and the remaining iron-group elements from EW analysis. The reader should be cautious in interpreting the Co I, Ni II, and Zn I abundances, as they were determined with only 1–2 lines each. There are insufficient data to define an abundance pattern of Ni II at this point. Our $[\text{Ni I/Fe}]$ values are generally near solar for moderately metal-poor stars ($[\text{Fe/H}] > 2.0$). The larger star-to-star scatter for very metal-poor stars ($[\text{Fe/H}] < 2.0$) is probably not real, as only one weak Ni I line was used in our analysis, resulting in uncertain Ni abundances for individual stars.

Zinc has multiple abundant isotopes ($^{64,66,67,68}\text{Zn}$), but the isotopic/hyperfine substructure of Zn I lines are not large and the observed features are weak (Timmes et al. 1995). Therefore we treated Zn I lines as single absorbers. The discussion of $[\text{Zn/Fe}]$ will be given in §8.1.

6.5. The neutron capture elements: Strontium, Yttrium, Zirconium, Barium, Lanthanum and Europium

We derived the strontium abundances using available Sr II 4077 Å, 4161 Å and 4215 Å lines. These lines are particularly hard to analyze in RHB stars because they are strong and/or partially blended. For example, the 4077.8 Å resonance line can be affected by Dy II 4078.0 Å and possibly La II 4077.3 Å. We illustrate this in Figure 16, which shows an example

of the Sr II 4077Å synthesis superimposed on the observed spectrum of an RHB star. The Dy abundance cannot be determined reliably with the spectra. Therefore, the adopted Dy abundance was arbitrarily changed to produce the best fit to the red wing of the observed Sr II line profile.

The star-to-star scatter in Sr abundances is large (see Figure 10). These variations are intrinsic to the stars, as can be easily seen in the spectra. In Figure 17 we show a few examples. Comparison of stars with similar stellar parameters (i.e., CS 22186–005 and CS 22875–029 in this figure) shows that the large scatter in [Sr/Fe] ratios is real. We also note an offset (~ 0.5 dex) of Sr abundance ratios between the RHB and BHB stars, which is not present in Yttrium and Zirconium abundance ratios (see Figure 10 & 13). This offset may be related to the large Sr II line strength difference between the two HB groups. Additionally, contamination of the lines by other species, which plagues the RHB spectra, is not an issue in the BHB stars.

We performed EW analysis for Yttrium lines. The star-to-star scatter is also large in this element but the analytical uncertainties are smaller for Y abundances. We compare a Y II line in stars with similar metallicity in Figure 18. The comparison shows that stars with similar metallicity possess different [Y II/Fe].

Synthesis were performed for Zr II 4149 Å, 4161 Å, 4090 Å and 4317Å lines, whenever present in the spectra. Generally Zr appears to be overabundant as compared to its neighboring light n -capture elements Sr and Y. We caution that the Zr II lines are generally very weak, and the resulting abundance uncertainties are thus large.

Barium is a much-studied member of the heavier n -capture element group. Its lines are affected by both hyperfine substructure and isotopic splitting. A line list with full Ba II substructure is given in McWilliam (1998). We adopted the solar abundance ratio distribution among the $^{134-138}\text{Ba}$ isotopes (Lodders 2003), and synthesized the Ba II lines at 4554 Å, 5853 Å, 6141 Å, and 6496 Å, whenever present in the spectra. We note that the 4554 Å line is always substantially stronger than the other lines, and Ba abundances derived from this line can be severely affected by microturbulence and damping.

The spectral lines of La have significant hyperfine substructure, and those of Eu have both hyperfine substructure and isotopic substructure. There are two natural occurring isotopes, $^{151,153}\text{Eu}$, for which we adopted the solar abundance ratio distribution (Lodders 2003). We employed La II 4086 Å and 4123 Å lines and Eu II 4129 and 4205 Å lines for abundance analysis. In general, Eu and La lines are very weak. None are detectable in BHB stars, and only 1–2 lines are available in RHB stars.

7. Evolutionary States

7.1. $T_{\text{eff}} - \log g$ Plane

We investigated the physical properties of our HB samples, by comparing our derived temperatures and gravities using the α -enhanced, HB models of Pietrinferni et al. (2006). These models implemented the low T -opacities of Ferguson et al. (2005) and an α -enhanced metal distribution that represents typical Galactic halo and bulge stars. The α -enhancement treatment is particularly important because the α -elements are overabundant in metal-poor stellar atmospheres, and they are major donors of electrons for the H^- continuum opacity. We adopted the HB canonical models of various metallicities with $\eta = 0.4$. The models of Pietrinferni et al. were chosen because they provide a fine grid of masses and time steps in contrast to other available HB models.

In order to convert the bolometric luminosities L/L_{\odot} of the models for each mass to $\log g$ values, we adopted Eq. (2) of Preston et al. (2006a),

$$\log g = \log(M/M_{\odot}) + 4\log T_{\text{eff}} - \log(L/L_{\odot}) - 10.607, \quad (2)$$

in which the constant was evaluated by using the solar T_{eff} and $\log g$ values. In Figure 19, we show the spectroscopic T_{eff} and $\log g$ values of our stars and the field RR Lyraes that are based on spectroscopic T_{eff} and $\log g$ of Lambert et al. (1996), and, photometric T_{eff} and Baade-Wesselink $\log g$ of Clementini et al. (1995), on the $T_{\text{eff}} - \log g$ plane. Both their data and our samples exhibit similar gravity scatter at fixed temperature.

To estimate the uncertainties associated with the Pietrinferni et al. (2006) HB models, we compare their luminosities (as translated into $\log g$) for a given mass with Lee & Demarque (1990)'s HB model (i.e., $[\text{Fe}/\text{H}] = -2.26$, $Z = 0.0001$, $Y = 0.23$).¹¹ The comparison is summarized in Table 12. The difference in $\log g$ in the two studies is $\lesssim 0.1$ dex, much smaller than the uncertainties in our spectroscopic $\log g$ values. Therefore, model choice is not an issue in contributing significant error on the mass derivation.

7.2. Derivation of HB Masses

Our mass estimation uses HB evolutionary tracks in the $T_{\text{eff}} - \log g$ plane. As discussed in §5.1, spectroscopic $\log g$ values are generally lower than the photometric ones, which

¹¹ Dorman et al. (1993) also published HB models with similar parameters, but their time steps are too large to be useful in this exercise.

would result in deriving more of low mass HB stars. Therefore, a correction of the spectroscopic gravities is necessary and adopting the photometric gravities is more appropriated to represent the physical gravities.

Preston et al. (2006a) derived an empirical relation for computing photometric gravities ($\log g_{\text{phot}}$) by using their spectroscopic gravities ($\log g_{\text{spec}}$) in conjunction with the existing $\log g_{\text{phot}}$ of M15. We adopted this relation,

$$\log g_{\text{phot}} = \log g_{\text{spec}} + 28.802 - 7.655 \log T_{\text{eff,spec}} \quad (3)$$

to obtain the $\log g_{\text{phot}}$ for all our RHB stars. While there are published $\log g_{\text{phot}}$ data for BHB stars in other GCs (Behr 2003a), there are no useful $\log g_{\text{spec}}$ values for comparison (Behr 2003a suggested that their measurements are too uncertain to provide any useful information on this issue). Additionally, Preston et al. showed that the corrections to $\log g_{\text{spec}}$ decline with increasing T_{eff} and essentially disappear at the red edge of RR Lyr IS (see their Figure 17). This can be understood by noting that the continuous opacity of a hotter star is dominated by H^- , and the dominant electron donor is hydrogen itself rather than the metals. The electron density rises sharply with increasing T_{eff} among RHB stars. Examination of atmosphere models for the M15 RHBs (from Preston et al.) suggests that in the line-forming regions, the electron pressure increases by a factor of more than 30 from the coolest ($T_{\text{eff}} = 5000$ K) to the warmest ($T_{\text{eff}} = 6250$ K) stars. This higher electron pressure helps to enforce LTE in the ionization equilibria in warmer HB stars. Thus, we assume the spectroscopic $\log g$ for our BHB stars is correct and no correction is applied. Future spectroscopic investigation of $\log g$ for BHB stars in GCs would be welcome.

After calculating RHB $\log g_{\text{phot}}$ values, we estimated the masses of individual HB star by employing an interpolation scheme. To account for different metallicities of our program stars, we first chose two models that closely match a star’s $[\text{Fe}/\text{H}]$ and superimposed them on the $T_{\text{eff}}\text{-}\log g$ plane along with the $T_{\text{eff,spec}}$ and $\log g_{\text{phot}}$. Then, calculating the linear interpolation between these two metallicities and masses:

$$M_{\text{star}} = M_1 + \frac{(M_2 - M_1)}{([\text{Fe}/\text{H}]_2 - [\text{Fe}/\text{H}]_1)} \times ([\text{Fe}/\text{H}]_{\text{star}} - [\text{Fe}/\text{H}]_1) \quad (4)$$

where M_1 , M_2 are estimated masses from the two models, and $[\text{Fe}/\text{H}]_1, [\text{Fe}/\text{H}]_2$ are the two models’ iron abundances. For stars positioned outside the model mass range ($0.503M_{\odot} \leq M \leq 0.80M_{\odot}$), we chose the mass that is within the $\log g$ and T_{eff} errors of the star on $T_{\text{eff}}\text{-}\log g$ plane. If there is no mass track lies within the errors, we constrain the upper mass limit to be $0.8 M_{\odot}$, the approximate turnoff mass of a old metal-poor main-sequence star. In Figure 20, we show an example of a set of HB stars superimposed on the HB tracks ($[\text{M}/\text{H}] = -1.79$ and -2.27) that were used to derive their masses. We summarize the derived

masses as a histogram in Figure 21 and parameters used to derive the masses is listed in Table 13.

The inferred mass distributions have means at $0.59 M_{\odot}$ and $0.56 M_{\odot}$ for RHB and BHB stars, respectively (see Figure 21). If we exclude those RHB stars that have masses set to the upper limit ($M > 0.8 M_{\odot}$), the mean masses for RHB and BHB stars are both $0.56 M_{\odot}$, and the median masses are $0.54 M_{\odot}$ and $0.56 M_{\odot}$.

This estimated mean mass is smaller than the HB masses found in some GCs, e.g. M3, for which Valcarce & Catelan (2008) derived mean masses of $0.633 M_{\odot}$ and $0.650 M_{\odot}$ for RHB and BHB stars, respectively. We also do not find a bimodal or multi-modal HB mass distribution that appears to exist in many GC’s (see Valcarce & Catelan; Catelan 2004). Several reasons could contribute to these differences. (1) GC’s are mostly mono-metallic, in contrast to the large metallicity range of our FHB stars. We have needed to multiple evolutionary tracks that correspond most closely to the individual metallicities of our FHB stars (refer back to the interpolation method as described above). (2) Our sample sizes of RHB and BHB stars are too small to clearly indicate statistically significant mass distributions. (3) We have used an empirical correction to spectroscopically-determined $\log g$ values, which directly impacts the derived masses. (3) Our samples consist more of RHB than BHB stars, where the majority agglomerate near the low mass end, resulting in more low mass HB estimates. (4) Finally, Valcarce & Catelan cautioned about over-interpretation of masses derived from the GC CMD method, because they are biased against stars in later evolutionary states. Thus, it is not clear that our mean masses are substantially different than those reported for M3.

Additionally, other GC HB mass study have reported mean mass in reasonable agreement with ours. For example, de Boer et al. (1993) obtained $\langle M_{\text{HB}} \rangle = 0.5 M_{\odot}$ for NGC 6397. Masses of nearby HB stars derived via *Hipparcos* parallaxes have slightly smaller mean masses, $\langle M_{\text{HB}} \rangle = 0.38 M_{\odot}$, than ours (de Boer et al. 1997). Finally, the evolutionary and structural models of Sweigart (1987) suggest a wide range of individual HB masses ($0.2 - 1.2 M_{\odot}$). We conclude that our derived mean masses for the field HB stars are reasonable.

7.3. Blue and Red Edges of the RR Lyrae Instability Strip: $[\text{Fe}/\text{H}] > -2.5$

Locations of the blue and red edges (BE and RE) of the RR Lyr IS provide powerful constraints on stellar pulsation theory. They can be determined directly by examining the color-magnitude diagram of GCs that are well populated with RR Lyrs. Unfortunately, this requirement eliminates most clusters.

Additionally, accurate cluster reddenings must be known to transformation from colors to T_{eff} values. Determining the blue and red edges from bright field RR Lyr stars via spectroscopic method can avoid these complications. For the metallicity regime $[\text{Fe}/\text{H}] < -2.0$, Preston et al. (2006a) estimated the fundamental red edge from the T_{eff} distributions of field RHB stars and GC RR Lyrs. Since HB colors are affected by metallicity, shifting slightly blueward with decreasing $[\text{Fe}/\text{H}]$ (e.g., see Figure 1 of Sandage 1990), we repeated the exercise with our sample. We considered only those stars with $[\text{Fe}/\text{H}] > -2.5$, and compared the T_{eff} distributions of our field RHB and BHB with the distribution for field RR Lyr stars.

In Figure 22, the top and bottom panels show the distributions of spectroscopic and photometric T_{eff} 's of BHB and RHB stars with $[\text{Fe}/\text{H}] > -2.5$, respectively. The data for field RR Lyr stars (fundamental mode RRab and first overtone RRc variables) in both middle panels are extracted from Lambert et al. (1996) and Clementini et al. (1995). It shows the RR Lyr distribution drops at $T_{\text{eff}} = 5900$ K and 7000 K. Both photometric and spectroscopic T_{eff} RHB distributions decline at $T_{\text{eff}} > 5700$ K and overlap with the RR Lyr distributions (bottom panels). We suggest that the weak overlap region, $\simeq 5900$ K, is the red edge of field HB with $[\text{Fe}/\text{H}] > -2.5$. The T_{eff} 's of our BHB sample have no overlap with those of the RR Lyr stars. This is expected since RRc type variables, which are bluer than the RRab type variables, are generally used for determining the BE, and there are only two RRc type variables from Lambert et al. (1996) being included in the histogram (middle panels). Assuming the RRc type variables defined the blue edge in this case, we approximated it to be 7400 K.

While field HB stars can be used for deriving red and blue edges, we warn that the method is not very robust. The lack of large BHB samples and uncertainties in T_{eff} values of field RRc stars are limiting factors on our blue edge estimates. The overlapping distributions of field RHB and RRab stars also limit the red edge accuracy. Perhaps semi-empirical work (i.e., simulations to map the observed distributions) would provide a better constraints on the red and blue edges of FHB stars. Before then, deriving T_{eff} 's for a large sample of field BHB and RRc will be needed.

8. Discussion

In this paper we have explored the chemical compositions of non-variable RHB and BHB field stars. Here we will compare our results with abundances in other evolutionary groups of halo field stars, and discuss some of the possible nucleosynthetic implications. The comparisons of our $[\text{X}/\text{Fe}]$ values with those of field stars are presented in Figure 23–25, where neutral and ionized species abundances of several elements have been averaged. We

did not combine Cr I & Cr II abundances, since their distributions conspicuously diverge at lower metallicities (as discussed in §6.4). Data for field stars were mainly taken from the compilation of Venn et al. (2004). For those $[X/Fe]$ that are not listed in Venn et al. (2004), we assembled the comparison samples from several references, which we summarize in Table 14.

8.1. Light and Iron-peak Elements

Enrichment of α -elements in metal-poor stars has been known for decades. The explanation for this behavior presumes predominance of nucleosynthetic contributions from short-lived massive stars that died in core-collapse type II supernovae (SNe II) in early Galactic times. The resulting explosions contributed large amounts of light α -elements (e.g., O, Ne, Mg and Si), smaller amounts of heavier α -elements (e.g., Ca and Ti) and small amounts of Fe-peak elements to the ISM (Woosley & Weaver 1995). Longer-lived, lower-mass stars began to contribute their ejecta by adding more Fe-peak elements through Type Ia supernovae (SNe Ia) from lower-mass progenitors which exploded in thermonuclear runaway processes at later times. When SNe Ia became significant polluters of the ISM, a lowering of the $[\alpha/Fe]$ values (at higher metallicities) occurred.

In general our HB α -element abundances agree with those of other halo star populations. We illustrate this in Figure 23, where $[Mg\ I/Fe]$ and $[Ti\ I/Fe]$ of our RHB and BHB are in close accord with other field stars. The $\langle [Si\ I+II/Fe] \rangle$ and $\langle [Ca\ I+II] \rangle$ of RHB stars follow the general field star trend but these ratios tend to be lower for BHB stars in the same metallicity range (i.e., ~ 0.35 dex lower). The offset of mean Ca abundances is mainly due to the lower $[Ca\ I/Fe]$ of BHB stars (see description in §6.1). Similar lines were used in both BHB and RHB stars, as such, line selection is probably not the cause of the offset. As for $\langle [Si\ I+II/Fe] \rangle$, the star-to-star scatter is large and the offset between RHB and BHB stars is dominated by the RHB star $[Si\ I/Fe]$ dependence on T_{eff} (see §6.2).

Our BHB and RHB sodium abundance pattern looks quite different than in other field stars. However, little weight should be attached to our results because they have large uncertainties. We must rely solely on the Na D lines, and they are very strong in RHB stars. Aluminum is produced in massive stars, similarly to magnesium, but significantly deficient with respect to iron in metal-poor stars. The production of Al rises as it reaches the disk-to-halo transition at higher metallicity, i.e., $[Fe/H] \gtrsim 1.5$ (e.g., Timmes et al. 1995). Our abundances confirm this, with the caution that our derived trend with metallicity depends solely on RHB stars at low $[Fe/H]$ and all BHB stars at high $[Fe/H]$.

Iron-peak elements (with the exception of Ti, discussed above) are believed to be largely produced during Type Ia and Type II SNe explosion events. In our metallicity regime the iron-peak abundances of main-sequence and RGB stars generally have their solar values, with the exception of Mn and Cu. The derived Fe-peak abundance ratios (i.e., Sc II, Cr I, and V II) of our RHB and BHB stars are also in agreement with those found in field dwarfs and giants (see Figure 24). Most of them are expected to be constant in all metallicity regimes. Manganese and Zinc are the exceptions. In common with previous studies, [Mn/Fe] ratios of our HB stars increase as metallicity increases, but the slope of this relation may be larger in our sample. We do not have a clear physical explanation to this, and caution that, (a) the trend is based on relatively few points, and (b) [Mn/Fe] is quite sensitive to stellar parameter choices (refer to Table 10 & 11). Again, we refer the reader to Sobeck et al. (2006) for the production of Mn.

For nickel abundances we must rely on Ni I lines for RHB stars and Ni II lines for BHB stars. The low Ni II abundances of BHB stars should not be given large weight, as they are solely derived from one line. The very large [Ni I/Fe] values of several RHB stars, substantially at variance with the general trend of field stars, are most likely due to the lack of many detectable lines. The RHB stars with more than four lines contributing to their Ni abundance have ratios in good agreement with the field stars.

We find [Zn/Fe] \simeq 0.0 throughout the metallicity regime of [Fe/H] $>$ -2.0 , which is consistent with the study of Sneden et al. (1991). Recent work by Cayrel et al. (2004) shows increasing [Zn/Fe] at decreasing metallicities. Such a trend could indicate an α -rich freezeout process contribution to Fe-group element production at low metallicities. Our Zn abundance at low metallicity range, i.e., [Fe/H] $<$ -2.0 , perhaps consistent with this recent finding, but our data points are too sparse for firm conclusions on this point. Unfortunately, the comparison can only be made for RHB stars since the Zn I lines in BHB stars are too weak to be detected.

8.2. Neutron-Capture Elements

Elements heavier than the iron-peak ($Z > 30$) cannot be efficiently synthesized by charged-particle fusion because of Coulomb repulsion and the endothermic nature of such reactions. They are produced in the late stages of stellar evolution via neutron-capture events, namely the s - and r -processes (see review by Sneden et al. 2008). The s -process occurs quiescently in the He-fusion zones of low or intermediate mass AGB stars, while the r -process is believed to occur explosively in neutron rich sites, e.g., Type II SNe or merging events of two neutron stars (Rosswog et al. 1999).

We have abundances for six n -capture elements in HB stars. Strontium, Yttrium and Zirconium are relatively light n -capture elements. In the solar system, they are attributed mostly to the “main” s -process (Arlandini et al. 1999). Barium and Lanthanum are heavier n -capture elements also primarily s -process elements in solar-system material. Europium is our sole representative of solar-system r -process elements.

Our HB n -capture abundance ratios are generally in accord with field stars studies (see Figure 25). The offset of $[\text{Sr}/\text{Fe}]$ between RHB and BHB stars are discussed in §6.5. Unfortunately, we do not have $[\text{Sr}/\text{Fe}]$ for field stars with $[\text{Fe}/\text{H}] > -2.0$ for comparison. The resonance lines of Sr II are very strong for moderately metal-poor cooler stars and thus Strontium is not well represented in previous field-star surveys in this metallicity regime. We conclude that $\langle [\text{Sr}/\text{Fe}] \rangle \sim 0$ for $[\text{Fe}/\text{H}] > -2.0$.

Increasing star-to-star scatter with decreasing metallicity is apparent in the heavier n -capture elements Ba, La, and Eu, in accord with trends seen in other field star samples. A sharp downward trend of $[\text{Ba II}/\text{Fe}]$ with decreasing metallicity becomes apparent for $[\text{Fe}/\text{H}] < -2.0$. This pattern is present in field stars studies as well. The $[\text{La}/\text{Fe}]$ should roughly correlate with $[\text{Ba}/\text{Fe}]$. Unfortunately, we cannot easily detect La II lines in HB stars below $[\text{Fe}/\text{H}] \simeq -2.5$, where the drop in Ba abundance becomes apparent. The simplest explanation for the rise of $[\text{Ba}/\text{Fe}]$ at $[\text{Fe}/\text{H}] > -2.0$ is that the r -process dominates Ba production at lowest metallicities while the s -process plays a more important role at higher metallicities (Busso et al. 1999).

The initial examination of our derived Europium abundances yielded six RHB stars with $[\text{Eu}/\text{Fe}] > 0.5$, well above the mean trend. However, high $[\text{Eu}/\text{Fe}]$ has also been found in some field stars (as shown in Figure 25). For example, n -capture rich star CS 22892–052 has $[\text{Eu}/\text{Fe}] = +1.64$ (Snedden et al. 2003) and CS 31082–001 has $[\text{Eu}/\text{Fe}] = +1.63$ (Hill et al. 2002). The other n -capture elements of three of the Eu-rich RHB stars in our samples, i.e., CS 22875–029, CS 22886–043 and BD+17° 3248 are also high, implying that these three are truly n -capture rich stars. The overall n -capture abundance distributions for the other three RHB stars with Eu excesses are less certain. These six RHB stars deserve followup spectroscopic investigation of the n -capture elements.

8.3. Heavier vs Lighter Neutron-Capture Elements

Abundances of light n -capture elements Sr, Y, and Zr appear to be highly correlated with each other, and clearly they share a common nucleosynthetic origin (e.g., McWilliam et al. 1995; François et al. 2007; Aoki et al. 2005). In Figure 26, we compare the mean Sr-Y-Zr

abundances the heavier element Ba for our HB stars, adding in the data of François et al. (2007). Only stars with detections of all of these elements are included in this plot. The comparison shows a tight correlation (i.e., increasing overabundant as decreasing Barium abundances), which suggests the correlation exists regardless of metallicity regime and evolutionary state.

To examine the contributions of the r and s -process ratios of metal-poor stars, abundances of Y, Ba, La and Eu are generally used. As discussed above, Y, Ba and La can be formed via r and s -processes, while Eu is largely formed via the r -process. In Figure 27, we plotted the [La/Eu], [Ba/Eu] and [Y/Eu] vs [Fe/H] of our HB samples along with those of Venn et al. (2004), Simmerer et al. (2004) and Woolf et al. (1995), and compare them with estimated pure r -process solar system abundances (Arlandini et al. 1999; Sneden et al. 2008).

The top panel shows the [La/Eu] distribution, which the rise of [La/Eu] as metallicity increases progresses slower than [Ba/Eu] and [Y/Eu]. The comparison between [La/Eu] and middle panel of [Ba/Eu] demonstrates that the larger scatter of [Ba/Eu] is due to the Barium not Europium abundances. The middle and bottom panels of [Ba/Eu] and [Y/Eu] show large scatter in very metal-poor stars regime, which suggests an inhomogeneous mixing in early Galactic time. We also find a slow increase of [Ba/Eu] and [Y/Eu] as the metallicity increases. The rise is further evidence of the increasing contribution of the s -process as metallicity increases (with time in the Galaxy). The slope of [Ba/Eu] for our HB stars is steeper than the field stars but the overall trend is indistinguishable from the large scatter. Also, the [Y/Eu] abundances are above the estimated pure r -process solar-system abundances, which again suggests that the s -process (from AGB stars) play a significant role in Yttrium production.

8.4. CS 22186–005

The RHB star CS 22186–005 has an extremely low Sr abundance, i.e., [Sr II/Fe] = -1.03 (see Figures 17 & 25). As expected, there is no detection of the weaker Zr II and Y II in this star. However, we detected Barium, with an abundance ratio of [Ba II/Fe] = -0.58 . Its Barium abundance follows the general declining trend of metal-poor stars that has metallicity below -2.0 (see Figure 25). The resulting abundance ratio, [Ba/Sr] = $+0.45$, is somewhat surprising because in most n -capture metal-poor cases, the heavier n -capture elements are underabundant with respect to lighter ones (as summarized in see Figure 7 of Sneden et al. 2008). Other heavier n -capture elements (i.e., Eu and La) were not detectable with our spectra of CS 22186–005, This star does not appear to have obvious abundance anomalies

among the lighter elements.

In Figure 28, we extend Sneden et al’s Figure 7 by adding in Sr and Ba abundances of our RHB and BHB stars. It is clear that CS 22186–005 is not the only metal-poor star that exhibits unusually large [Ba/Sr] ratios at low [Ba/Fe]. Such stars have mainly been found among the very metal-poor giant sample of François et al. (2007). Clearly these stars provide further evidence that n -capture synthesis events cannot easily be characterized by single nucleosynthesis processes. Followup observations at higher S/N and resolution of this type of star should be undertaken.

9. Conclusions

We present the first large-sample detailed chemical composition study of non-variable field RHB and BHB stars. The high resolution spectra for our work were obtained with the 2.7 m telescope at the McDonald Observatory. The sample was selected from the survey of Behr (2003b). Additional RHB spectra from Preston et al. (2006a) were also added to the analysis. We derived the model stellar atmospheric parameters, T_{eff} , $\log g$, [Fe/H], and v_t for all program stars based on spectroscopic constraints. Of some interest is that the microturbulence of RHB stars increase with increasing T_{eff} , in agreement with Preston et al. (2006a), while microturbulence appears to decline with increasing T_{eff} in BHB stars. More data on BHB stars to solidify this conclusion would be welcome.

Employing these stellar parameters, we derived relative abundance ratios, [X/Fe], of the α -elements, Fe-peak elements and n -capture elements for these stars. The abundance ratios vs metallicity of our RHB and BHB stars are generally in accord with other field star studies. In particular, the α -elements are overabundant, [Al I/Fe] (RHB stars only) and [Mn I/Fe] are underabundant for metal-poor stars. Large star-to-star scatter is present in [n -capture/Fe] abundance ratios.

Finally we investigated the physical properties of our RHB and BHB stars by locating them in the $T_{\text{eff}}-\log g$ plane, and comparing them to HB evolutionary tracks of Pietrinferni et al. (2006), in order to estimate individual stellar masses. The mass distribution suggests that the majority of our stars have $M \sim 0.56 M_{\odot}$. By comparing the T_{eff} distribution of our field RHB and BHB stars with the field RR Lyraes of Lambert et al. (1996) and Clementini et al. (1995), we estimated the temperatures of red and blue edges of the RR Lyr IS for stars with [Fe/H] > -2.5 . We derived 5900 K and 7400 K, respectively for these edges.

The general consistency of HB abundance ratios with those of other dwarf and giant

halo star samples justifies that HB stars can be used routinely in the future for Galactic structure-metallicity studies (such as investigations of stellar streams). More importantly, this work provides a starting point for our future study on chemical compositions of RR Lyrs (For et al., in prep). Determinations of abundances of these stars throughout their pulsational cycles will be examined in detail with the same methods as have been employed in this paper.

B.-Q. For acknowledges the invaluable assistance from the mountain support staff at the McDonald observatory, and travel assistance from a SigmaXi grant-in-aid. We are grateful to Bradford Behr and George Preston for helpful discussions and advice on their earlier studies. This research was supported by U.S. National Science Foundation grants AST-0607708 and AST-0908978.

REFERENCES

- Adelman, S. J., & Hill, G. 1987, *MNRAS*, 226, 581
- Adelman, S. J., & Philip, A. G. D. 1990, *MNRAS*, 247, 132
- Allende Prieto, C. 2001, *ArXiv Astrophysics e-prints*
- Allende Prieto, C., García López, R. J., Lambert, D. L., & Gustafsson, B. 1999, *ApJ*, 527, 879
- Alonso, A., Arribas, S., & Martínez-Roger, C. 1994, *A&A*, 282, 684
- Alonso, A., Arribas, S., & Martínez-Roger, C. 1999, *A&AS*, 140, 261
- Altmann, M. & de Boer, K. S. 2000, *A&A*, 353, 135
- Anders, E., & Grevesse, N. 1989, *Geochim. Cosmochim. Acta*, 53, 197
- Aoki, W., et al. 2005, *ApJ*, 632, 611
- Arlandini, C., Käppeler, F., Wisshak, K., Gallino, R., Lugaro, M., Busso, M., & Straniero, O. 1999, *ApJ*, 525, 886
- Arpigny, C., & Magain, P. 1983, *A&A*, 127, L7
- Barklem, P. S., & O’Mara, B. J. 1998, *MNRAS*, 300, 863
- Barklem, P. S., et al. 2005, *A&A*, 439, 129

- Baumuellner, D., Butler, K., & Gehren, T. 1998, *A&A*, 338, 637
- Baumuellner, D., & Gehren, T. 1997, *A&A*, 325, 1088
- Beers, T. C., Preston, G. W., & Shectman, S. A. 1992, *AJ*, 103, 1987
- Behr, B. B. 2003a, *ApJS*, 149, 67
- . 2003b, *ApJS*, 149, 101
- Blackwell, D. E., & Shallis, M. J. 1977, *MNRAS*, 180, 177
- Burstein, D., & Heiles, C. 1982, *AJ*, 87, 1165
- Busso, M., Gallino, R., & Wasserburg, G. J. 1999, *ARA&A*, 37, 239
- Cassisi, S., Castellani, M., Caputo, F., & Castellani, V. 2004, *A&A*, 426, 641
- Castelli, F., Gratton, R. G., & Kurucz, R. L. 1997, *A&A*, 318, 841
- Catelan, M. 2004, *ApJ*, 600, 409
- Cayrel, R., et al. 2004, *A&A*, 416, 1117
- Clementini, G., Carretta, E., Gratton, R., Merighi, R., Mould, J. R., & McCarthy, J. K. 1995, *AJ*, 110, 2319
- Cohen, J. G., et al. 2004, *ApJ*, 612, 1107
- de Boer, K. S., Geffert, M., Tucholke, H., & Schmidt, J. H. K. 1997, in *ESA Special Publication, Vol. 402, Hipparcos - Venice '97*, ed. R. M. Bonnet, E. Høg, P. L. Bernacca, L. Emiliani, A. Blaauw, C. Turon, J. Kovalevsky, L. Lindegren, H. Hassan, M. Bouffard, B. Strim, D. Heger, M. A. C. Perryman, & L. Woltjer, 331–334
- de Boer, K. S., Schmidt, J. H., & Heber, U. 1993, in *Astronomische Gesellschaft Abstract Series, Vol. 9, Astronomische Gesellschaft Abstract Series*, ed. G. Klare, 173–+
- Demarque, P., Zinn, R., Lee, Y., & Yi, S. 2000, *AJ*, 119, 1398
- Dorman, B., Rood, R. T., & O’Connell, R. W. 1993, *ApJ*, 419, 596
- Ferguson, J. W., Alexander, D. R., Allard, F., Barman, T., Bodnarik, J. G., Hauschildt, P. H., Heffner-Wong, A., & Tamanai, A. 2005, *ApJ*, 623, 585
- Fitzpatrick, M. J., & Sneden, C. 1987, in *Bulletin of the American Astronomical Society, Vol. 19, Bulletin of the American Astronomical Society*, 1129–+

- François, P., et al. 2007, *A&A*, 476, 935
- Francois, P. 1984, *Academie des Science Paris Comptes Rendus Serie B Sciences Physiques*, 299, 195
- Fulbright, J. P. 2000, *AJ*, 120, 1841
- Fusi Pecci, F., Ferraro, F. R., Bellazzini, M., Djorgovski, S., Piotto, G., & Buonanno, R. 1993, *AJ*, 105, 1145
- Gratton, R. G., et al. 2007, *A&A*, 464, 953
- Heber, U. 2009, *ARA&A*, 47, 211
- Hill, V., et al. 2002, *A&A*, 387
- Hoyle, F., & Schwarzschild, M. 1955, *ApJS*, 2, 1
- Hubrig, S., Castelli, F., de Silva, G., González, J. F., Momany, Y., Netopil, M., & Moehler, S. 2009, *A&A*, 499, 865
- Johnson, C. I., Kraft, R. P., Pilachowski, C. A., Sneden, C., Ivans, I. I., & Benman, G. 2005, *PASP*, 117, 1308
- Khalack, V. R., Leblanc, F., Behr, B. B., Wade, G. A., & Bohlender, D. 2008, *A&A*, 477, 641
- Khalack, V. R., Leblanc, F., Bohlender, D., Wade, G. A., & Behr, B. B. 2007, *A&A*, 466, 667
- Lai, D. K., Bolte, M., Johnson, J. A., Lucatello, S., Heger, A., & Woosley, S. E. 2008, *ApJ*, 681, 1524
- Lambert, D. L., Heath, J. E., Lemke, M., & Drake, J. 1996, *ApJS*, 103, 183
- Lee, Y., & Demarque, P. 1990, *ApJS*, 73, 709
- Lee, Y., Demarque, P., & Zinn, R. 1994, *ApJ*, 423, 248
- Lodders, K. 2003, *ApJ*, 591, 1220
- McWilliam, A. 1998, *AJ*, 115, 1640
- McWilliam, A., Preston, G. W., Sneden, C., & Searle, L. 1995, *AJ*, 109, 2757

- Meléndez, J., Shchukina, N. G., & Vasiljeva, I. E. and Ramírez, I. 2006, *ApJ*, 642, 1082
- Möhler, S. 2004, in *IAU Symposium*, Vol. 224, *The A-Star Puzzle*, ed. J. Zverko, J. Ziznovsky, S. J. Adelman, & W. W. Weiss, 395–402
- Nilsson, H., Ljung, G., Lundberg, H., & Nielsen, K. E. 2006, *A&A*, 445, 1165
- Nissen, P. E., Akerman, C., Asplund, M., Fabbian, D., Kerber, F., Kaufl, H. U., & Pettini, M. 2007, *A&A*, 469, 319
- Perryman, M. A. C., et al. 1997, *A&A*, 323, L49
- Peterson, R. C., Rood, R. T., & Crocker, D. A. 1995, *ApJ*, 453, 214
- Pietrinferni, A., Cassisi, S., Salaris, M., & Castelli, F. 2006, *ApJ*, 642, 797
- Pilachowski, C. A., Sneden, C., & Kraft, R. P. 1996, *AJ*, 111, 1689
- Preston, G. W., & Sneden, C. 2000, *AJ*, 120, 1014
- Preston, G. W., Sneden, C., Thompson, I. B., Sheckman, S. A., & Burley, G. S. 2006a, *AJ*, 132, 85
- Preston, G. W., Thompson, I. B., Sneden, C., Stachowski, G., & Sheckman, S. A. 2006b, *AJ*, 132, 1714
- Ramírez, I., & Meléndez, J. 2005, *ApJ*, 626, 465
- Reddy, B. E., Tomkin, J., Lambert, D. L., & Allende Prieto, C. 2003, *MNRAS*, 340, 304
- Rood, R. T., & Seitzer, P. O. 1981, in *IAU Colloq. 68: Astrophysical Parameters for Globular Clusters*, ed. A. G. D. Philip & D. S. Hayes, 369–+
- Rosenberg, A., Aparicio, A., Saviane, I., & Piotto, G. 2000, *A&AS*, 145, 451
- Rosswog, S., Liebendörfer, M., Thielemann, F., Davies, M. B., Benz, W., & Piran, T. 1999, *A&A*, 341, 499
- Sandage, A. 1990, *ApJ*, 350, 603
- Sandage, A., & Wallerstein, G. 1960, *ApJ*, 131, 598
- Schlegel, D. J., Finkbeiner, D. P., & Davis, M. 1998, *ApJ*, 500, 525
- Searle, L., & Zinn, R. 1978, *ApJ*, 225, 357

- Shi, J. R., Gehren, T., Mashonkina, L., & Zhao, G. 2009, *A&A*, 503, 533
- Simmerer, J., Sneden, C., Cowan, J. J., Collier, J., Woolf, V. M., & Lawler, J. E. 2004, *ApJ*, 617, 1091
- Skrutskie, M. F., et al. 2006, *AJ*, 131, 1163
- Sneden, C., Cowan, J. J., & Gallino, R. 2008, *ARA&A*, 46, 241
- Sneden, C., Gratton, R. G., & Crocker, D. A. 1991, *A&A*, 246, 354
- Sneden, C., & Lawler, J. E. 2008, in *American Institute of Physics Conference Series*, Vol. 990, *First Stars III*, ed. B. W. O’Shea & A. Heger, 90–103
- Sneden, C., et al. 2003, *ApJ*, 591, 936
- Sneden, C. A. 1973, PhD thesis, THE UNIVERSITY OF TEXAS AT AUSTIN.
- Sobeck, J. S., Ivans, I. I., Simmerer, J. A., Sneden, C., Hoefflich, P., Fulbright, J. P., & Kraft, R. P. 2006, *AJ*, 131, 2949
- Sobeck, J. S., Lawler, J. E., & Sneden, C. 2007, *ApJ*, 667, 1267
- Stephens, A., & Boesgaard, A. M. 2002, *AJ*, 123, 1647
- Sweigart, A. V. 1987, *ApJS*, 65, 95
- . 1997, *ApJ*, 474, L23+
- Thévenin, F., & Idiart, T. P. 1999, *ApJ*, 521, 753
- Timmes, F. X., Woosley, S. E., & Weaver, T. A. 1995, *ApJS*, 98, 617
- Valcarce, A. A. R., & Catelan, M. 2008, *A&A*, 487, 185
- Venn, K. A., Irwin, M., Shetrone, M. D., Tout, C. A., Hill, V., & Tolstoy, E. 2004, *AJ*, 128, 1177
- Wallerstein, G. and Greenstein, J. L., Parker, R., Helfer, H. L., & Aller, L. H. 1963, *ApJ*, 137, 280
- Wilhelm, R., Beers, T. C., Kriessler, J. R., Pier, J. R., Sommer-Larsen, J., & Layden, A. C. 1996, in *Astronomical Society of the Pacific Conference Series*, Vol. 92, *Formation of the Galactic Halo...Inside and Out*, ed. H. L. Morrison & A. Sarajedini, 171–+

Woolf, V. M., Tomkin, J., & Lambert, D. L. 1995, *ApJ*, 453, 660

Woosley, S. E., & Weaver, T. A. 1995, *ApJS*, 101, 181

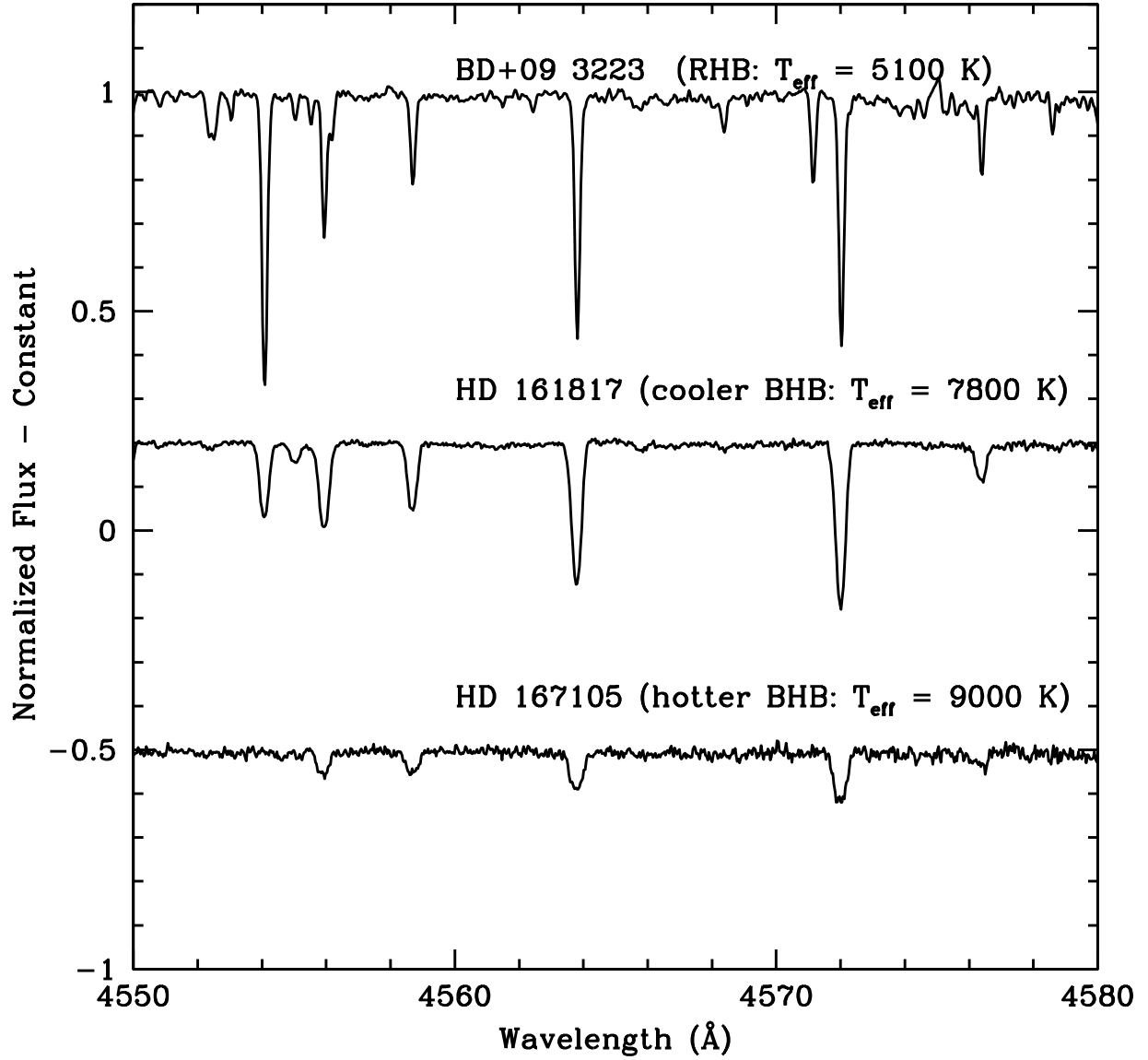


Fig. 1.— Typical reduced, normalized spectra of RHB and BHB stars obtained at McDonald 2.7 m telescope. Large rotational velocity is seen in hotter BHB stars.

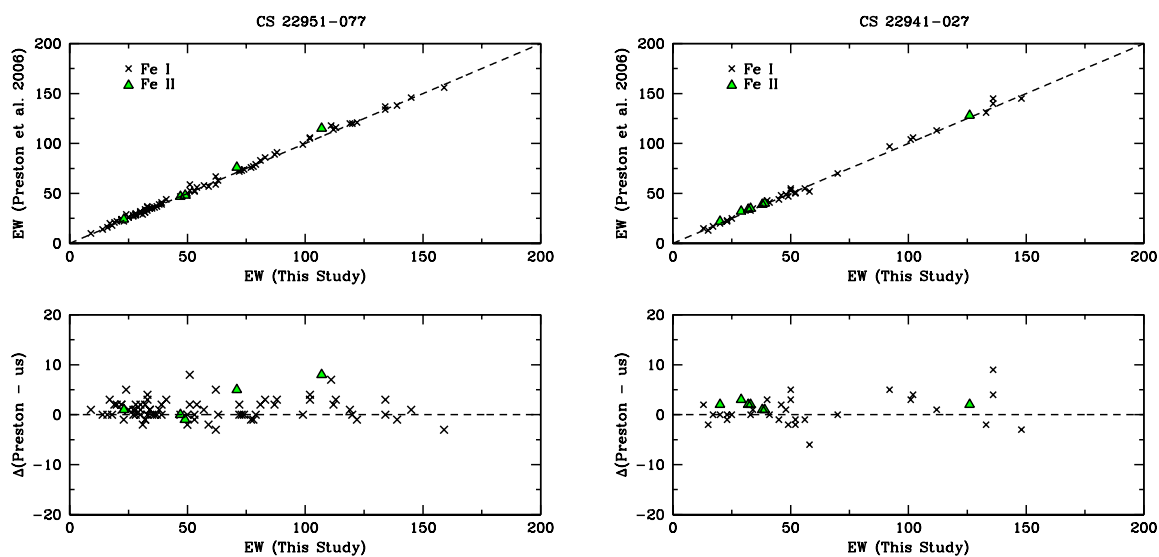


Fig. 2.— Comparisons of our measured Fe I & II EWs of cooler (CS 22951–077) and hotter (CS 22941–027) MPFRHB stars with Preston et al. (2006a). The top panels show 1:1 comparison of EW measurements. The bottom panels show the difference between our EW measurements and Preston et al. (2006a). The crosses and triangles represent Fe I and Fe II lines, respectively.

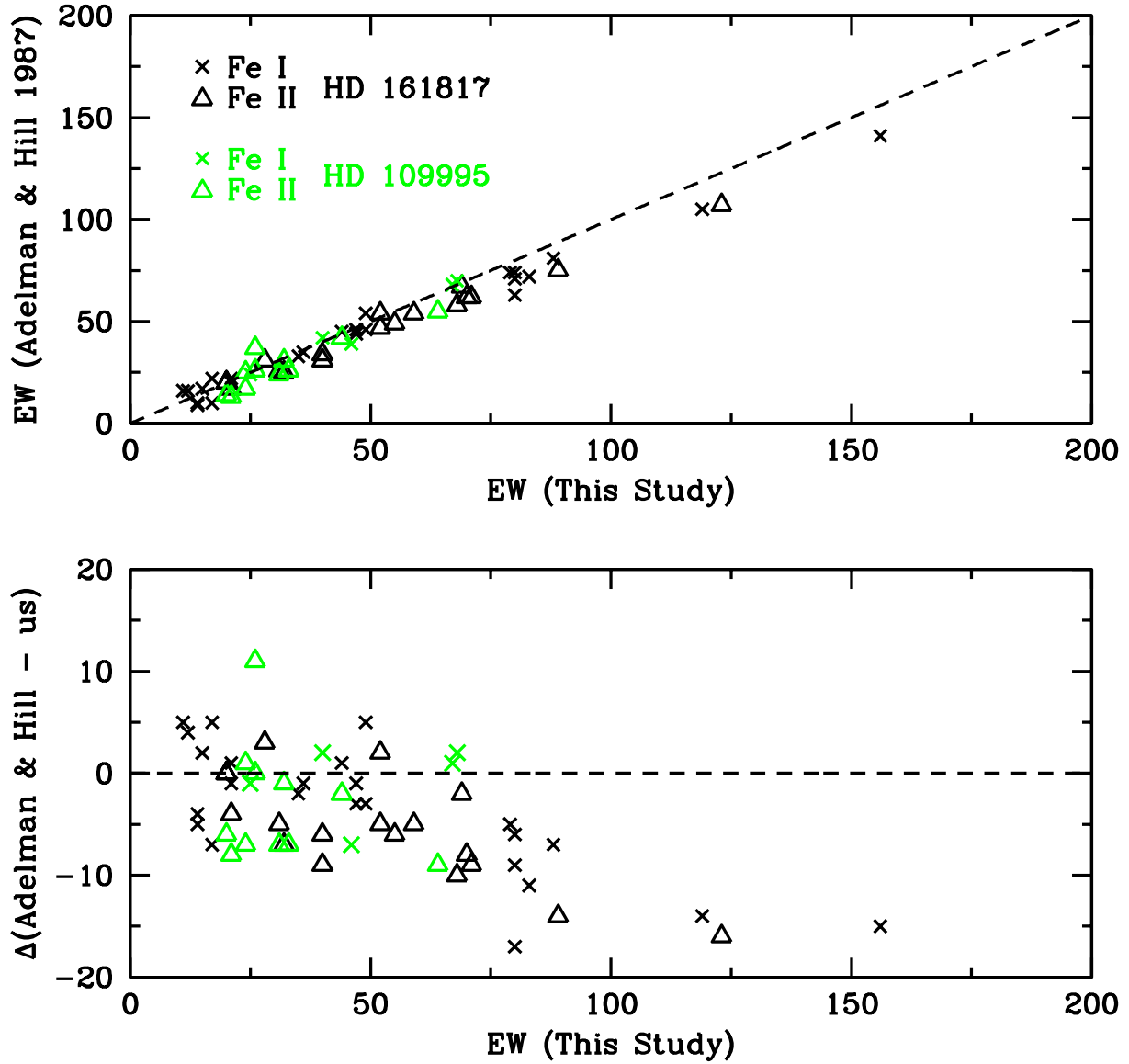


Fig. 3.— Comparisons of our measured Fe I & II EWs of HD 161817 and HD 109995 with Adelman & Hill (1987). The top panel shows 1:1 comparison of EW measurement. The bottom panel shows the difference between our EW measurements and Adelman & Hill (1987). See text for explanation on the large deviation between ours and Adelman & Hill (1987) measurements. The crosses and triangles represent Fe I and Fe II lines. The green and black correspond to lines measured in HD 109995 and HD 161817, respectively.

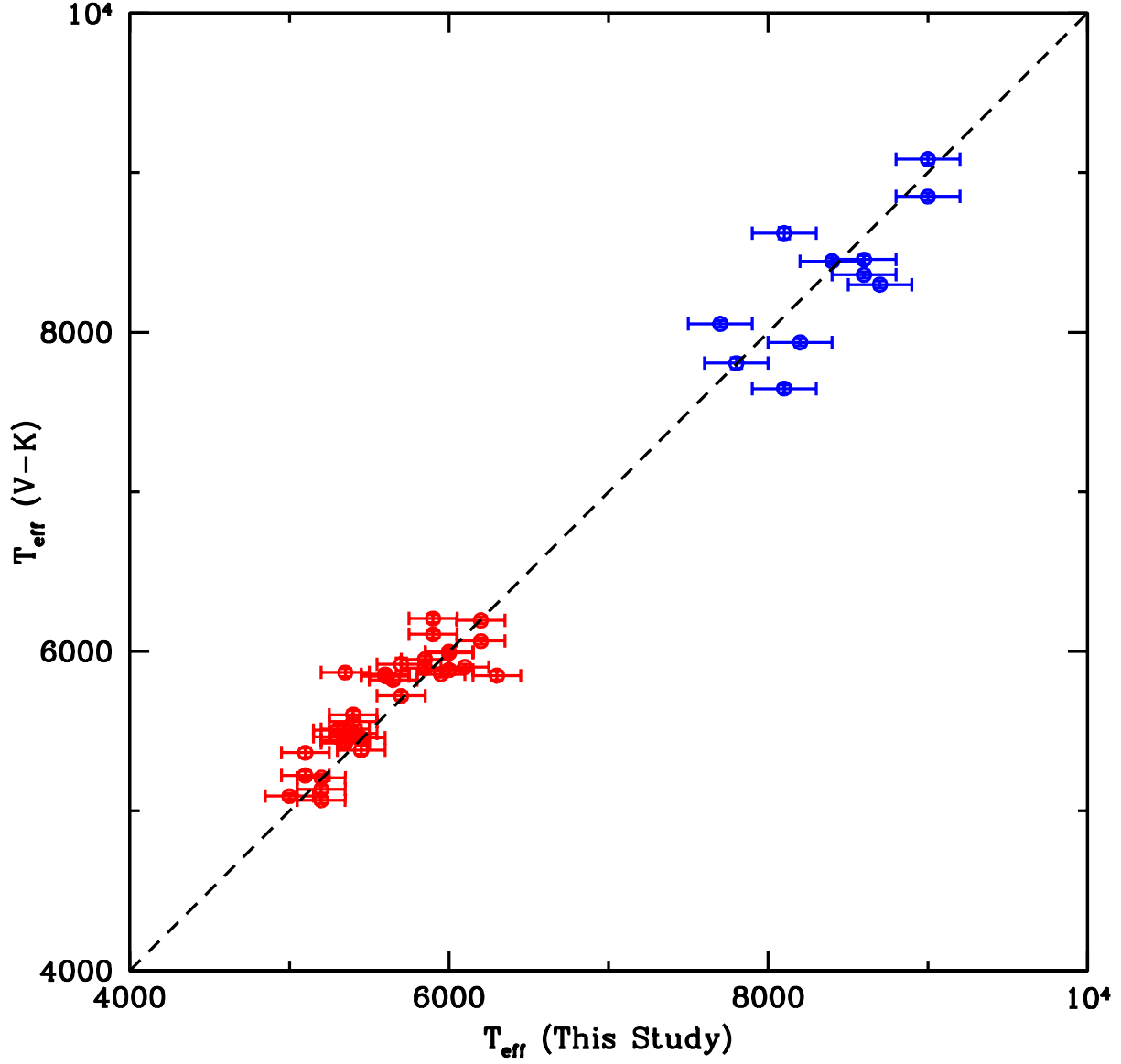


Fig. 4.— Comparison of spectroscopic T_{eff} with photometric T_{eff} derived from $(V - K)_{\text{TCS}}$ metallicity-dependent T_{eff} -color formula of Alonso et al. (1999). The error of photometric T_{eff} is equal to or smaller than the size of the dots.

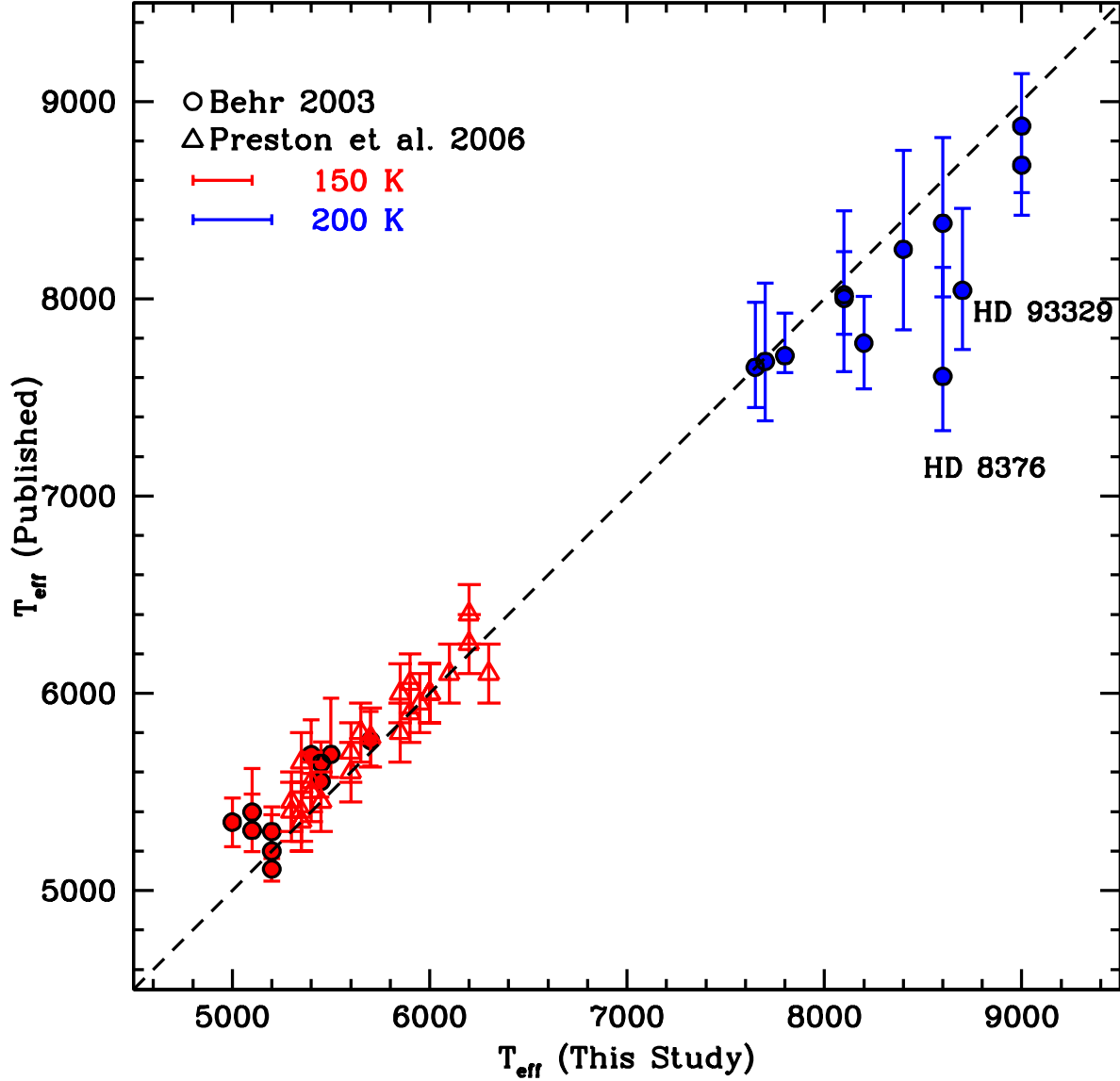


Fig. 5.— Comparison of spectroscopic T_{eff} derived from this study with T_{eff} values from Preston et al. (2006a) and Behr (2003b). The triangles and circles represent Preston et al. (2006a) and Behr (2003b) study, respectively. The red and blue colors correspond to RHB and BHB stars. For clarity in the figure, we do not plot error bars from our work for each star, but instead indicate typical T_{eff} uncertainties for this study, 150 K and 200 K for RHB and BHB stars. Comparison of BHB stars can only be made with Behr (2003b).

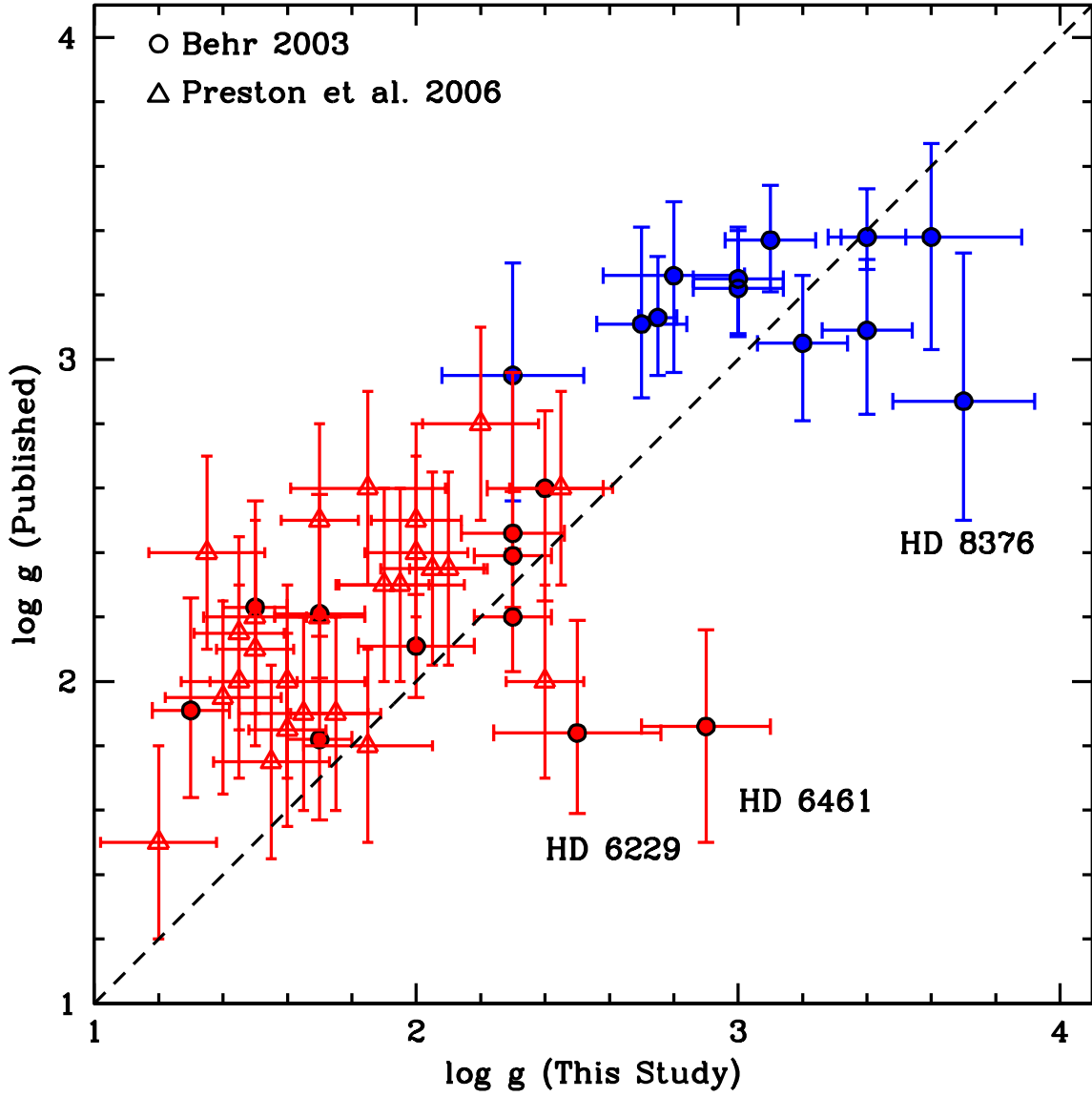


Fig. 6.— Comparison of spectroscopic $\log g$ derived from this study with $\log g$ derived by Preston et al. (2006a) and Behr (2003b). The triangles and circles represent Preston et al. (2006a) and Behr (2003b) study, respectively. The red and blue colors correspond to RHB and BHB stars.

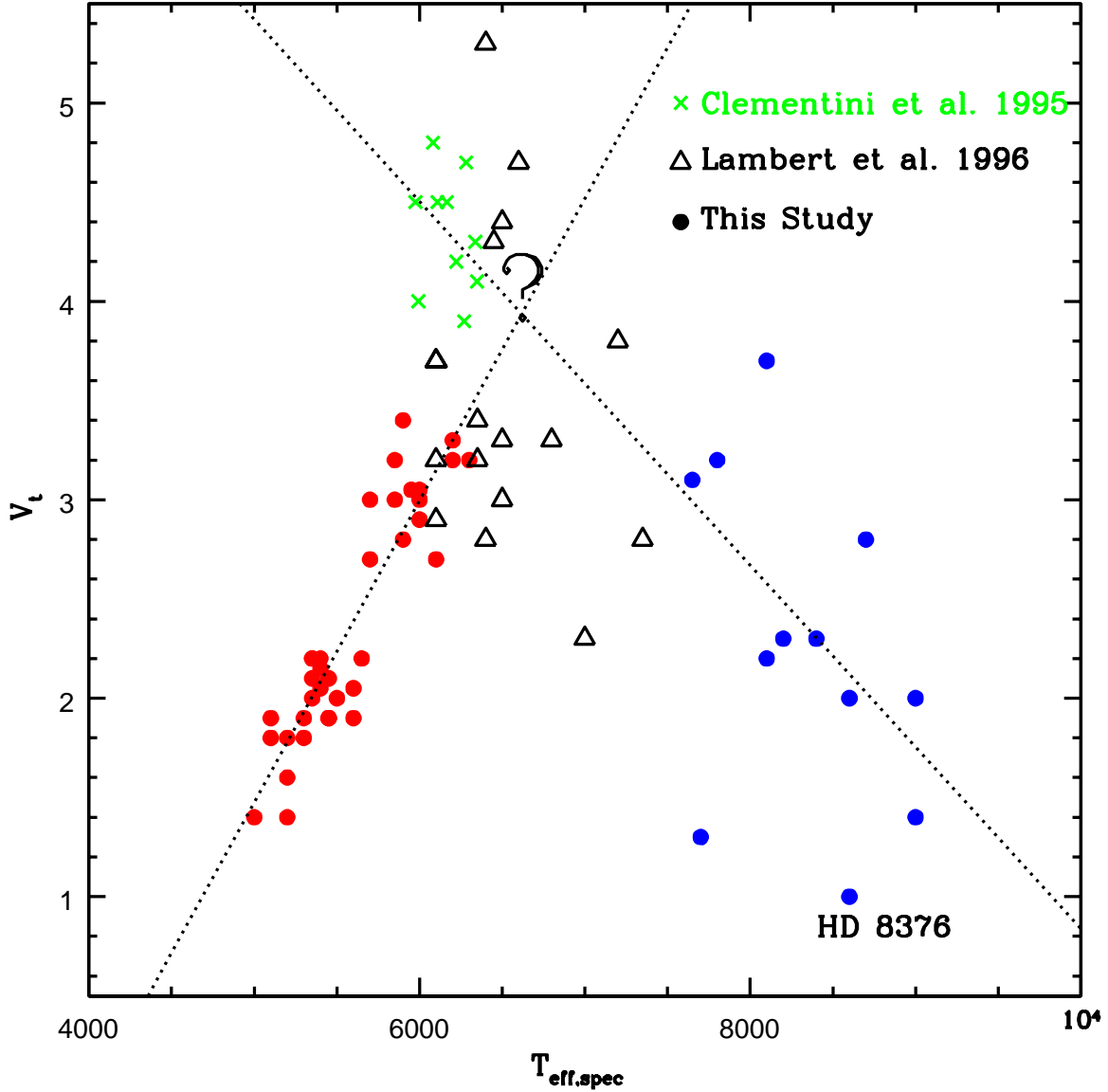


Fig. 7.— The correlation and anti-correlation between v_t and T_{eff} for RHB and BHB stars. Linear least square equations were fitted to all the RHB stars and BHB stars, excluding HD 8376. The crosses and open triangles represent the v_t and T_{eff} of RR Lyrs studies by Clementini et al. (1995) and Lambert et al. (1996), respectively. The readers are warned that there is no correlation in the RR Lyr IS region and beyond the intersection of dashed lines, where question mark is marked.

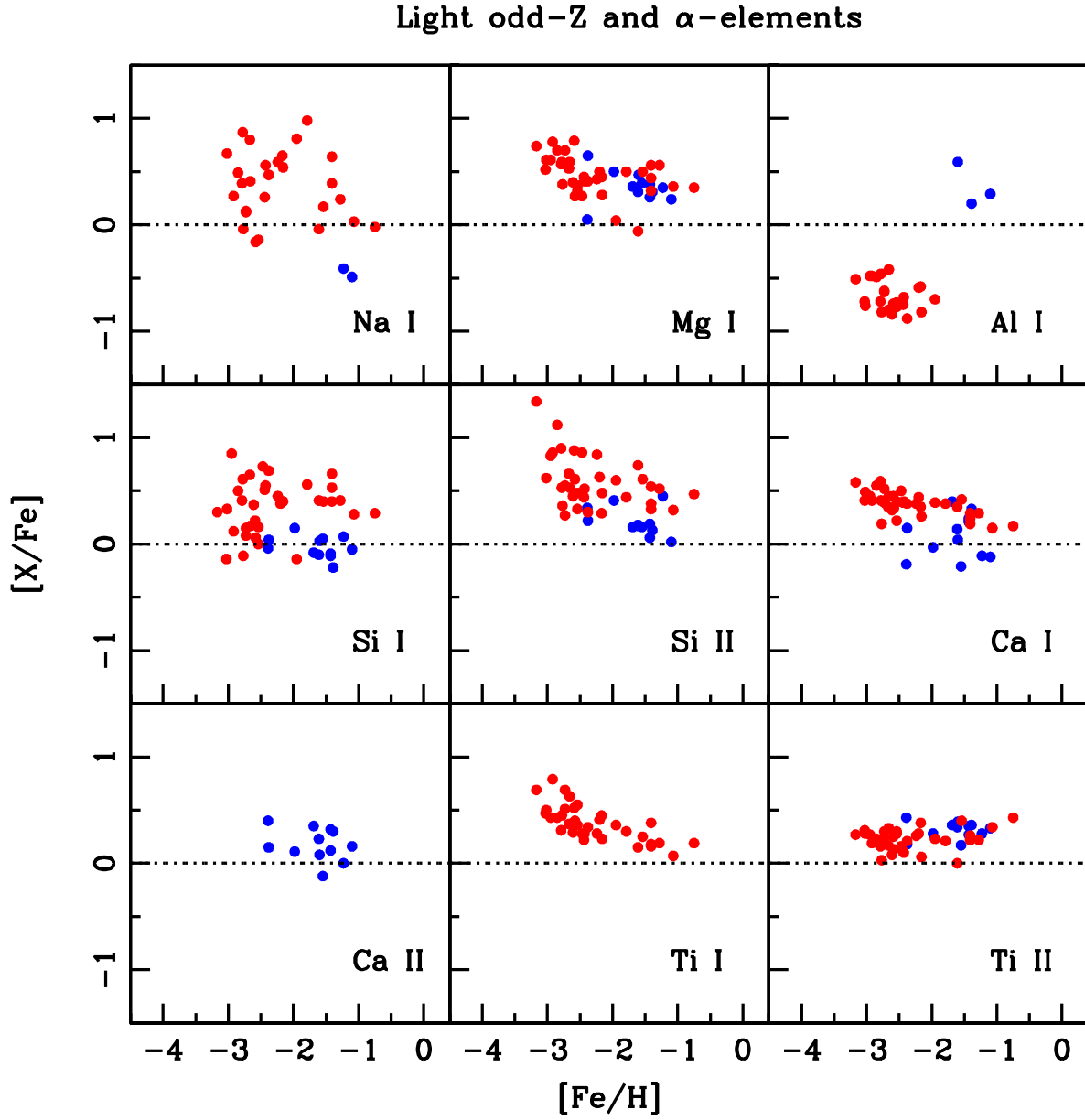


Fig. 8.— Abundance ratios of odd-Z and α -elements as a function of metallicity. NLTE corrections applied to Na I, Al I, Si I & Si II as described in text. The red and blue dots represent RHB and BHB stars.

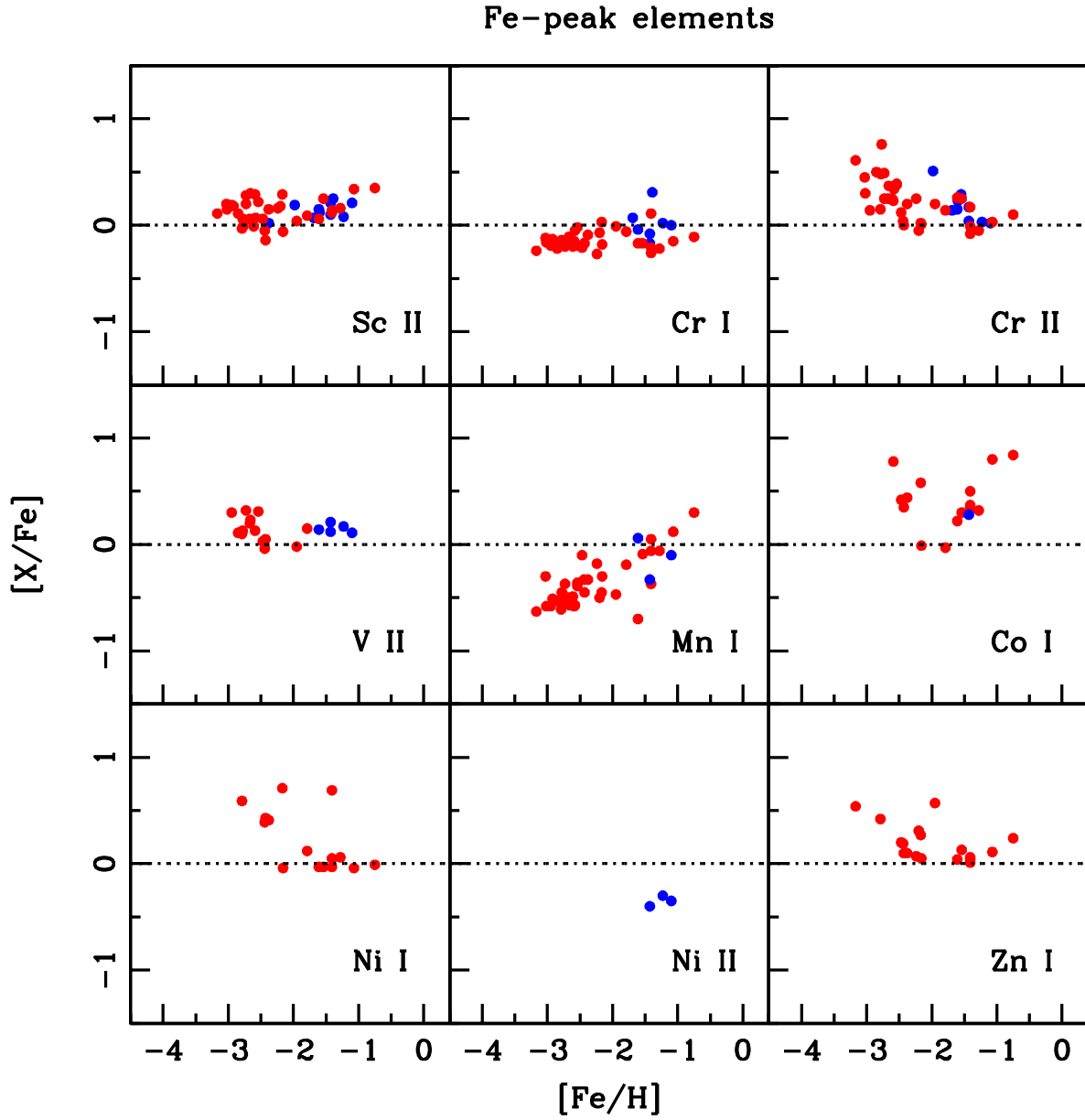


Fig. 9.— Abundance ratios of Fe-peak elements as a function of metallicity. The red and blue dots represent RHB and BHB stars.

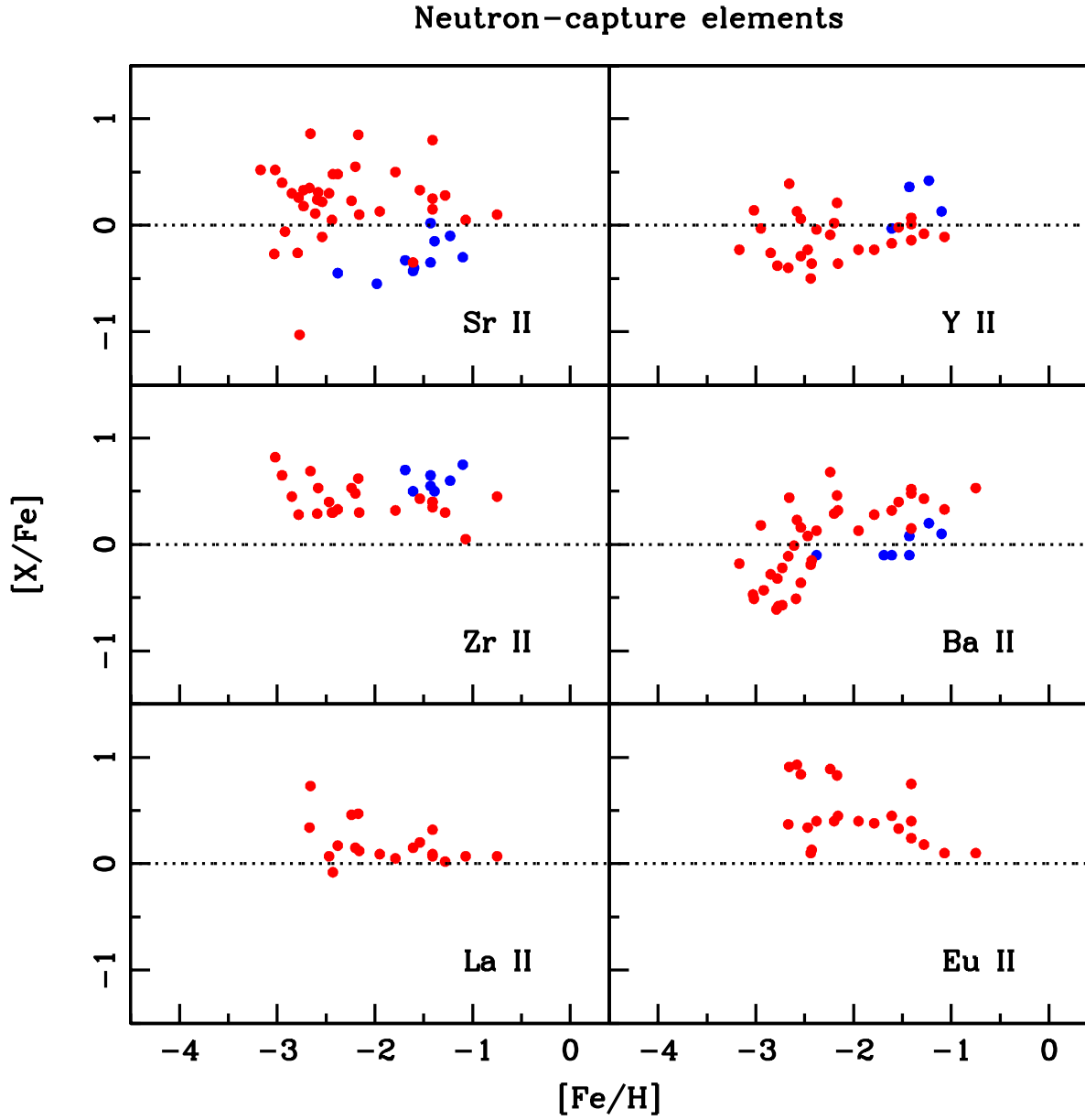


Fig. 10.— Abundance ratios of neutron-capture elements as a function of metallicity. The red and blue dots represent RHB and BHB stars.

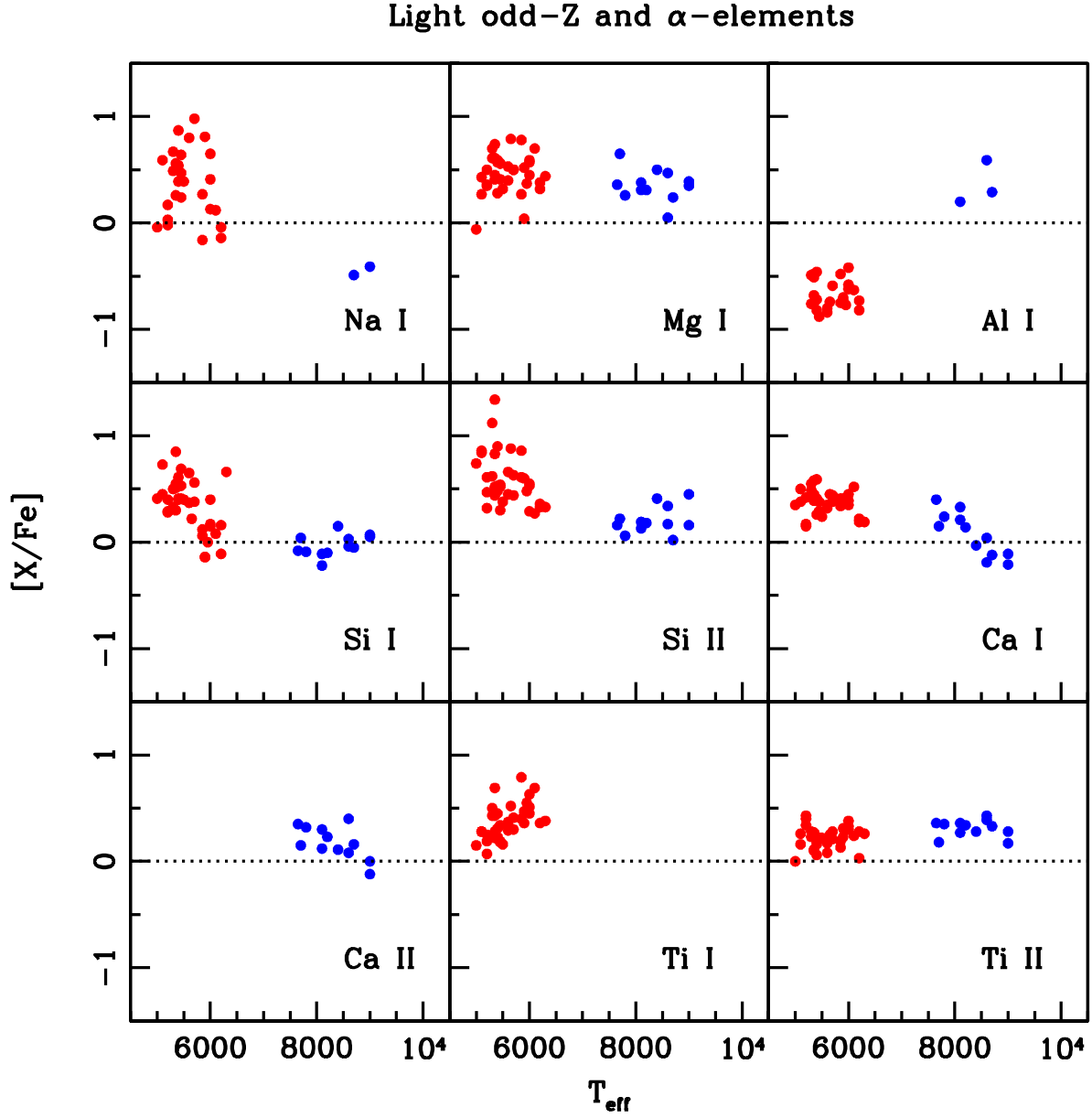


Fig. 11.— Abundance ratios of odd-Z and α -elements as a function of spectroscopic T_{eff} . NLTE corrections applied to Na I, Al I, Si I & Si II as described in text. The red and blue dots represent RHB and BHB stars.

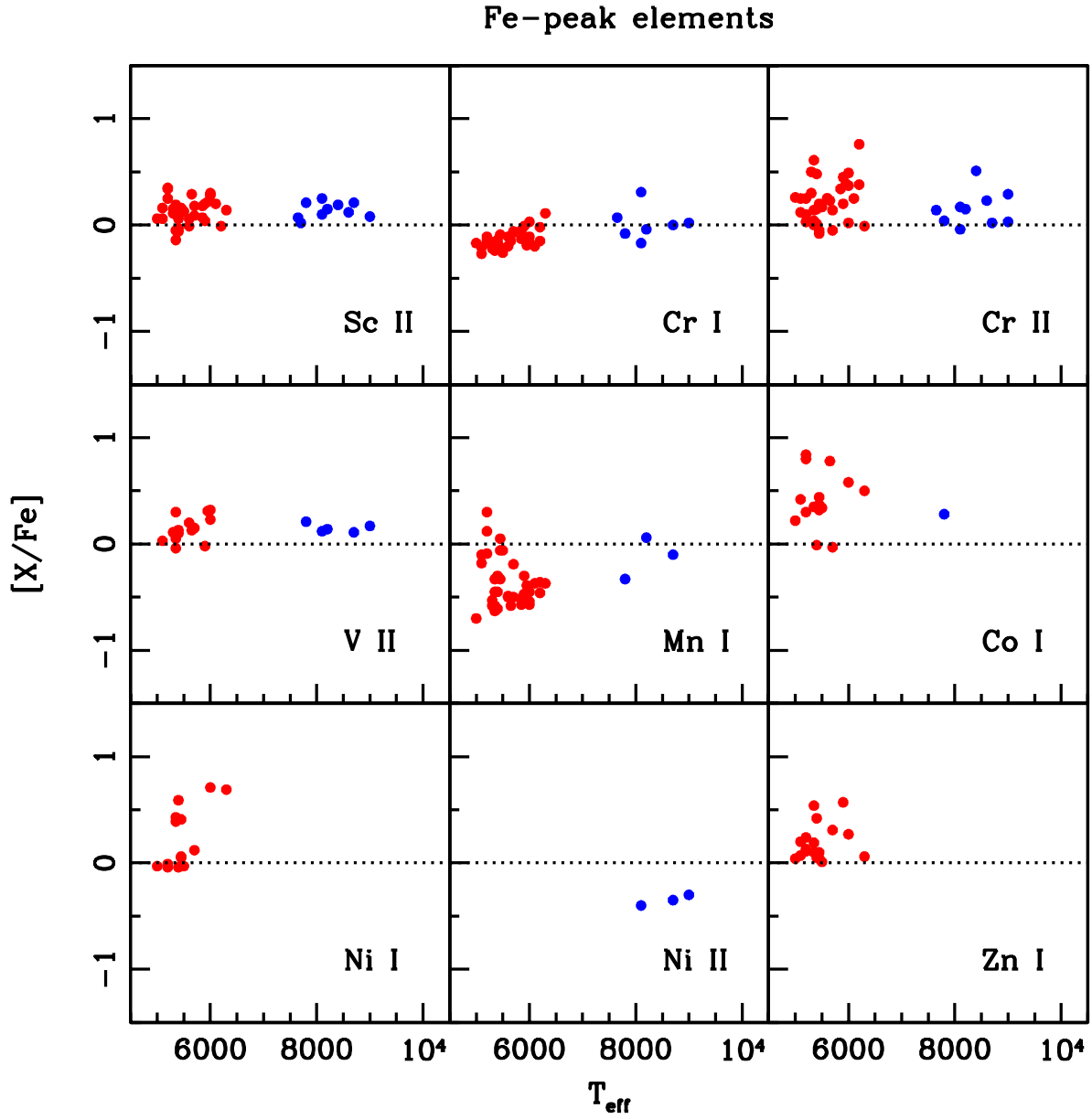


Fig. 12.— Abundance ratios of Fe-peak elements as a function of spectroscopic T_{eff} . The red and blue dots represent RHB and BHB stars.

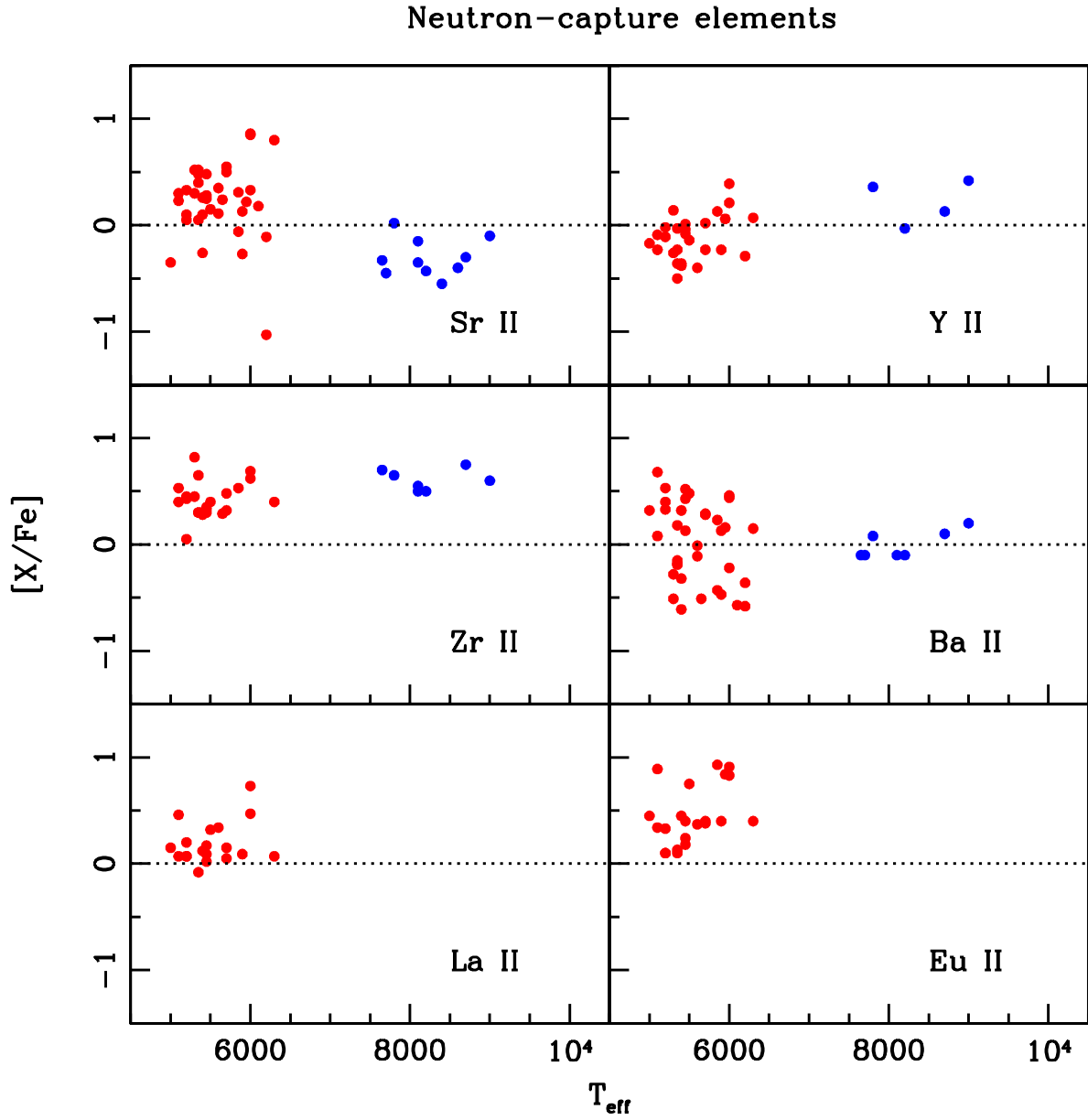


Fig. 13.— Abundance ratios of neutron-capture elements as a function of spectroscopic T_{eff} . The red and blue dots represent RHB and BHB stars.

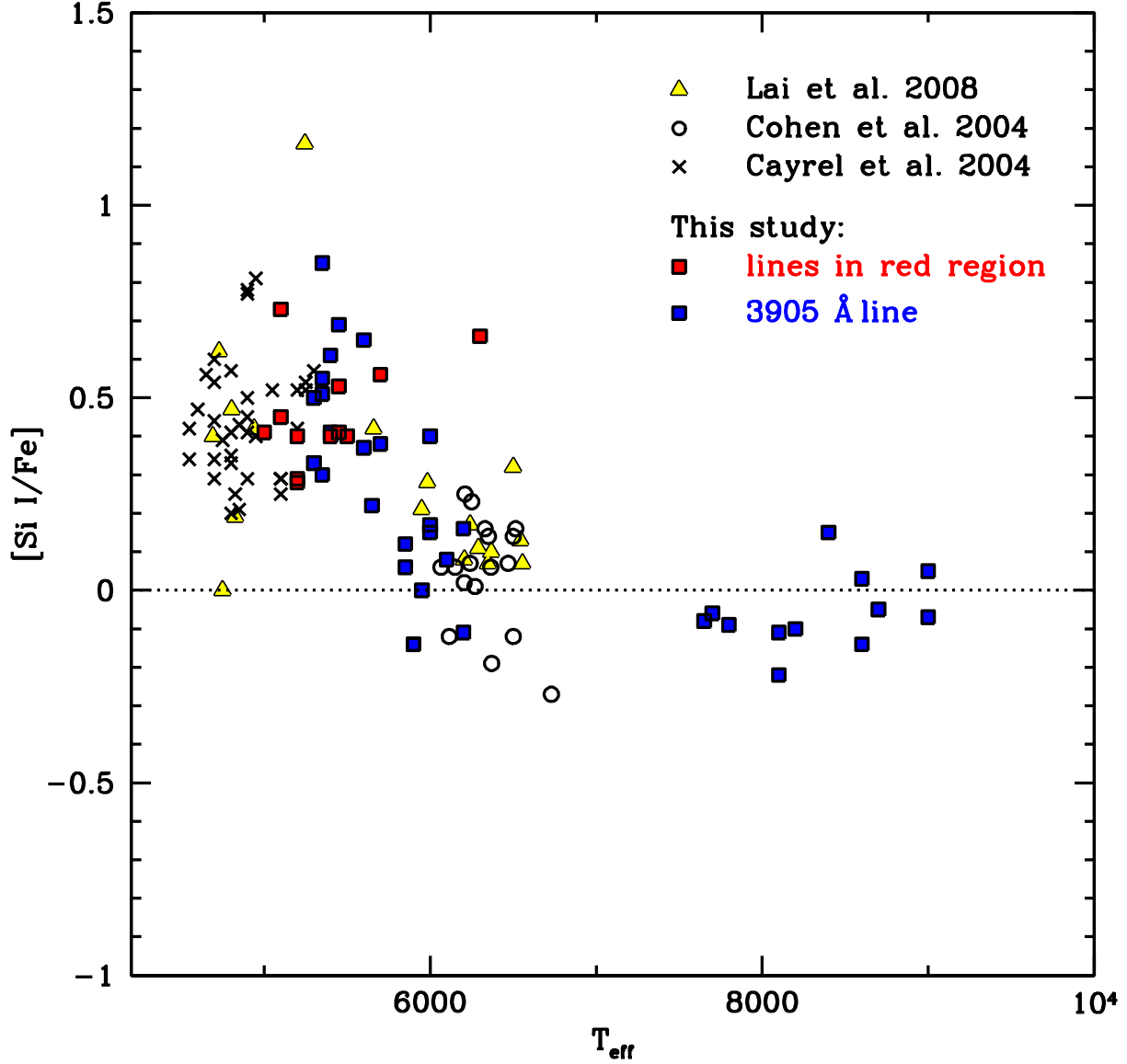


Fig. 14.— Abundance ratios of $[\text{Si I}/\text{Fe}]$ vs spectroscopic T_{eff} , with the addition of data of very metal-poor stars giants from Cayrel et al. (2004) (crosses), low-luminosity near-turnoff stars from Cohen et al. (2004) (open circles) and stars in different evolutionary states from Lai et al. (2008) (yellow triangles). The derived $[\text{Si I}/\text{Fe}]$ in this study is represented by filled rectangles. NLTE correction applied to $[\text{Si I}/\text{Fe}]$ as described in text. The red and blue colors represent Si I lines in red spectral region and 3905 Å line, respectively.

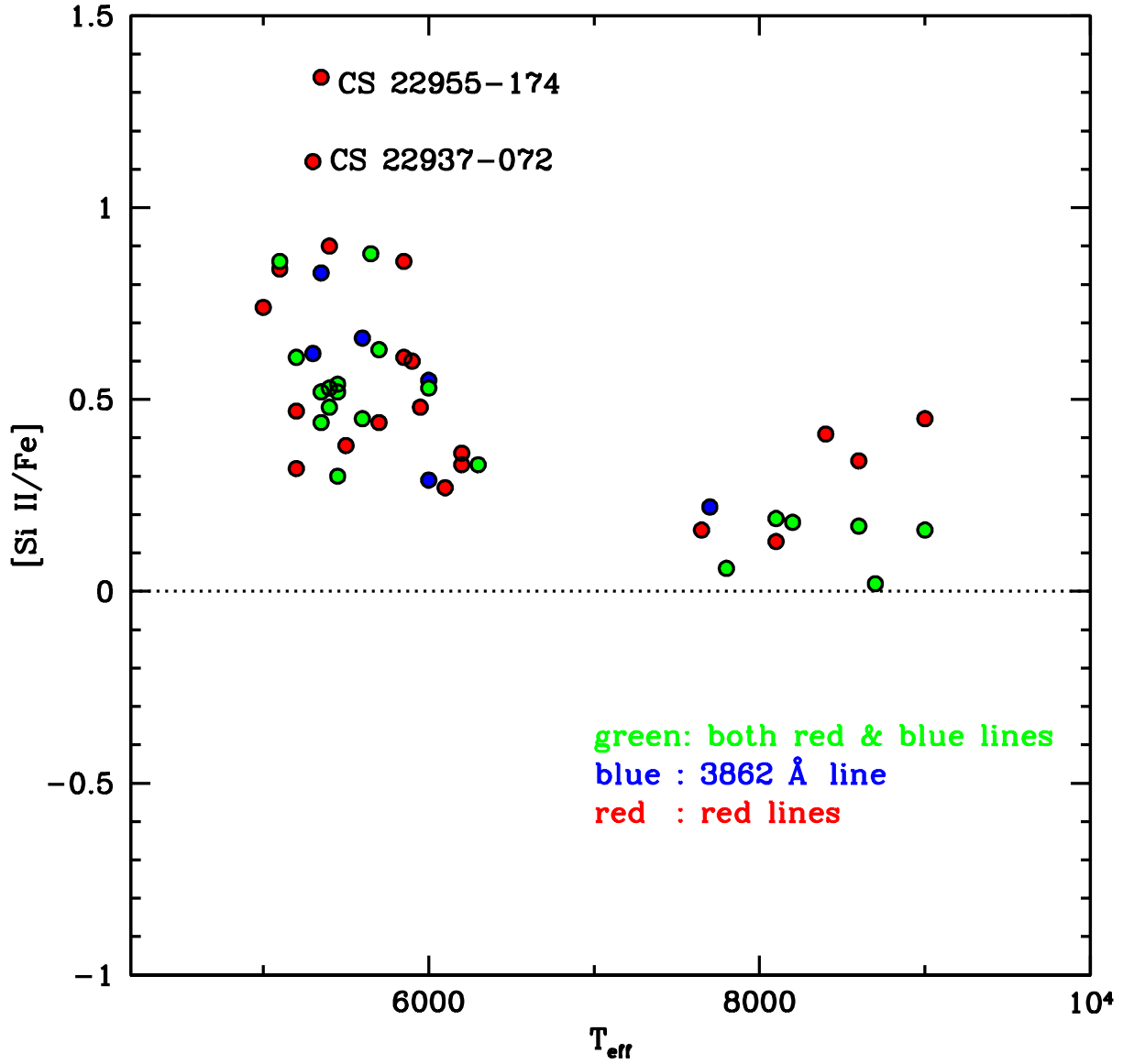


Fig. 15.— Abundance ratios of $[\text{Si II}/\text{Fe}]$ vs spectroscopic T_{eff} . NLTE correction applied to $[\text{Si II}/\text{Fe}]$ as described in text. The colors represent the usage of lines in different spectral regions for EW analysis.

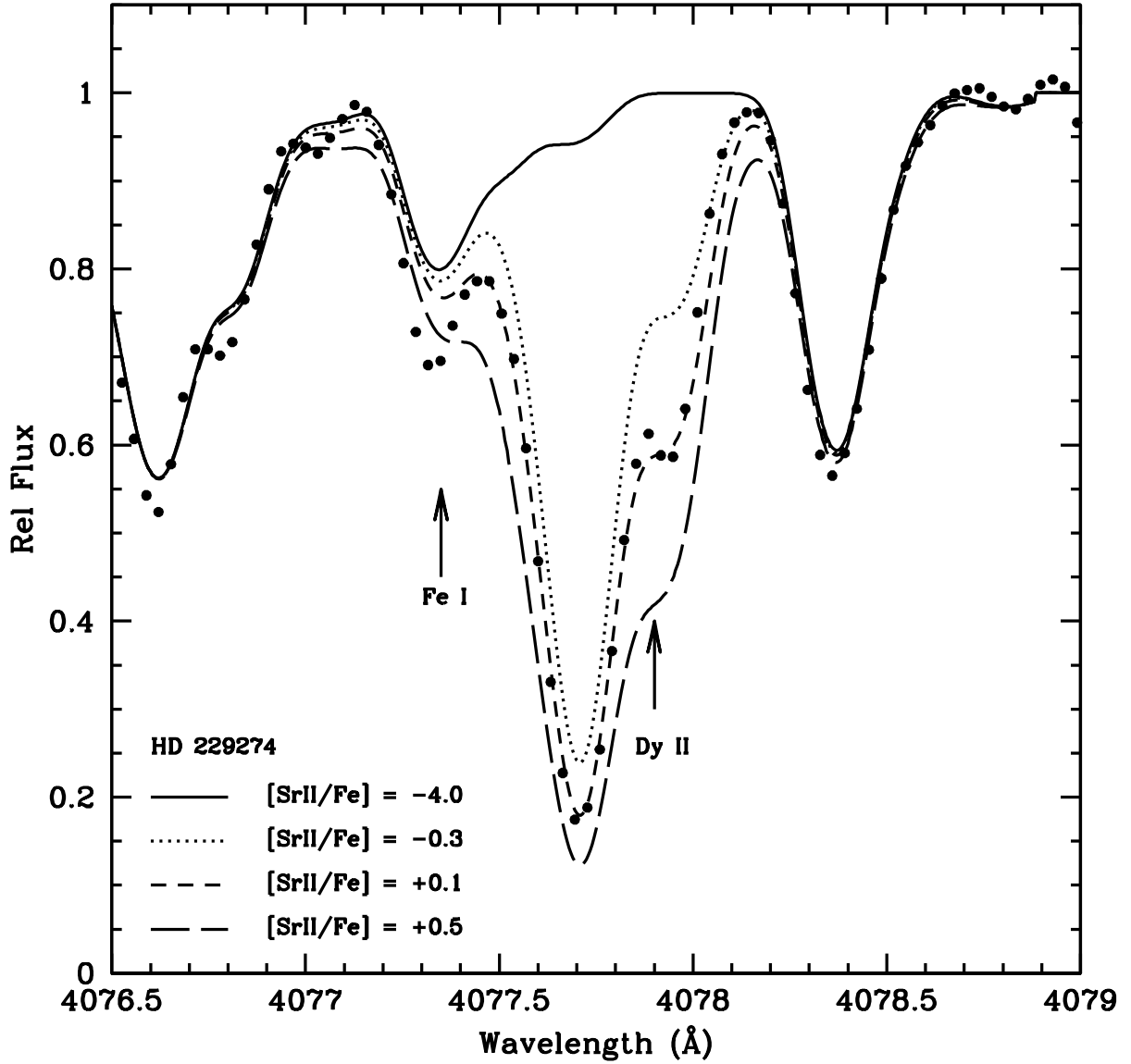


Fig. 16.— An example of synthesized Sr II 4077 Å line superimposed on the observed spectrum. The assumed Fe abundance is the same as the metallicity used in the stellar parameters. The solid and medium dashed lines represent no Sr contribution and derived Sr abundance ratio for this line. The dotted and long dashed lines are ± 0.4 dex of derived Sr abundance ratio.

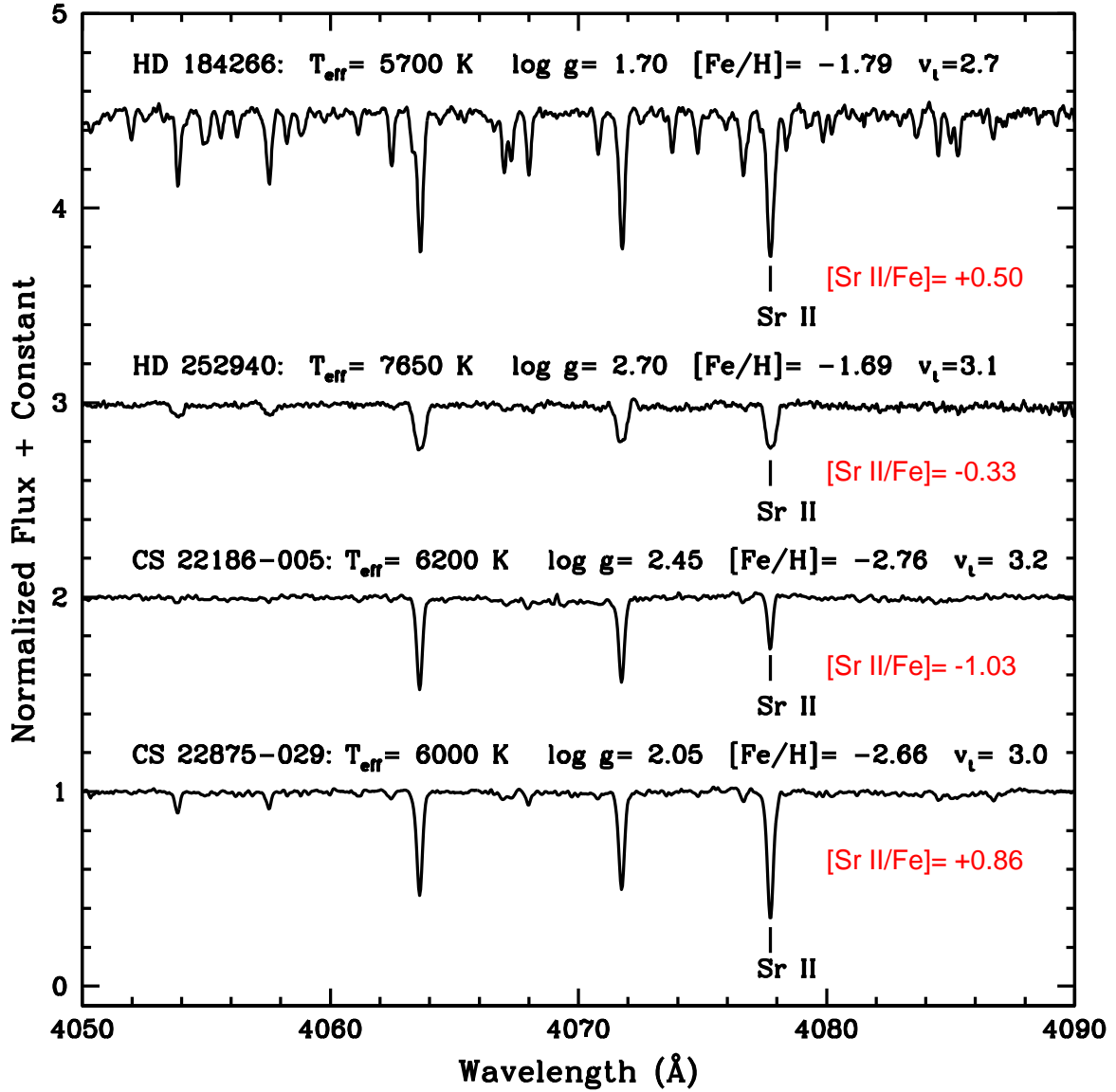


Fig. 17.— The top two spectra show the different Sr II line strength between RHB and BHB stars. As shown, Sr II line in BHB stars is not as strong as in RHB stars. The bottom two stars possess similar stellar parameters but show different line strength in Sr II line.

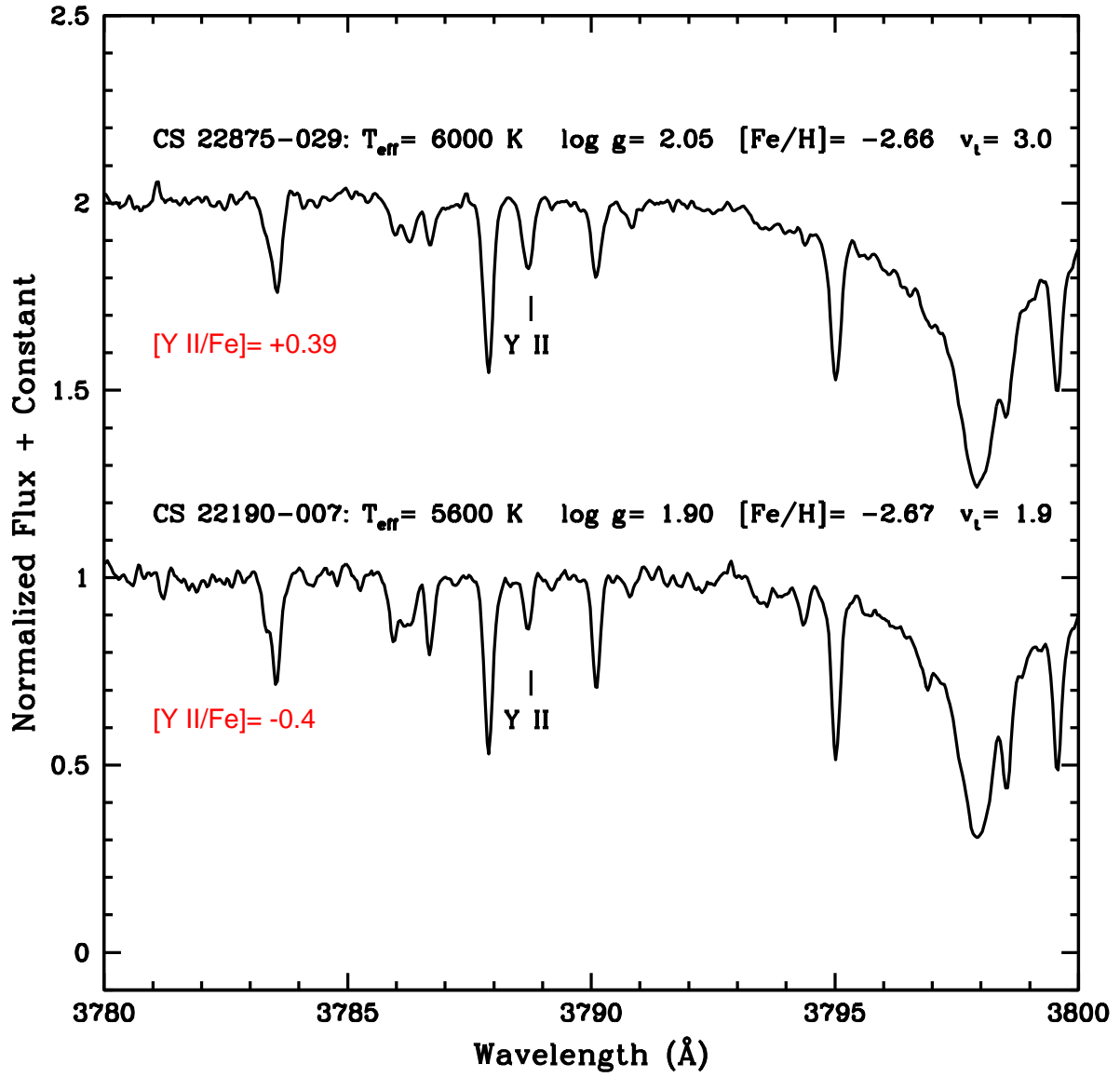


Fig. 18.— Comparison of Y II line strength of stars with similar $[\text{Fe}/\text{H}]$. The low and high Y II abundance ratios of these two stars contribute to the scatter of $[\text{Y II}/\text{Fe}]$ vs $[\text{Fe}/\text{H}]$.

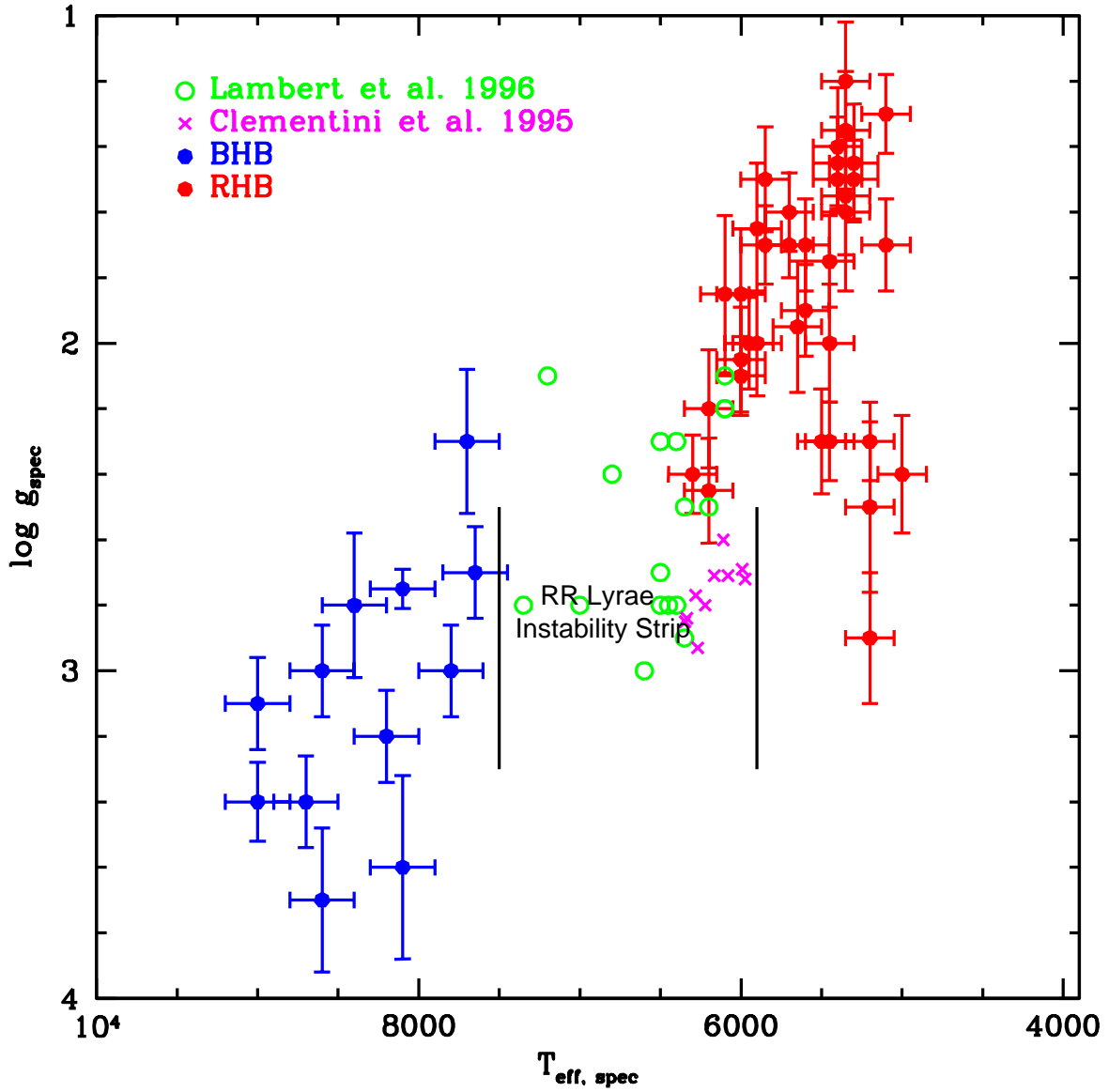


Fig. 19.— The spectroscopic T_{eff} and $\log g$ of our RHB and BHB stars (red and blue dots), and T_{eff} and $\log g$ of field RR Lyraes from Lambert et al. 1996 and Clementini et al. 1995 (green open circles & magenta crosses) on the $T_{\text{eff}}\text{--}\log g$ plane.

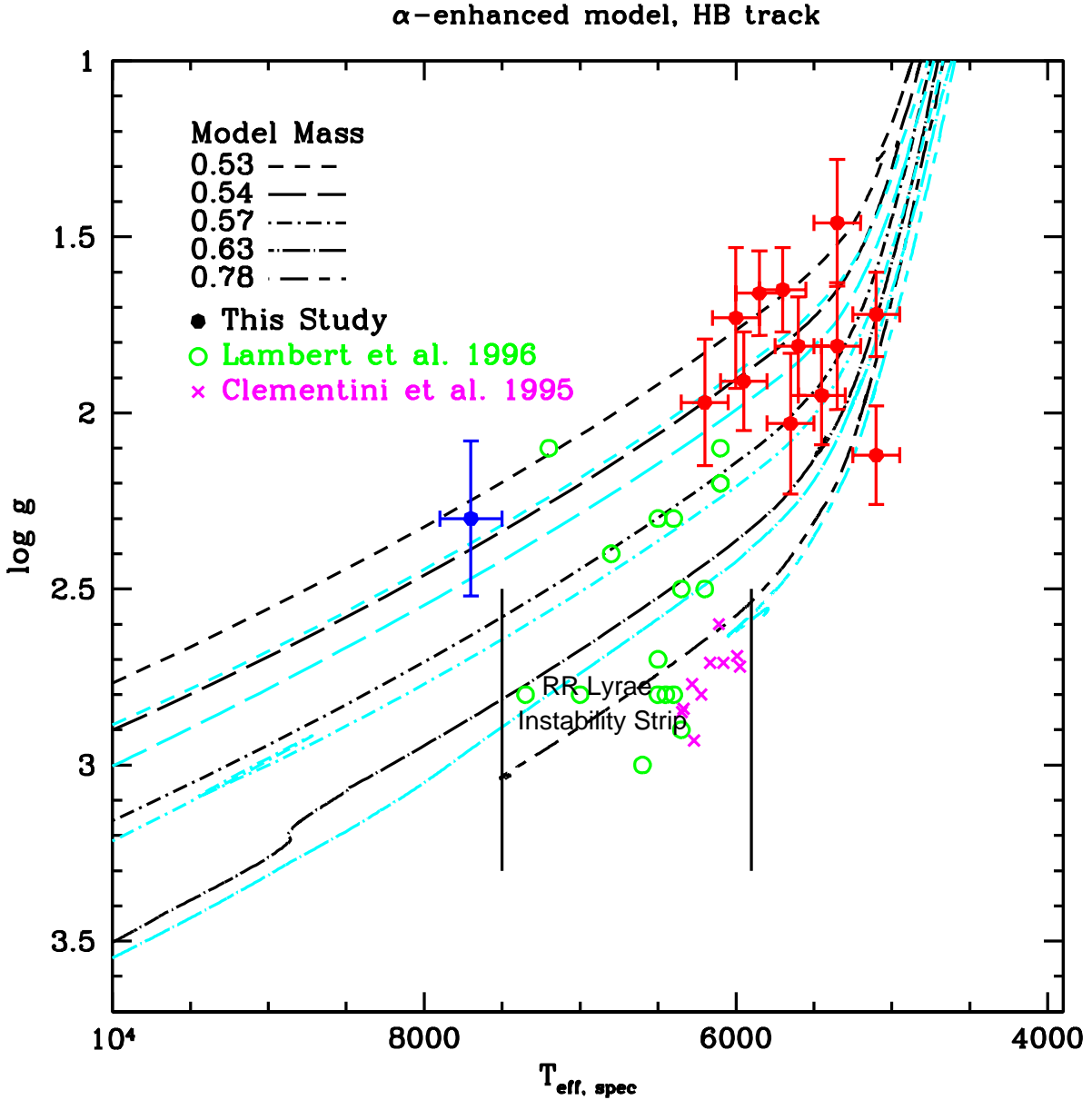


Fig. 20.— The spectroscopic T_{eff} and photometric/spectroscopic $\log g$ of a set of our RHB and BHB stars (red and blue dots) overlaid on α -enhanced HB tracks of $[M/H] = -1.79$, $Z = 0.0003$, $Y = 0.245$ (black) and $[M/H] = -2.27$, $Z = 0.0001$, $Y = 0.245$ (cyan). These HB tracks were used to derive the masses of this set of HB stars. The T_{eff} and $\log g$ of field RR Lyraes are from Lambert et al. 1996 and Clementini et al. 1995 (green open circles & magenta crosses).

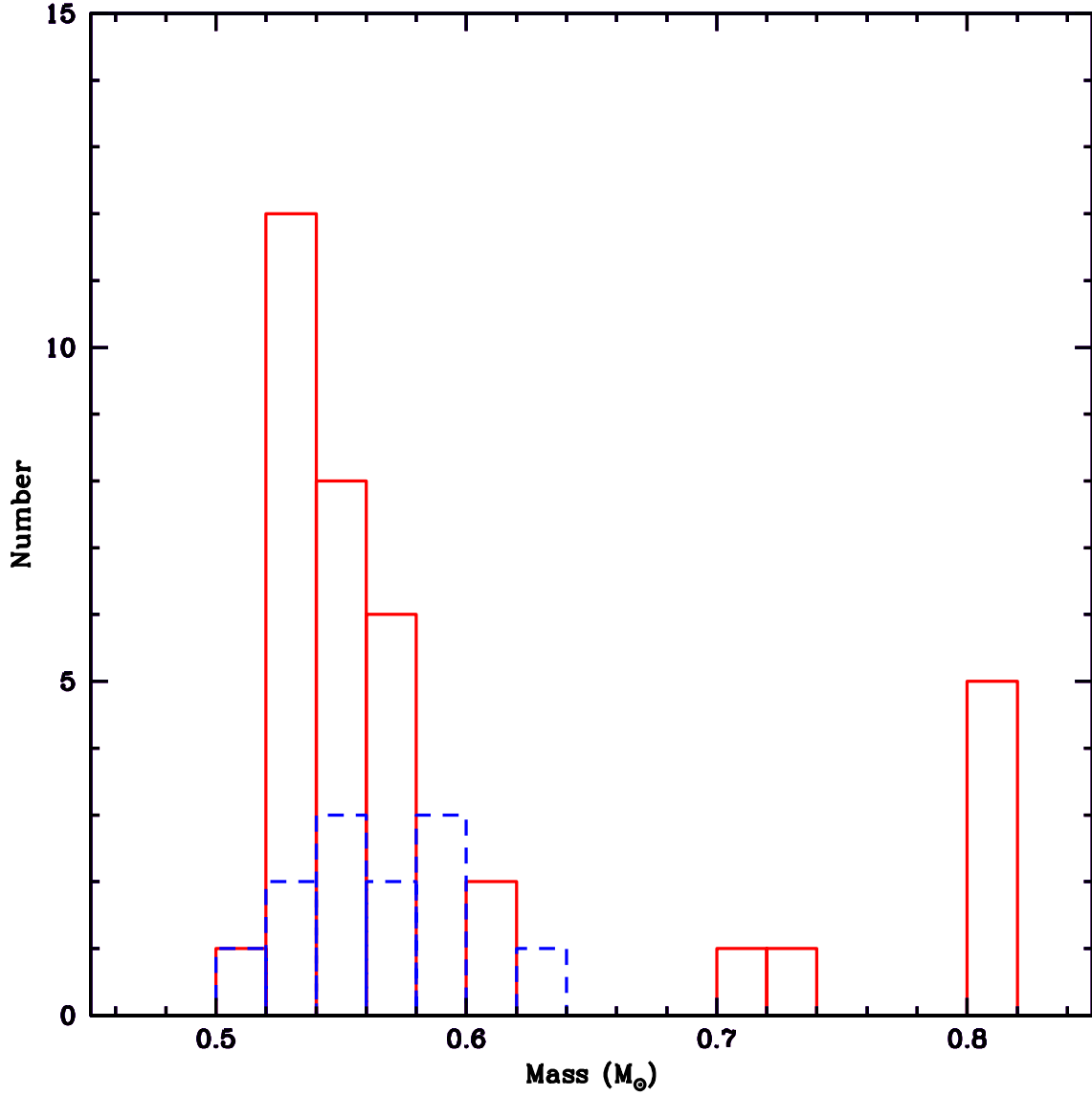


Fig. 21.— The red (solid) and blue (dashed) histograms represent the estimated RHB and BHB masses. The mean masses for RHB and BHB stars are $0.59 M_{\odot}$ and $0.56 M_{\odot}$. Excluding the upper mass limit RHB stars ($M > 0.7 M_{\odot}$), the mean masses are $0.56 M_{\odot}$ for both RHB and BHB stars. The median masses for RHB and BHB stars are $0.54 M_{\odot}$ and $0.56 M_{\odot}$, respectively.

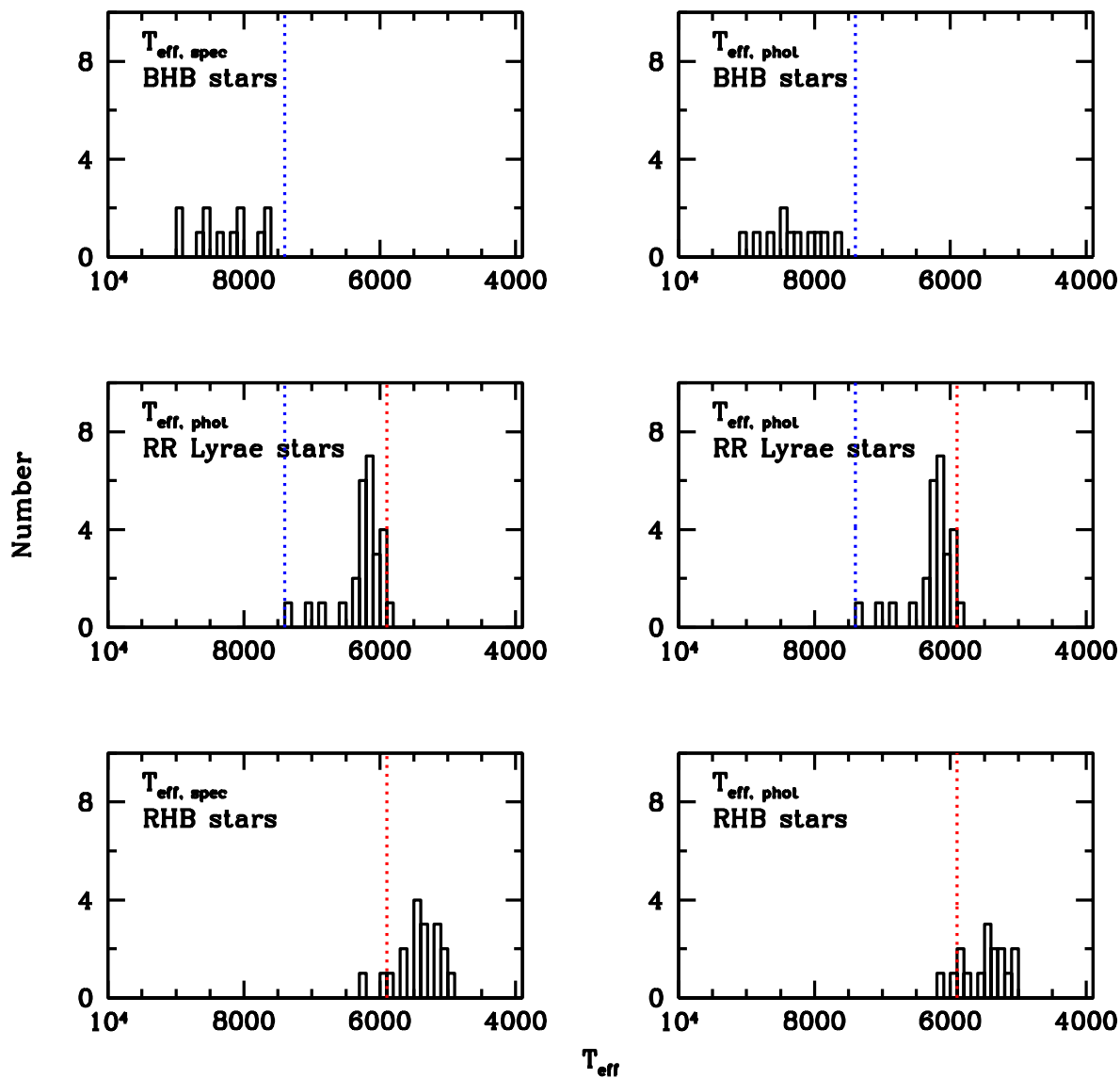


Fig. 22.— The top and bottom panels show the histograms of spectroscopic and photometric T_{eff} of BHB and RHB stars. The middle panels (same) are the photometric T_{eff} of field RR Lyr stars extracted from Lambert et al. (1996) and Clementini et al. (1995). The red and blue dotted lines represent the estimated fundamental red and blue edges of field RR Lyr IS for $[\text{Fe}/\text{H}] > -2.5$.

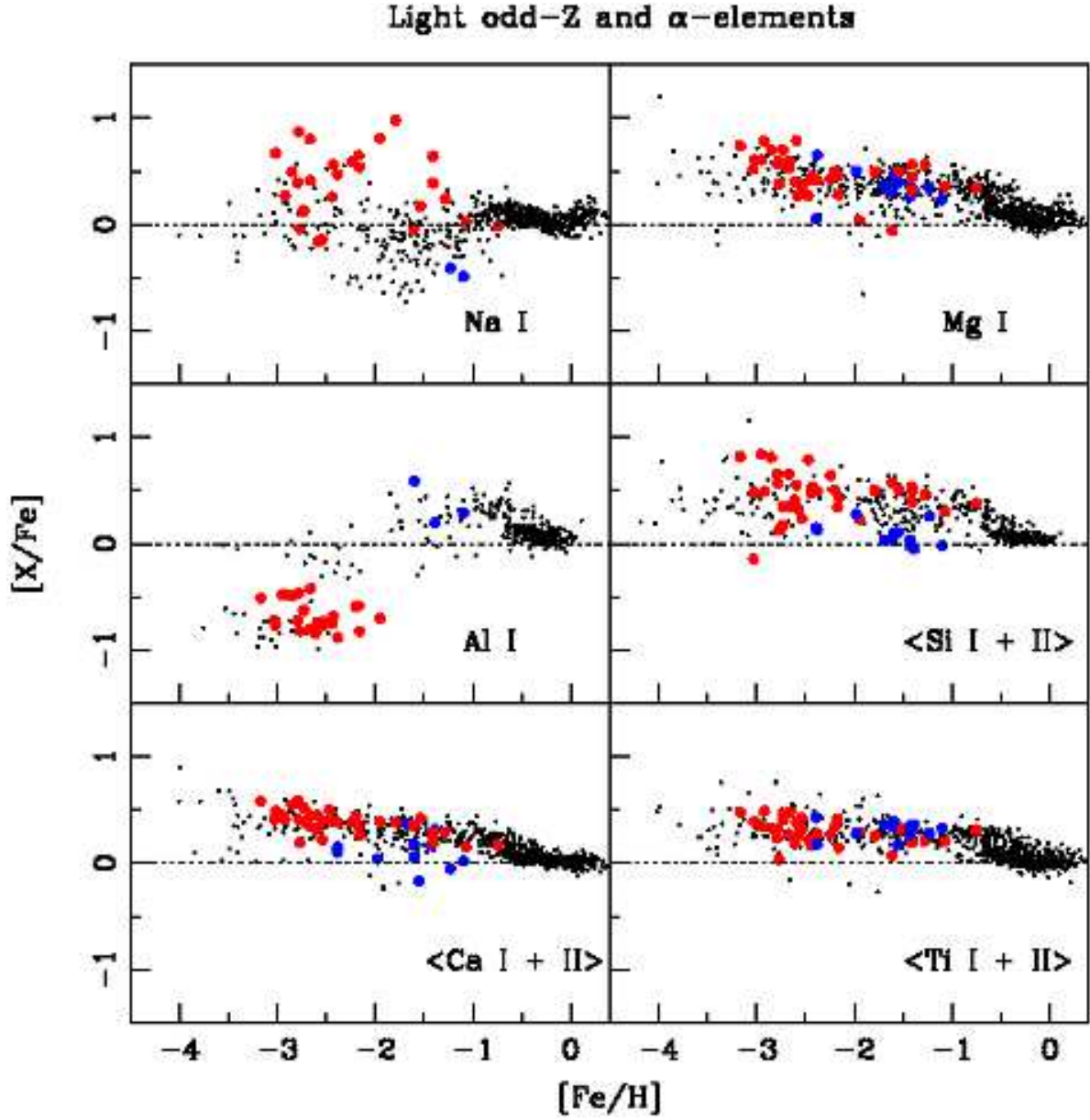


Fig. 23.— Abundance ratios of light odd-Z and α -elements in this study superimposed on the data assembled by Venn et al. (2004) and us. Mean of neutral and ionized species are used for comparisons. NLTE corrections applied to Na I, Al I, Si I & Si II for our HB stars. The red and blue dots correspond to RHB and BHB stars.

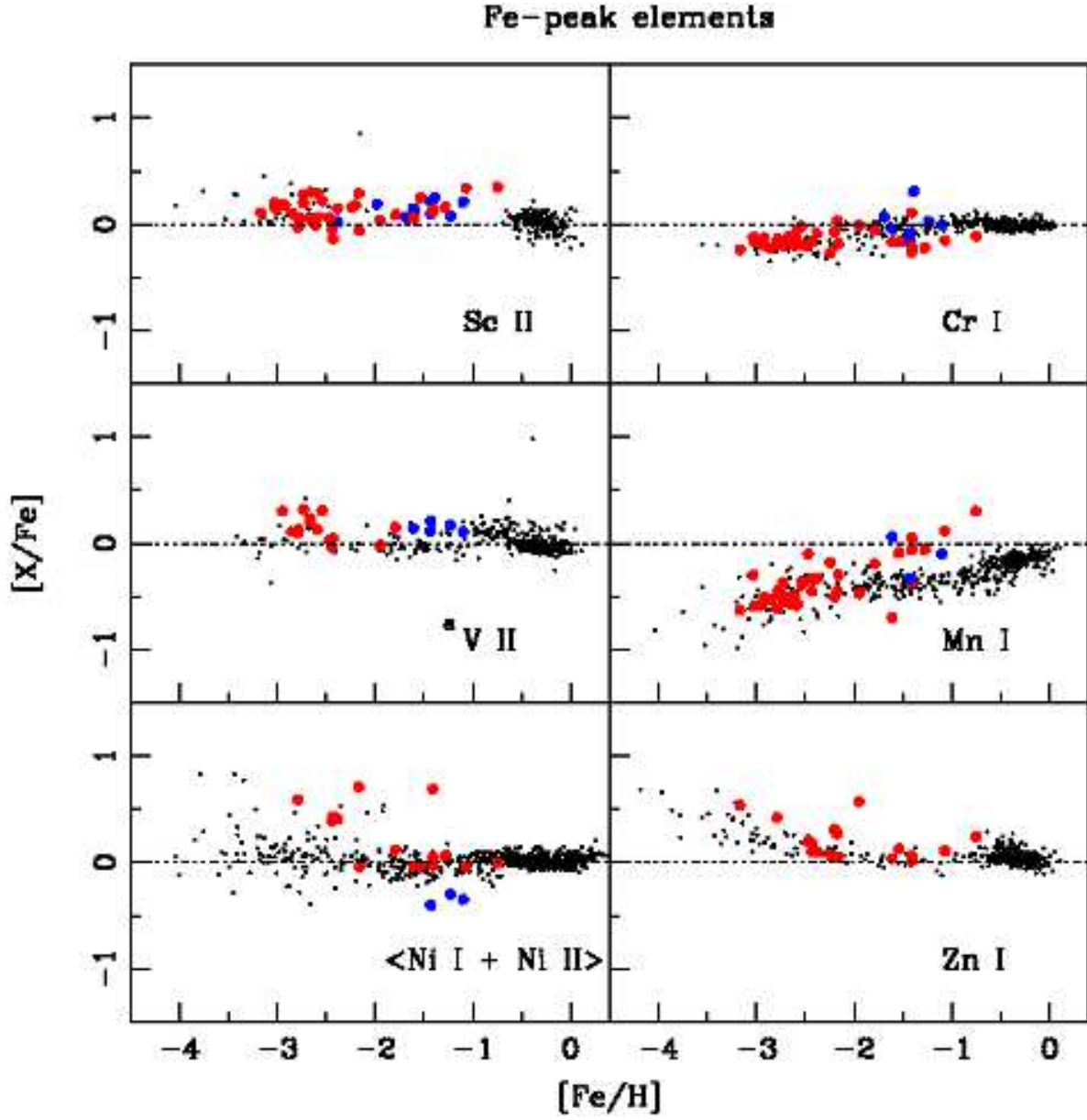


Fig. 24.— Same as Figure 23, except for Fe-peak elements. a: $[V I/Fe]$ for stars possess $[Fe/H] > 2.0$ is used for comparison. The red and blue dots correspond to RHB and BHB stars.

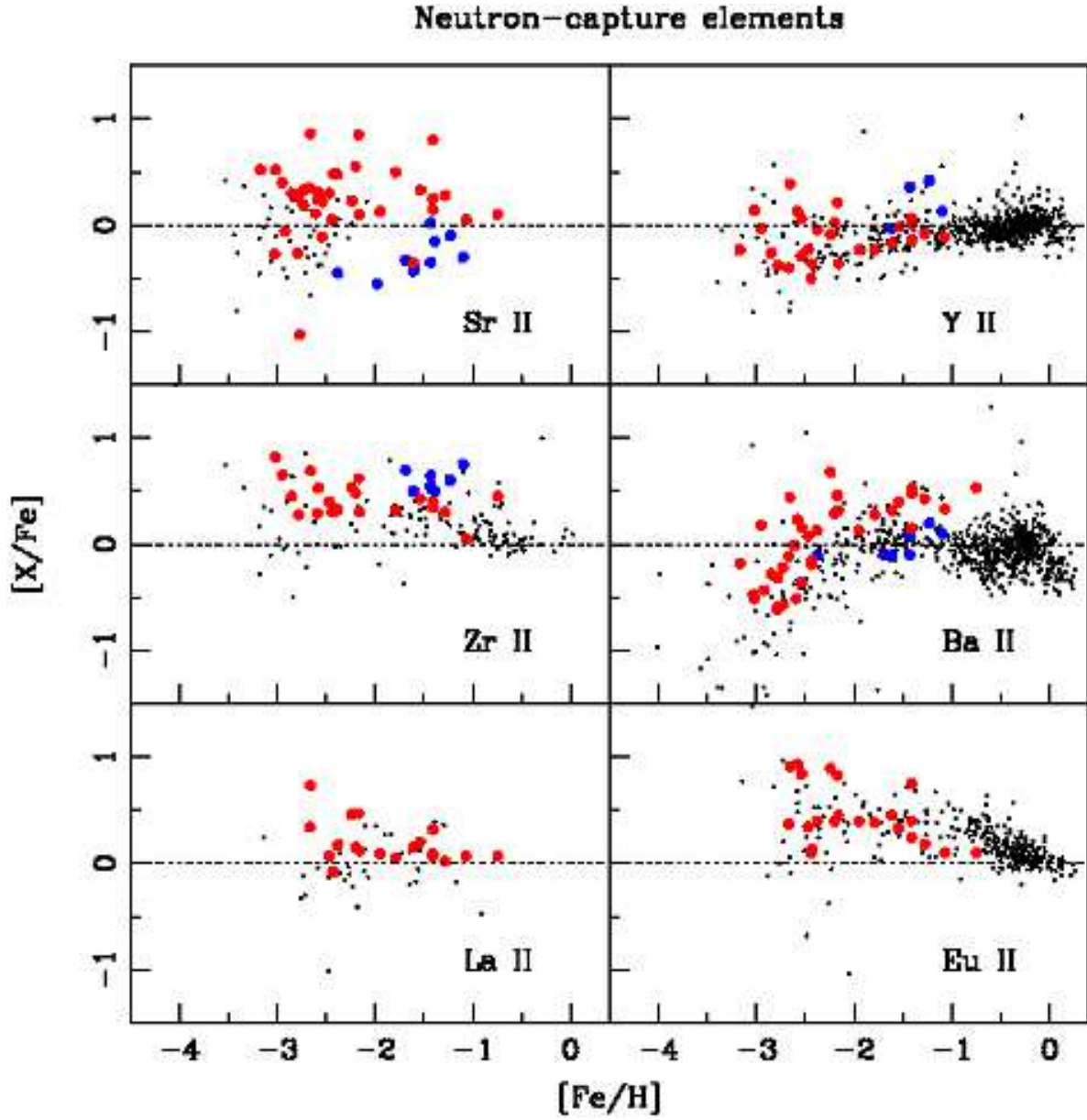


Fig. 25.— Same as Figure 23, except for n -capture elements. The red and blue dots correspond to RHB and BHB stars.

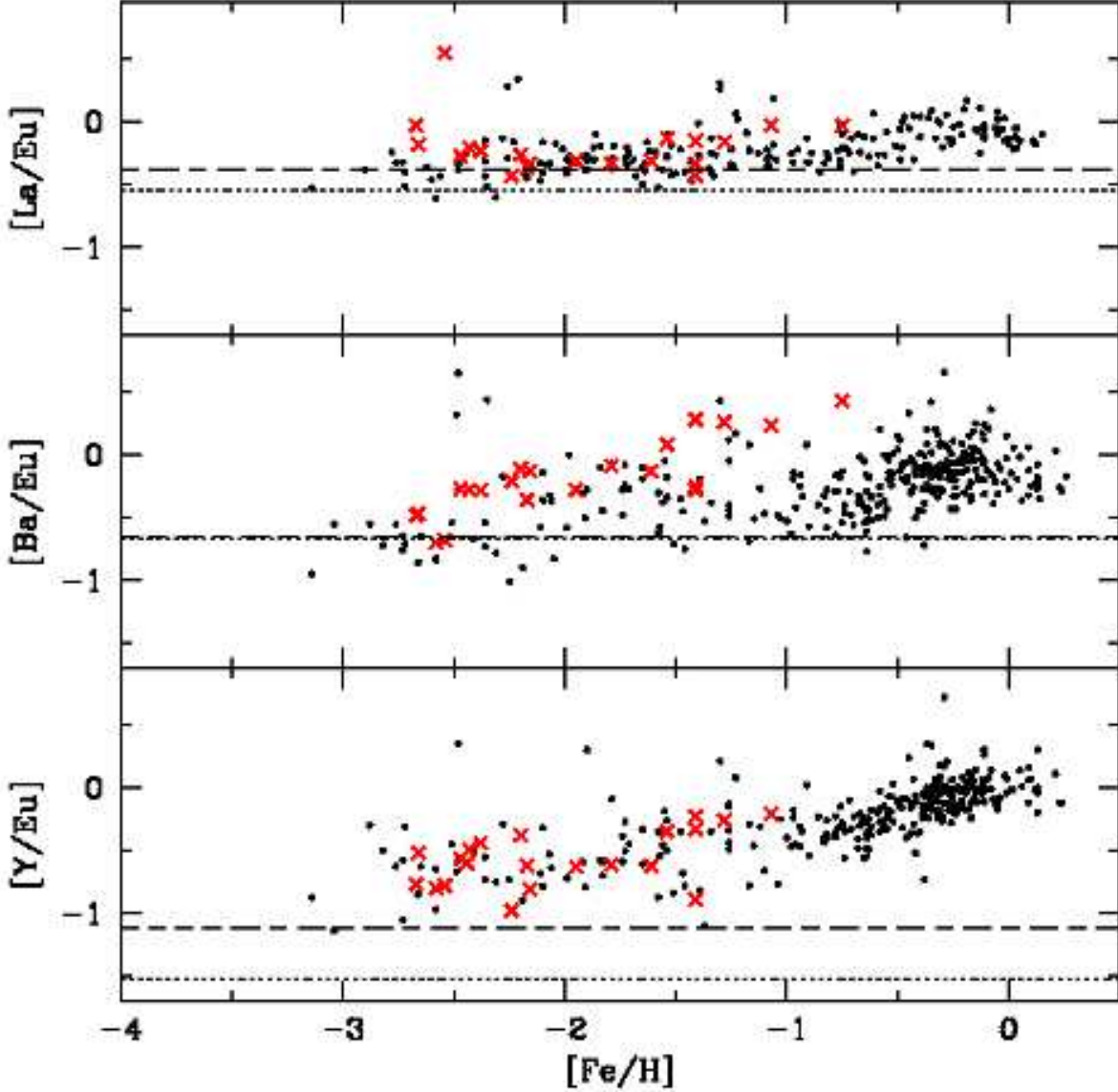


Fig. 27.— Comparison of light vs heavier n -capture elemental abundance ratios as a function of metallicity. These ratios are used to examine s and r -process enrichment. The dashed and dotted lines represent the estimated pure r -process from solar system abundances of Arlandini et al. (1999) and Sneden et al. (2008), respectively. The red crosses correspond to our RHB stars. The black dots represent La, Ba, Y, Eu from Venn et al. (2004), La, Eu from Simmerer et al. (2004) and Woolf et al. (1995).

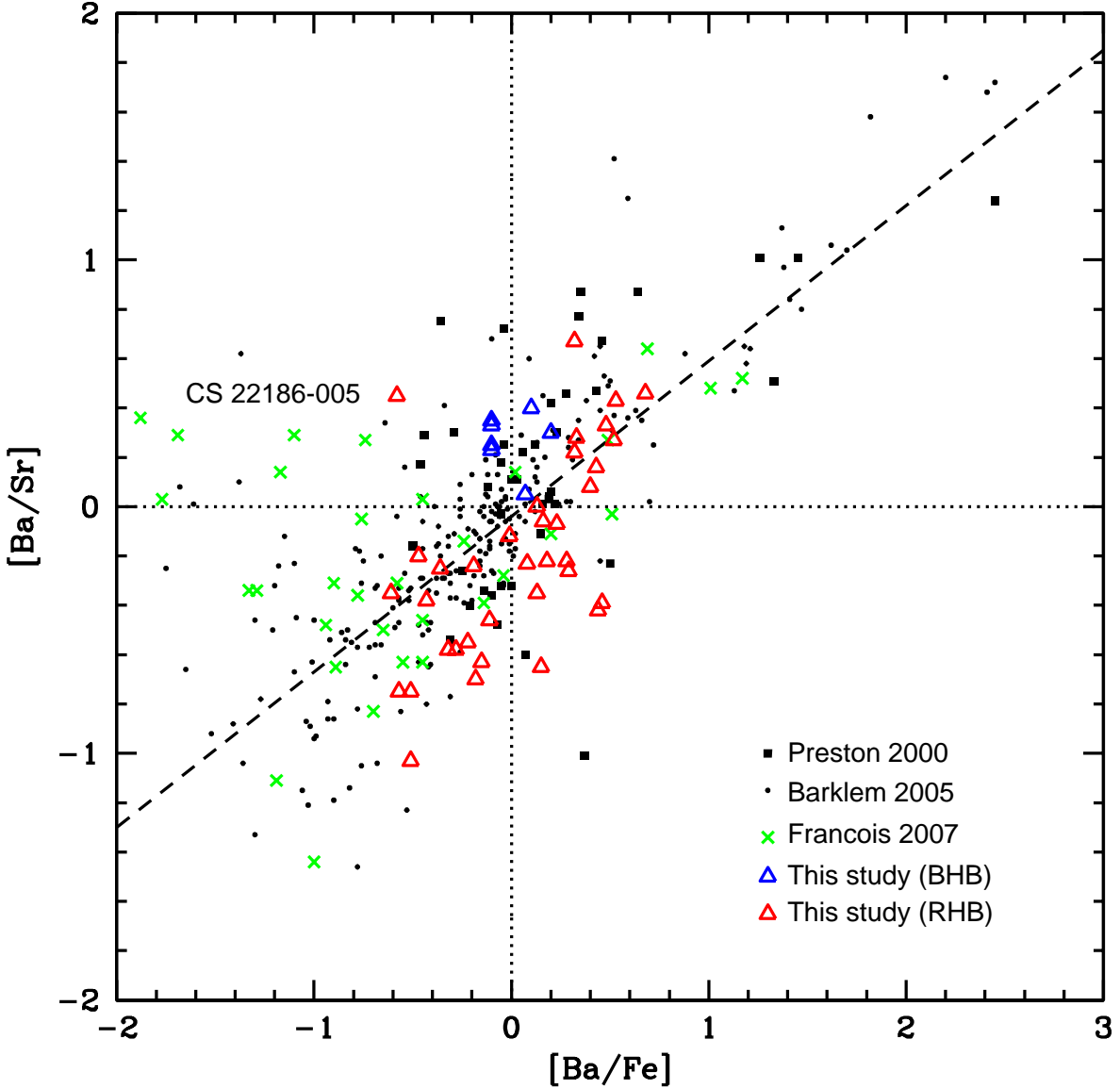


Fig. 28.— Abundance ratios of $[Ba/Sr]$ vs $[Ba/Fe]$. The long dashed line represent the linear correlation between $[Ba/Sr]$ and $[Ba/Fe]$ (see Sneden et al. 2008). Solid, black rectangulars and dots represent studies of Preston & Sneden (2000) and Barklem et al. (2005), respectively. Study by François et al. (2007) is represented in green crosses. Our RHB and BHB stars are represented by red and blue open triangles.

Table 1. Program stars.

Star	R.A.(J2000) (hr m s)	Decl.(J2000) ($^{\circ}$ $'$ $''$)	B^a (mag)	$V^{a,b}$ (mag)	J^c (mag)	H^c (mag)	K_s^c (mag)	$B - V$ (mag)	$V - K$ (mag)	$E(B - V)^d$ (mag)	$cE(B - V)$ (mag)
RHB											
HD 6229	01 03 36.5	+23 46 06.4	9.31	8.60	7.088	6.646	6.575	0.71	2.025	0.034	0.021
HD 6461	01 05 25.4	−12 54 12.1	8.4	7.65	6.149	5.676	5.587	0.75	2.063	0.025	0.013
HD 25532	04 04 11.0	+23 24 27.1	8.85	8.24	6.688	6.327	...	0.61	1.057	0.191	0.162
HD 105546	12 09 02.7	+59 01 05.1	9.4	8.61	7.152	6.756	6.674	0.79	0.980	0.022	0.010
HD 119516	13 43 26.7	+15 34 31.1	9.52	9.13	7.771	7.431	7.366	0.39	1.764	0.031	0.018
BD+18 $^{\circ}$ 2890	14 32 13.5	+17 25 24.3	10.49	9.77	8.241	7.837	7.744	0.72	2.026	0.020	0.008
BD+11 $^{\circ}$ 2998	16 30 16.8	+10 59 51.7	9.70	9.07	7.619	7.271	7.185	0.63	1.885	0.057	0.041
BD+09 $^{\circ}$ 3223	16 33 35.6	+09 06 16.3	9.81	9.25	7.760	7.335	7.277	0.56	1.007	0.076	0.058
BD+17 $^{\circ}$ 3248	17 28 14.5	+17 30 35.8	9.99	9.37	7.876	7.391	7.338	0.62	0.956	0.059	0.043
HD 184266	19 34 15.4	−16 19 00.2	8.16	7.57	6.252	5.913	5.830	0.59	1.740	0.142	0.118
HD 229274	20 24 36.1	+41 30 02.6	9.63	9.06	7.622	7.288	7.213	0.57	1.847
CS 22882−001	00 20 25.3	−31 39 04.0	15.22	14.82	13.677	13.362	13.317	0.40	1.503	0.018	0.006
CS 22190−007	03 52 21.7	−16 24 30.0	14.66	14.20	13.059	12.706	12.656	0.46	1.544	0.031	0.018
CS 22186−005	04 13 09.1	−35 50 38.7	13.33	12.96	11.902	11.625	11.581	0.37	1.379	0.012	0.001
CS 22191−029	04 47 42.2	−39 07 26.0	14.46	14.05	12.947	12.646	12.614	0.41	1.436	0.019	0.007
CS 22883−037	14 24 19.4	+11 29 25.0	15.28	14.73	13.733	13.425	13.378	0.55	1.352	0.028	0.015
CS 22878−121	16 47 50.1	+11 39 12.0	14.53	13.99	12.620	12.288	12.169	0.54	1.821	0.043	0.029
CS 22891−184	19 26 12.5	−60 34 09.0	14.33	13.83	12.574	12.274	12.187	0.50	1.643	0.070	0.053
CS 22896−110	19 35 48.0	−53 26 17.0	14.09	13.56	12.180	11.791	11.780	0.53	1.780	0.060	0.044
CS 22940−077	20 41 33.5	−59 50 36.0	14.66	14.13	12.679	12.300	12.220	0.53	1.910	0.070	0.053
CS 22955−174	20 42 05.0	−23 49 12.7	14.88	14.38	13.179	12.843	12.770	0.50	1.610	0.049	0.034
CS 22940−070	20 42 39.2	−61 40 41.0	15.35	14.87	13.686	13.368	13.312	0.48	1.558	0.056	0.040
CS 22879−103	20 47 10.1	−37 26 52.6	14.79	14.30	13.095	12.747	12.661	0.49	1.639	0.044	0.030
CS 22879−097	20 48 46.6	−38 30 49.4	14.68	14.22	13.031	12.684	12.617	0.46	1.603	0.048	0.033
CS 22940−121	20 55 10.8	−58 00 54.0	14.71	14.16	12.738	12.339	12.267	0.55	1.893	0.053	0.038
CS 22898−043	21 10 36.8	−21 44 51.8	14.49	14.06	12.909	12.674	12.650	0.43	1.410	0.050	0.035
CS 22937−072	21 14 40.6	−37 24 51.8	14.55	14.02	12.646	12.301	12.221	0.53	1.799	0.040	0.026
CS 22948−006	21 33 17.7	−39 39 42.8	15.56	15.07	13.774	13.405	13.334	0.49	1.736	0.030	0.017
CS 22944−039	21 45 12.2	−14 41 22.0	14.85	14.30	12.976	12.616	12.500	0.55	1.800	0.049	0.034
CS 22951−077	21 57 53.4	−43 08 06.0	14.11	13.61	12.258	11.944	11.845	0.50	1.765	0.016	0.004
CS 22881−039	22 09 35.4	−40 25 51.2	15.52	15.12	13.915	13.746	13.646	0.40	1.474	0.014	0.003
CS 22886−043	22 22 33.9	−10 14 11.0	15.18	14.72	13.564	13.247	13.178	0.46	1.542	0.047	0.032
CS 22875−029	22 29 25.1	−38 57 47.5	14.08	13.68	12.584	12.298	12.267	0.40	1.413	0.013	0.002
CS 22888−047	23 20 19.9	−33 45 46.9	15.01	14.61	13.460	13.194	13.127	0.40	1.483	0.019	0.007
CS 22941−027	23 34 58.1	−36 52 05.7	14.40	14.05	13.060	12.721	12.747	0.35	1.303	0.016	0.004
CS 22945−056	23 53 19.8	−65 29 41.0	14.485	14.09	12.984	12.692	12.616	0.40	1.474	0.020	0.008
BHB											
HD 2857	00 31 53.8	−05 15 42.9	10.12	9.95	9.481	9.354	9.323	0.17	0.627	0.041	0.027
HD 8376	01 23 28.3	+31 47 12.3	9.72	9.59	9.248	9.163	9.130	0.13	0.460	0.051	0.036
HD 252940	06 11 37.3	+26 27 30.1	9.4	9.096	8.440	8.371	8.302	0.30	0.794
HD 60778	07 36 11.8	−00 08 15.6	9.19	9.12	8.746	8.662	8.666	0.07	0.454	0.104	0.084
HD 74721	08 45 59.3	+13 15 48.7	8.76	8.71	8.521	8.525	8.522	0.05	0.188	0.031	0.018
HD 86986	10 02 29.6	+14 33 25.2	8.11	8.01	7.610	7.499	7.499	0.10	0.511	0.031	0.018

Table 1—Continued

Star	R.A.(J2000) (hr m s)	Decl.(J2000) ($^{\circ}$ $'$ $''$)	B^a (mag)	$V^{a,b}$ (mag)	J^c (mag)	H^c (mag)	K_s^c (mag)	$B - V$ (mag)	$V - K$ (mag)	$E(B - V)^d$ (mag)	$cE(B - V)$ (mag)
HD 87047	10 03 12.7	+31 03 19.0	9.86	9.72	9.309	9.251	9.214	0.14	0.506	0.019	0.007
HD 93329	10 46 36.6	+11 11 02.9	8.86	8.76	8.475	8.399	8.416	0.10	0.344	0.029	0.016
HD 109995	12 38 47.6	+39 18 31.6	7.643	7.598	7.304	7.317	7.265	0.04	0.333	0.017	0.005
BD+25 $^{\circ}$ 2602	13 09 25.6	+24 19 25.1	10.18	10.14	9.877	9.844	9.800	0.04	0.340	0.017	0.005
HD 161817	17 46 40.6	+25 44 57.0	7.123	6.988	6.413	6.339	6.290	0.14	0.698	0.093	0.074
HD 167105	18 11 06.3	+50 47 32.4	8.97	8.93	8.743	8.748	8.735	0.04	0.195	0.049	0.034

^aSIMBAD. <http://simbad.u-strasbg.fr/simbad/>

^bBeers et al. (1992).

^c2MASS All-Sky Point Source Catalog(Skrutskie et al. 2006). <http://tdc-www.harvard.edu/catalogs/tmpsc.html>

^dNasa/IPAC extragalactic database.

Table 2. Observation Log.

Star	UT Date	No. Integration	t_{exp} (s)	S/N at 7000Å	S/N at 5000Å	S/N at 4000Å	Comments
BD+09° 3223	30 Jun 2007	3	1800	223	230	95	1
BD+11° 2998	01 Jul 2007	3	1800	230	128	88	1
BD+18° 2890	02 Jul 2007	3	1800	210	124	30	1
HD 180903	02 Jul 2007	3	1800	210	88	40	1,4
HD 229274	02 Jul 2007	3	1800	320	147	100	1
HD 119516	03 Jul 2007	3	1800	320	132	60	1
HD 184266	04 Jul 2007	2	900	360	140	75	1
BD+17° 3248	04 Jul 2007	2	1800	280	108	66	1
HD 252940	20 Feb 2008	3	1800	188	135	63	1
HD 117880	21 Feb 2008	3	1800	196	96	86	1,3
HD 60778	21 Feb 2008	4	1×1200, 1×1800	200	125	64	1
HD 87112	21, 22 Feb 2008	5	1800	250	112	56	1,3
HD 25532	22 Feb 2008	3	1800	247	235	122	1
HD 82590	23 Apr 2008	4	900	226	103	66	1,3
BD+25° 2602	24 Feb 2008	4	1800	176	70	45	1
BD+42° 2309	24 Feb 2008	4	1800	134	100	64	1,3
HD 86986	11 Apr 2009	4	2×1200, 2×1800	226	164	79	2
HD 109995	11 Apr 2009	4	3×1200, 1×870	370	124	72	2
HD 74721	11 Apr 2009	4	1×1200, 3×1800	200	156	86	2
HD 161817	11 Apr 2009	4	1200	430	270	73	2
HD 167105	11, 13 Apr 2009	4	3×1800, 1×2400	260	162	67	2
HD 93329	13 Apr 2009	5	1×1000, 3×2400	290	109	163	2
HD 87047	14 Apr 2009	3	2400	150	96	67	2
HD 105546	14 Apr 2009	4	3×1800, 1×1400	250	190	70	2
HD 8376	06 Oct 2009	3	1800	200	105	67	2
HD 2857	08, 09 Oct 2009	4	3×1800, 1×1000	170	100	34	2
HD 6229	09 Oct 2009	3	1200	200	166	74	2

¹The echelle grating was blazed to obtain more red portion of the spectrum. See text for explanation.

²The echelle grating was blazed to obtain optima red and blue portion of the spectrum.

³Initial analysis was performed. Stellar parameters cannot be obtained due to the lack of measurable Fe I or Fe II lines. Excluded from this study.

⁴RR Lyr, excluded from this study.

Table 3. Equivalent width measurements of program stars.

Wavelength (Å)	Species	E.P. (eV)	log gf	Ref.	EW (mÅ)
HD 6229					
5682.63	Na I	2.102	-0.71	1	49
5688.19	Na I	2.104	-0.46	1	...
5339.93	Fe I	3.266	-0.72	1	101
5341.02	Fe I	1.608	-1.95	1	141
.
.
.

Note. — Table 3 is published in its entirety in the electronic edition of the *Astronomical Journal*. A portion is shown here for guidance regarding its form and content.

Table 4. Input stellar atmosphere parameters and derived Fe metallicities.

Star	T_{eff} (K)	$\log g$ (dex)	$[M/H]^a$	v_t (km s ⁻¹)	$[\text{Fe I}/H]$	σ	N	$[\text{Fe II}/H]$	σ	N
RHB										
HD 6229	5200	2.50	-1.07	1.60	-1.07	0.13	98	-1.06	0.13	20
HD 6461	5200	2.90	-0.75	1.40	-0.75	0.12	94	-0.74	0.10	13
HD 25532	5450	2.00	-1.41	2.10	-1.41	0.06	44	-1.42	0.09	8
HD 105546	5200	2.30	-1.54	1.80	-1.54	0.08	65	-1.54	0.06	20
HD 119516	5400	1.50	-2.16	2.20	-2.16	0.06	49	-2.16	0.05	15
BD+18° 2890	5000	2.40	-1.61	1.40	-1.61	0.07	51	-1.61	0.09	8
BD+11° 2998	5450	2.30	-1.28	1.90	-1.28	0.08	59	-1.29	0.06	10
BD+09° 3223	5100	1.30	-2.47	1.90	-2.47	0.05	48	-2.46	0.06	11
BD+17° 3248	5100	1.70	-2.24	1.80	-2.24	0.06	38	-2.23	0.07	13
HD 184266	5700	1.70	-1.79	2.70	-1.79	0.06	32	-1.78	0.05	8
HD 229274	5500	2.30	-1.41	2.00	-1.41	0.08	44	-1.42	0.08	12
CS 22882-001	5950	2.00	-2.50	3.05	-2.54	0.10	55	-2.54	0.07	14
CS 22190-007	5600	1.90	-2.50	1.90	-2.67	0.09	93	-2.67	0.07	15
CS 22186-005	6200	2.45	-2.50	3.20	-2.77	0.07	13	-2.78	0.08	6
CS 22191-029	6000	2.10	-2.50	2.90	-2.73	0.09	53	-2.72	0.06	10
CS 22883-037	5900	1.65	-1.95	2.80	-1.95	0.11	73	-1.94	0.10	17
CS 22878-121	5450	1.75	-2.38	1.90	-2.38	0.12	110	-2.37	0.07	24
CS 22891-184	5600	1.70	-2.50	2.05	-2.61	0.07	86	-2.61	0.07	16
CS 22896-110	5400	1.45	-2.50	2.05	-2.78	0.09	78	-2.78	0.07	16
CS 22940-077	5300	1.45	-2.50	1.90	-3.02	0.08	70	-3.02	0.09	15
CS 22955-174	5350	1.35	-2.50	2.20	-3.17	0.09	45	-3.17	0.08	7
CS 22940-070	6300	2.40	-1.41	3.20	-1.41	0.07	24	-1.42	0.06	7
CS 22879-103	5700	1.60	-2.20	3.00	-2.20	0.08	94	-2.20	0.06	16
CS 22879-097	5650	1.95	-2.50	2.20	-2.59	0.10	76	-2.58	0.10	14
CS 22940-121	5350	1.60	-2.50	2.10	-2.95	0.09	73	-2.94	0.12	14
CS 22898-043	5900	2.00	-2.50	3.40	-3.03	0.05	12	-3.03	0.08	2
CS 22937-072	5300	1.50	-2.50	1.80	-2.85	0.09	86	-2.85	0.06	16
CS 22948-006	5400	1.40	-2.50	2.15	-2.79	0.09	83	-2.79	0.09	13
CS 22944-039	5350	1.20	-2.43	2.20	-2.43	0.10	99	-2.44	0.09	16
CS 22951-077	5350	1.55	-2.44	2.00	-2.44	0.09	97	-2.43	0.09	13
CS 22881-039	6100	1.85	-2.50	2.70	-2.73	0.08	37	-2.72	0.12	7
CS 22886-043	6000	1.85	-2.17	3.05	-2.17	0.11	52	-2.17	0.10	21
CS 22875-029	6000	2.05	-2.50	3.00	-2.66	0.09	62	-2.66	0.08	12
CS 22888-047	5850	1.70	-2.50	3.20	-2.58	0.08	58	-2.57	0.06	11
CS 22941-027	6200	2.20	-2.50	3.30	-2.54	0.07	36	-2.53	0.09	10
CS 22945-056	5850	1.50	-2.50	3.00	-2.92	0.07	33	-2.92	0.08	7
BHB										
HD 2857	8100	3.60	-1.39	3.70	-1.39	0.13	12	-1.38	0.14	14
HD 8376	8600	3.70	-2.39	1.00	-2.39	0.11	9	-2.38	0.11	6
HD 252940	7650	2.70	-1.69	3.10	-1.69	0.07	11	-1.68	0.07	10
HD 60778	8100	2.75	-1.43	2.20	-1.43	0.06	20	-1.43	0.03	11
HD 74721	9000	3.40	-1.23	1.40	-1.23	0.05	13	-1.21	0.06	13
HD 86986	8200	3.20	-1.61	2.30	-1.61	0.09	34	-1.59	0.07	23

Table 4—Continued

Star	T_{eff} (K)	$\log g$ (dex)	$[M/H]^a$	v_t (km s ⁻¹)	$[\text{Fe I}/H]$	σ	N	$[\text{Fe II}/H]$	σ	N
HD 87047	7700	2.30	-2.38	1.30	-2.38	0.03	4	-2.37	0.11	7
HD 93329	8700	3.40	-1.10	2.80	-1.10	0.07	35	-1.11	0.07	27
HD 109995	8600	3.00	-1.60	2.00	-1.60	0.05	7	-1.59	0.07	18
BD+25° 2602	8400	2.80	-1.98	2.30	-1.98	0.07	5	-1.98	0.11	8
HD 161817	7800	3.00	-1.43	3.20	-1.43	0.09	57	-1.45	0.07	28
HD 167105	9000	3.10	-1.55	2.00	-1.55	0.03	3	-1.54	0.07	18

^aInput model metallicity.

Table 5. Abundance ratios from Mg, Si and Ca

Star	[Na I/Fe]	σ	N	[Mg I/Fe]	σ	N	[Si I/Fe]	σ	N	[Si II/Fe]	σ	N	[Ca I/Fe]	σ	N	[Ca II/Fe]	σ	N
RHB																		
HD 6229	0.03	0.06	5	0.36	0.04	3	0.28	0.06	5	0.32	0.03	2	0.15	0.11	12
HD 6461	-0.02	0.10	3	0.35	0.15	2	0.29	0.02	6	0.47	0.16	2	0.17	0.09	13
HD 25532	0.64	...	1	0.56	...	1	0.53	0.07	5	0.54	0.18	2	0.29	0.05	4
HD 105546	0.17	...	1	0.50	0.08	3	0.40	0.10	6	0.61	0.20	3	0.42	0.09	12
HD 119516	0.54	...	1	0.28	...	1	0.40	...	1	0.48	0.17	2	0.26	0.07	7
BD+18° 2890	-0.04	0.02	4	-0.06	...	1	0.41	0.08	6	0.74	...	1	0.35	0.07	12
BD+11° 2998	0.24	...	1	0.56	0.12	2	0.41	0.07	5	0.52	0.07	3	0.29	0.09	7
BD+09° 3223	0.27	...	1	0.73	...	1	0.86	0.16	2	0.50	0.06	11
BD+17° 3248	0.59	...	1	0.43	0.26	2	0.45	...	1	0.84	...	1	0.38	0.05	7
HD 184266	0.98	...	1	0.50	0.03	2	0.56	0.02	2	0.44	...	1	0.38	0.09	7
HD 229274	0.39	0.02	2	0.32	0.05	3	0.40	0.08	7	0.38	0.17	2	0.24	0.07	7
CS 22882-001	0.37	0.01	2	0.00	...	1	0.48	0.06	2	0.40	0.09	6
CS 22190-007	0.80	0.10	2	0.53	0.13	3	0.65	...	1	0.66	...	1	0.35	0.08	10
CS 22186-005	-0.04	...	1	0.38	0.06	2	-0.11 ^a	...	1	0.36 ^a	...	1	0.19	...	1
CS 22191-029	0.13	0.02	2	0.57	0.15	4	0.15 ^a	...	1	0.55	...	1	0.39	0.10	9
CS 22883-037	0.81	...	1	0.04	...	1	-0.14	...	1	0.60	0.20	2	0.40	0.08	8
CS 22878-121	0.47	0.26	2	0.41	0.08	5	0.69	...	1	0.30	0.14	2	0.38	0.08	13
CS 22891-184	0.40	0.13	5	0.37	...	1	0.45	0.08	2	0.32	0.05	9
CS 22896-110	0.87	0.02	2	0.59	0.10	3	0.61	...	1	0.53	0.12	3	0.41	0.06	8
CS 22940-077	0.67	0.00	2	0.61	0.07	4	0.33	...	1	0.62	...	1	0.49	0.08	9
CS 22955-174	0.74	0.04	4	0.30	...	1	1.34	...	1	0.58	0.09	6
CS 22940-070	0.44	...	1	0.66	0.11	4	0.33	0.05	2	0.19	0.06	6
CS 22879-103	0.50	0.09	3	0.38	...	1	0.63	0.05	3	0.44	0.06	12
CS 22879-097	0.79	0.03	2	0.22	...	1	0.88	0.20	2	0.45	0.10	9
CS 22940-121	0.61	0.04	4	0.85	...	1	0.83	...	1	0.45	0.07	4
CS 22898-043	0.52	0.02	3	-0.14	...	1	0.41	0.03	3
CS 22937-072	0.49	0.08	2	0.70	0.10	3	0.50	...	1	1.12	0.02	2	0.55	0.07	8
CS 22948-006	0.39	0.13	2	0.57	0.06	2	0.41	...	1	0.90	0.16	2	0.59	0.09	12
CS 22944-039	0.56	0.15	2	0.41	0.02	2	0.55	...	1	0.52	0.15	2	0.40	0.07	10
CS 22951-077	0.26	0.04	2	0.45	0.09	4	0.51	...	1	0.44	0.01	2	0.39	0.07	15
CS 22881-039	0.12	0.05	2	0.70	0.01	2	0.08 ^a	...	1	0.27 ^a	...	1	0.52	0.09	4
CS 22886-043	0.65	0.18	2	0.45	0.08	3	0.40 ^a	...	1	0.29	...	1	0.35	0.09	6
CS 22875-029	0.41	...	1	0.59	...	1	0.17 ^a	...	1	0.53 ^a	0.10	3	0.45	0.04	6
CS 22888-047	-0.16	...	1	0.27	0.01	2	0.06	...	1	0.61	...	1	0.34	0.09	7
CS 22941-027	-0.14	0.10	2	0.32	0.10	2	0.16 ^a	...	1	0.33 ^a	...	1	0.22	0.11	4
CS 22945-056	0.27	...	1	0.78	0.18	2	0.12	...	1	0.86	...	1	0.41	0.11	3
BHB																		
HD 2857	0.31	0.14	2	-0.22 ^a	...	1	0.13 ^a	0.08	2	0.33	...	1	0.30	...	1
HD 8376	0.05	0.05	2	-0.04 ^a	...	1	0.34 ^a	...	1	-0.19	...	1	0.40	...	1
HD 252940	0.36	0.01	2	-0.08 ^a	...	1	0.16 ^a	...	1	0.40	0.07	4	0.35	...	1
HD 60778	0.38	0.02	2	-0.11 ^a	...	1	0.19 ^a	0.22	2	0.21	0.08	5	0.12	...	1
HD 74721	-0.41 ^a	...	1	0.35	0.02	2	0.07 ^a	...	1	0.45 ^a	0.21	2	-0.11	...	1	0.00	...	1
HD 86986	0.31	0.02	2	-0.10 ^a	...	1	0.18 ^a	0.18	3	0.14	0.07	2	0.23	...	1
HD 87047	0.65	...	1	0.04 ^a	...	1	0.22 ^a	...	1	0.15	...	1	0.15	...	1
HD 93329	-0.49 ^a	...	1	0.24	...	1	-0.05 ^a	...	1	0.02 ^a	0.22	3	-0.12	...	1	0.16	...	1
HD 109995	0.47	...	1	0.03 ^a	...	1	0.17 ^a	0.18	3	0.04	...	1	0.08	...	1

Table 5—Continued

Star	[Na I/Fe]	σ	N	[Mg I/Fe]	σ	N	[Si I/Fe]	σ	N	[Si II/Fe]	σ	N	[Ca I/Fe]	σ	N	[Ca II/Fe]	σ	N
BD+25 ^o 2602	0.50	0.05	2	0.15 ^a	...	1	0.41 ^a	0.17	2	-0.03	...	1	0.11	...	1
HD 161817	0.26	0.00	2	-0.09 ^a	...	1	0.06 ^a	0.15	3	0.24	0.05	8	0.32	...	1
HD 167105	0.39	0.06	2	0.05 ^a	...	1	0.16 ^a	0.20	3	-0.21	...	1	-0.12	...	1

^aNLTE correction.

Table 6. Abundance ratios of Al, Ti, Sc and Cr

Star	[Al I/Fe]	σ	N	[Ti I/Fe]	σ	N	[Ti II/Fe]	σ	N	[Sc II/Fe]	σ	N	[Cr I/Fe]	σ	N	[Cr II/Fe]	σ	N
RHB																		
HD 6229	0.07	0.08	13	0.34	0.14	10	0.34	0.12	4	-0.15	0.08	5	0.03	0.14	5
HD 6461	0.19	0.10	13	0.43	0.10	9	0.35	0.11	4	-0.11	0.05	2	0.10	0.20	5
HD 25532	0.18	0.07	8	0.22	0.09	7	0.12	0.06	2	-0.21	0.12	4	-0.08	0.17	5
HD 105546	0.25	0.02	9	0.40	0.10	8	0.25	0.08	3	-0.17	0.11	7	0.25	0.19	6
HD 119516	-0.82	...	1	0.23	0.06	5	0.06	0.13	5	-0.06	...	1	-0.18	0.06	5	0.01	0.10	5
BD+18° 2890	0.15	0.09	6	0.00	0.08	3	0.06	0.09	2	-0.17	0.01	2	0.26	...	1
BD+11° 2998	0.19	0.04	10	0.22	0.12	6	0.16	0.05	3	-0.22	0.08	4	-0.05	0.12	3
BD+09° 3223	0.28	0.08	8	0.16	0.09	9	0.06	0.02	3	-0.21	0.07	4	0.12	0.18	2
BD+17° 3248	0.28	0.06	6	0.26	0.09	8	0.16	0.07	2	-0.27	0.08	5	0.25	0.09	4
HD 184266	0.30	0.07	6	0.21	0.10	5	0.09	0.02	3	-0.06	0.06	3	0.14	0.17	5
HD 229274	0.16	0.05	9	0.22	0.12	6	0.13	0.02	3	-0.26	0.03	3	0.17	0.18	4
CS 22882-001	-0.77	...	1	0.55	...	1	0.30	0.09	22	0.22	0.02	2	-0.19	...	1	0.39	...	1
CS 22190-007	-0.80	0.17	2	0.37	0.10	4	0.17	0.08	23	0.06	0.13	4	-0.11	0.16	6	0.25	0.04	2
CS 22186-005	-0.82	...	1	0.03	0.04	6	-0.01	...	1	-0.15	0.11	4	0.76	...	1
CS 22191-029	-0.62	0.08	2	0.51	0.03	3	0.30	0.09	14	0.28	0.05	3	-0.16	0.08	3	0.49	...	1
CS 22883-037	-0.70	...	1	0.36	...	1	0.23	0.11	10	0.04	0.04	3	-0.01	0.16	5	0.20	0.08	3
CS 22878-121	-0.88	...	1	0.34	0.11	6	0.21	0.10	27	0.15	0.09	6	-0.09	0.12	9	0.20	0.12	4
CS 22891-184	-0.84	0.05	2	0.29	0.04	4	0.08	0.06	21	-0.01	0.04	3	-0.20	0.06	5	0.25	0.06	2
CS 22896-110	-0.46	0.21	2	0.45	0.08	5	0.19	0.11	17	0.06	0.01	3	-0.14	0.14	6	0.48	0.11	2
CS 22940-077	-0.76	...	1	0.50	0.12	6	0.28	0.10	17	0.15	0.11	5	-0.16	0.13	5	0.30	...	1
CS 22955-174	-0.51	...	1	0.69	0.02	2	0.27	0.06	14	0.11	0.05	2	-0.24	0.10	3	0.61	0.05	2
CS 22940-070	0.38	0.09	4	0.26	0.06	9	0.14	0.04	2	0.11	...	1	-0.01	0.16	2
CS 22879-103	-0.59	0.14	2	0.41	0.09	6	0.28	0.06	15	0.18	0.00	2	-0.07	0.09	6	-0.05	0.07	3
CS 22879-097	-0.74	...	1	0.52	0.12	5	0.25	0.08	16	0.29	0.13	4	-0.15	0.15	3	0.23	0.16	3
CS 22940-121	-0.48	...	1	0.43	0.13	3	0.27	0.10	15	0.19	0.12	3	-0.19	0.13	4	0.14	...	1
CS 22898-043	-0.72	...	1	0.47	...	1	0.31	0.08	10	0.20	...	1	-0.12	0.11	2	0.45	...	1
CS 22937-072	-0.49	...	1	0.43	0.09	9	0.23	0.09	20	0.11	0.05	4	-0.22	0.07	3	0.50	...	1
CS 22948-006	-0.72	...	1	0.31	0.04	5	0.16	0.08	16	-0.03	0.01	2	-0.17	0.23	4	0.15	0.13	4
CS 22944-039	-0.68	0.16	2	0.28	0.14	3	0.10	0.11	19	-0.14	0.08	3	-0.17	0.05	4	0.00	0.06	4
CS 22951-077	-0.75	0.17	2	0.22	0.03	3	0.11	0.07	17	-0.05	0.14	3	-0.17	0.10	7	0.04	0.15	3
CS 22881-039	-0.63	0.02	2	0.69	...	1	0.24	0.08	15	0.20	0.05	2	-0.20	0.11	4	0.25	...	1
CS 22886-043	-0.58	0.14	2	0.45	0.05	3	0.38	0.13	6	0.29	0.18	2	0.03	0.13	6	0.02	0.11	2
CS 22875-029	-0.42	...	1	0.63	0.01	3	0.33	0.08	18	0.30	0.10	3	-0.11	0.08	3	0.37	0.11	3
CS 22888-047	-0.75	0.03	2	0.40	0.13	3	0.13	0.08	17	0.07	0.14	3	-0.05	0.11	4	0.34	0.13	2
CS 22941-027	-0.73	0.07	2	0.36	...	1	0.28	0.08	12	-0.02	0.12	3	0.38	0.10	5
CS 22945-056	-0.48	...	1	0.79	...	1	0.19	0.06	8	0.18	0.04	3	-0.13	0.06	3
BHB																		
HD 2857	0.20 ^a	...	1	0.36	0.07	8	0.25	0.08	2	0.31	...	1	-0.04	0.14	2
HD 8376	0.43	0.07	11
HD 252940	0.36	0.07	8	0.07	...	1	0.07	0.06	2	0.14	0.02	2
HD 60778	0.27	0.12	11	0.10	...	1	-0.17	...	1	0.17	0.06	2
HD 74721	0.28	0.09	11	0.08	0.05	2	0.02	0.06	4	0.03	0.15	7
HD 86986	0.34	0.05	12	0.15	0.04	2	-0.04	0.12	5	0.15	0.12	7
HD 87047	0.18	0.06	4	0.02	...	1
HD 93329	0.29 ^a	...	1	0.33	0.09	14	0.21	0.08	2	0.00	0.09	4	0.02	0.14	7
HD 109995	0.59 ^a	...	1	0.39	0.08	10	0.12	...	1	0.23	0.09	3

Table 6—Continued

Star	[Al I/Fe]	σ	N	[Ti I/Fe]	σ	N	[Ti II/Fe]	σ	N	[Sc II/Fe]	σ	N	[Cr I/Fe]	σ	N	[Cr II/Fe]	σ	N
BD+25° 2602	0.28	0.07	8	0.19	...	1	0.51	...	1
HD 161817	0.35	0.13	25	0.21	0.03	3	-0.08	0.09	3	0.04	0.14	8
HD 167105	0.17	0.05	6	0.29	0.11	3

^aNLTE correction.

Table 7. Abundance ratios of Fe-peak elements: V, Mn, Co, Ni and Zn

Star	[V II/Fe]	σ	N	[Mn I/Fe]	σ	N	[Co I/Fe]	σ	N	[Ni I/Fe]	σ	N	[Ni II/Fe]	σ	N	[Zn I/Fe]	σ	N
RHB																		
HD 6229	0.12	0.27	3	0.80	...	1	-0.04	0.09	9	0.11	0.04	2
HD 6461	0.30	...	1	0.84	...	1	-0.01	0.1	9	0.24	...	1
HD 25532	0.05	0.07	3	0.37	...	1	0.05	0.12	4	0.04	...	1
HD 105546	-0.09	0.16	5	0.30	0.08	2	-0.03	0.13	5	0.13	0.05	2
HD 119516	-0.30	0.08	3	-0.01	...	1	-0.04	...	1	0.05	0.04	2
BD+18° 2890	-0.70	0.08	3	0.22	...	1	-0.03	0.09	3	0.04	...	1
BD+11° 2998	-0.06	0.15	4	0.32	0.04	2	0.06	0.03	2
BD+09° 3223	0.03	...	1	-0.10	0.11	4	0.42	...	1	0.20	...	1
BD+17° 3248	-0.18	0.08	4	0.07	0.01	2
HD 184266	0.15	...	1	-0.19	0.11	4	-0.03	...	1	0.12	...	1
HD 229274	-0.06	0.24	4	0.34	0.15	2	-0.03	0.11	6	0.01	0.01	2
CS 22882-001	0.31	...	1	-0.39	0.05	3
CS 22190-007	0.20	...	1	-0.50	0.02	3
CS 22186-005	-0.46	0.05	3
CS 22191-029	0.32	...	1	-0.54	0.05	3
CS 22883-037	-0.02	...	1	-0.47	0.05	3	0.57	...	1
CS 22878-121	-0.33	0.17	3	0.44	...	1	0.41	...	1	0.10	...	1
CS 22891-184	-0.49	0.07	3
CS 22896-110	0.13	...	1	-0.45	0.09	3
CS 22940-077	-0.58	0.08	3
CS 22955-174	-0.63	0.02	3	0.54	...	1
CS 22940-070	-0.37	0.05	3	0.50	...	1	0.69	...	1	0.06	...	1
CS 22879-103	-0.50	0.04	3	0.31	...	1
CS 22879-097	0.13	0.02	2	-0.58	0.05	3	0.78	...	1
CS 22940-121	0.30	...	1	-0.58	0.02	3
CS 22898-043	-0.30	0.05	3
CS 22937-072	0.11	0.01	2	-0.53	0.06	3
CS 22948-006	0.10	...	1	-0.61	0.02	3	0.59	...	1	0.42	...	1
CS 22944-039	0.05	...	1	-0.45	0.04	3	0.35	...	1	0.43	...	1	0.10	...	1
CS 22951-077	-0.04	0.02	2	-0.33	0.17	3	0.39	...	1	0.19	...	1
CS 22881-039	-0.37	0.02	3
CS 22886-043	-0.45	0.04	3	0.58	...	1	0.71	...	1	0.27	...	1
CS 22875-029	0.23	...	1	-0.57	0.05	3
CS 22888-047	-0.57	0.08	3
CS 22941-027	-0.36	0.04	3
CS 22945-056	-0.51	0.05	3
BHB																		
HD 2857
HD 8376
HD 252940
HD 60778	0.12	...	1	-0.40	...	1
HD 74721	0.17	0.04	2	-0.30	...	1
HD 86986	0.14	0.09	2	0.06	0.32	3
HD 87047
HD 93329	0.11	0.07	2	-0.10	0.02	2	-0.35	...	1
HD 109995

Table 7—Continued

Star	[V II/Fe]	σ	N	[Mn I/Fe]	σ	N	[Co I/Fe]	σ	N	[Ni I/Fe]	σ	N	[Ni II/Fe]	σ	N	[Zn I/Fe]	σ	N
BD+25° 2602
HD 161817	0.21	0.06	2	-0.33	0.10	3	0.28	...	1	
HD 167105	

Table 8. Abundance ratios of neutron-capture elements: Sr, Y, Zr, Ba, La and Eu

Star	[Sr II/Fe]	σ	N	[Y II/Fe]	σ	N	[Zr II/Fe]	σ	N	[Ba II/Fe]	σ	N	[La II/Fe]	σ	N	[Eu II/Fe]	σ	N
RHB																		
HD 6229	0.05	0.05	2	-0.11	0.07	2	0.05	0.05	2	0.33	0.09	3	0.07	...	1	0.10	0.15	2
HD 6461	0.10	0.10	2	0.45	0.15	2	0.53	0.12	3	0.07	...	1	0.10	...	1
HD 25532	0.25	...	1	0.01	0.10	2	0.35	0.04	3	0.52	0.19	3	0.09	0.08	2	0.24	0.01	2
HD 105546	0.33	0.02	2	-0.02	0.04	4	0.43	0.06	3	0.40	0.16	3	0.20	0.08	2	0.33	0.03	2
HD 119516	0.10	...	1	-0.36	0.06	5	0.30	...	1	0.32	0.22	3	0.12	...	1	0.45	0.05	2
BD+18 2890	-0.35	...	1	-0.17	...	1	0.32	0.08	3	0.15	0.28	2	0.45	0.10	2
BD+11 2998	0.28	0.02	2	-0.08	0.12	2	0.30	...	1	0.43	0.09	3	0.02	0.02	2	0.18	0.03	2
BD+09 3223	0.30	0.10	2	-0.23	0.07	2	0.40	...	1	0.08	0.11	4	0.07	...	1	0.34	0.06	2
BD+17 3248	0.23	0.08	2	-0.09	0.08	2	0.53	0.03	2	0.68	0.16	3	0.46	0.04	2	0.89	0.01	2
HD 184266	0.50	...	1	-0.23	0.32	0.08	3	0.28	0.24	3	0.05	0.03	2	0.38	0.03	2
HD 229274	0.15	0.05	2	-0.14	0.06	2	0.40	...	1	0.48	0.18	2	0.32	0.05	2	0.75	0.02	2
Cs22882-001	0.22	0.03	2	0.06	0.04	2	0.16	0.02	3	0.84	...	1
Cs22190-007	0.35	0.03	2	-0.40	...	1	-0.11	0.06	3	0.34	...	1	0.37	...	1
Cs22186-005	-1.03	0.05	2	-0.58	...	1
Cs22191-029	0.33	0.05	2	-0.22	0.02	2
Cs22883-037	0.13	0.18	2	-0.23	0.02	2	0.13	0.08	4	0.09	0.02	2	0.40	0.02	2
Cs22878-121	0.48	0.13	2	-0.04	0.16	3	0.33	0.12	3	0.13	0.08	4	0.17	...	1	0.40	0.02	2
Cs22891-184	0.11	0.00	2	-0.01	0.02	3
Cs22896-110	0.26	0.02	2	-0.38	...	1	0.28	...	1	-0.32	0.02	3
Cs22940-077	0.52	0.02	2	0.14	...	1	0.82	...	1	-0.51	0.23	2
Cs22955-174	0.52	0.05	2	-0.23	...	1	-0.18	0.05	2
Cs22940-070	0.80	...	1	0.07	...	1	0.40	...	1	0.15	0.15	2	0.07	...	1	0.40	0.02	2
Cs22879-103	0.55	0.05	2	0.02	0.03	2	0.48	0.08	2	0.29	0.09	4	0.15	0.08	2	0.40	0.02	2
Cs22879-097	0.24	0.05	2	0.29	...	1	-0.51	0.07	3
Cs22940-121	0.40	0.05	2	-0.03	0.06	3	0.65	...	1	0.18	0.05	3
Cs22898-043	-0.27	0.10	2	-0.47	...	1
Cs22937-072	0.30	0.05	2	-0.26	0.05	2	0.45	...	1	-0.28	0.03	2
Cs22948-006	-0.26	0.05	2	-0.61	0.10	2
Cs22944-039	0.48	0.03	2	-0.36	0.06	3	0.30	...	1	-0.15	0.05	4	-0.08	0.05	2	0.13	0.03	2
Cs22951-077	0.05	0.05	2	-0.50	0.05	3	0.30	...	1	-0.19	0.05	4	0.10	0.05	2
Cs22881-039	0.18	0.05	2	-0.57	...	1
Cs22886-043	0.85	0.05	2	0.21	0.03	2	0.62	0.05	3	0.46	0.10	4	0.47	0.02	2	0.83	0.03	2
Cs22875-029	0.86	0.02	2	0.39	0.17	3	0.69	0.03	2	0.44	0.06	3	0.73	...	1	0.91	0.05	2
Cs22888-047	0.31	0.02	2	0.13	0.12	2	0.53	0.05	2	0.23	0.07	3	0.93	0.02	2
Cs22941-027	-0.11	0.05	2	-0.29	...	1	-0.36	...	1
Cs22945-056	-0.06	0.13	2	-0.43	...	1
BHB																		
HD 2857	-0.15	0.05	2	1	0.50	...	1
HD 8376
HD 252940	-0.33	0.03	2	0.70	...	1	-0.10	...	1
HD 60778	-0.35	0.02	2	0.55	0.05	2	-0.10	...	1
HD 74721	-0.10	0.02	2	0.42	...	1	0.60	...	1	0.20	...	1
HD 86986	-0.43	0.02	2	-0.03	...	1	0.50	...	1	-0.10	...	1
HD 87047	-0.45	0.02	2	-0.10	...	1
HD 93329	-0.30	0.02	2	0.13	...	1	0.75	0.05	2	0.10	...	1
HD 109995	-0.40	...	1

Table 8—Continued

Star	[Sr II/Fe]	σ	N	[Y II/Fe]	σ	N	[Zr II/Fe]	σ	N	[Ba II/Fe]	σ	N	[La II/Fe]	σ	N	[Eu II/Fe]	σ	N
BD+25 2602	-0.55	...	1
HD 161817	0.02	0.08	2	0.36	0.01	2	0.65	...	1	0.08	0.03	2
HD 167105

Table 9. Mean abundance ratios of various elements.

Element	RHB	N	BHB	N
Na I	0.37	27	-0.45	2
Mg I	0.47	36	0.36	12
Al I	-0.67	25	0.36	3
Si I	0.35	36	-0.03	12
Si II	0.59	35	0.21	12
Ca I	0.37	36	0.07	12
Ca II	0.18	12
Sc II	0.13	35	0.14	10
Ti I	0.37	35
Ti II	0.23	36	0.31	12
V II	0.14	14	0.15	5
Cr I	-0.14	36	0.02	7
Cr II	0.23	35	0.15	10
Mn I	-0.37	36	-0.13	3
Co I	0.41	15	0.28	1
Ni I	0.22	15
Ni II	-0.35	3
Zn I	0.19	18
Sr II	0.23	36	-0.30	10
Y II	-0.12	27	0.22	4
Zr II	0.42	23	0.61	7
Ba II	0.03	36	0.00	7
La II	0.19	19
Eu II	0.45	22

Table 10. Sensitivity of $[X/Fe]$ with stellar parameters.

Stellar Parameters	Species $\Delta[X/Fe]$	Star		
		CS 22898–043	HS 25532	BD+18° 2890
$T_{\text{eff}} + 150$	Na I	...	+0.16	+0.16
(K)	Mg I	+0.09	+0.08	+0.25
$\log g + 0.15$	Na I	...	–0.05	–0.03
(dex)	Mg I	+0.01	–0.02	–0.01
$[M/H] + 0.1$	Na I	...	–0.01	+0.00
(dex)	Mg I	...	–0.01	–0.01
$v_t + 0.2$	Na I	...	–0.01	–0.05
(km s^{-1})	Mg I	–0.05	–0.10	–0.07

Note. — Table 10 is published in its entirety in the electronic edition of the *Astronomical Journal*. A portion is shown here for guidance regarding its form and content.

Table 11. Sensitivity of $[X/Fe]$ with stellar parameters for BHB star.

Stellar Parameters	Species $\Delta[X/Fe]$	Star HD 93329
$T_{\text{eff}} + 200$ (K)	Na I Mg I	+0.18 +0.14
$\log g + 0.15$ (dex)	Na I Mg I	-0.03 -0.04
$[M/H] + 0.1$ (dex)	Na I Mg I	+0.01 +0.00
$v_t + 0.2$ (km s ⁻¹)	Na I Mg I	-0.02 -0.01

Note. — Table 11 is published in its entirety in the electronic edition of the *Astronomical Journal*. A portion is shown here for guidance regarding its form and content.

Table 12. Comparison of HB model

Model	Mass (M/M_{\odot})	$\log T_{\text{eff}}$ (K)	$\Delta \log g^{\text{a}}$	$\Delta \log L^{\text{a}}$
Lee & Demarque (1990)	0.56	4.22	+0.02	–0.02
Lee & Demarque (1990)	0.56	4.26	+0.11	–0.11
Lee & Demarque (1990)	0.78	3.86	–0.01	+0.01
Lee & Demarque (1990)	0.78	3.72	+0.09	–0.09

^aPietrinferni et al. (2006) minus Lee & Demarque (1990) model

Table 13. Estimated HB masses and Parameters Used

Stars	$T_{\text{eff,spec}}$ (K)	$\log g$ (dex)	[Fe/H] (dex)	Mass M_{\odot}
RHB				
HD 6229	5200	2.86 ^a	-1.07	0.80
HD 6461	5200	3.26 ^a	-0.75	0.80
HD 25532	5450	2.20 ^a	-1.41	0.60
HD 105546	5200	2.66 ^a	-1.54	0.80
HD 119516	5400	1.73 ^a	-2.16	0.54
BD+18° 2890	5000	2.89 ^a	-1.61	0.80
BD+11° 2998	5450	2.50 ^a	-1.28	0.72
BD+09° 3223	5100	1.72 ^a	-2.47	0.61
BD+17° 3248	5100	2.12 ^a	-2.24	0.80
HD 184266	5700	1.75 ^a	-1.79	0.52
HD 229274	5500	2.47 ^a	-1.41	0.73
CS 22882–001	5950	1.91 ^a	-2.54	0.54
CS 22190–007	5600	2.01 ^a	-2.67	0.58
CS 22186–005	6200	2.22 ^a	-2.77	0.57
CS 22191–029	6000	1.98 ^a	-2.73	0.55
CS 22883–037	5900	1.59 ^a	-1.95	0.52
CS 22878–121	5450	1.95 ^a	-2.38	0.57
CS 22891–184	5600	1.81 ^a	-2.61	0.54
CS 22896–110	5400	1.68 ^a	-2.78	0.54
CS 22940–077	5300	1.74 ^a	-3.02	0.56
CS 22955–174	5350	1.61 ^a	-3.17	0.54
CS 22940–070	6300	2.12 ^a	-1.41	0.53
CS 22879–103	5700	1.65 ^a	-2.20	0.52
CS 22879–097	5650	2.03 ^a	-2.59	0.57
CS 22940–121	5350	1.86 ^a	-2.95	0.57
CS 22898–043	5900	1.94 ^a	-3.03	0.55
CS 22937–072	5300	1.79 ^a	-2.85	0.57
CS 22948–006	5400	1.63 ^a	-2.79	0.54
CS 22944–039	5350	1.46 ^a	-2.43	0.52
CS 22951–077	5350	1.81 ^a	-2.44	0.56
CS 22881–039	6100	1.68 ^a	-2.73	0.53
CS 22886–043	6000	1.73 ^a	-2.17	0.52
CS 22875–029	6000	1.93 ^a	-2.66	0.54
CS 22888–047	5850	1.66 ^a	-2.58	0.53
CS 22941–027	6200	1.97 ^a	-2.54	0.54
CS 22945–056	5850	1.46 ^a	-2.92	0.52
BHB				
HD 2857	8100	2.48 ^b	-1.39	0.52
HD 8376	8600	2.38 ^b	-2.39	0.52
HD 252940	7650	1.77 ^b	-1.69	0.56
HD 60778	8100	1.63 ^b	-1.43	0.54
HD 74721	9000	1.93 ^b	-1.23	0.59
HD 86986	8200	2.04 ^b	-1.61	0.63

Table 13—Continued

Stars	$T_{\text{eff,spec}}$ (K)	$\log g$ (dex)	[Fe/H] (dex)	Mass M_{\odot}
HD 87047	7700	1.35 ^b	-2.38	0.53
HD 93329	8700	2.04 ^b	-1.10	0.59
HD 109995	8600	1.68 ^b	-1.60	0.56
BD+25° 2602	8400	1.56 ^b	-1.98	0.55
HD 161817	7800	2.01 ^b	-1.43	0.59
HD 167105	9000	1.63 ^b	-1.55	0.56

^aPhotometric $\log g$.

^bSpectroscopic $\log g$.

Table 14. Data Sources

References	Element
Venn et al. (2004)	Na, Mg, Ca, Ti, Ni, Y, Ba, La, Eu
Cohen et al. (2004)	Si, Al, Sc, Cr, Mn, Sr
Lai et al. (2008)	Si, Al, Sc, V, Mn, Zn, Sr, Zr
Fulbright (2000)	Si, Al, Cr, V, Zr
Reddy et al. (2003)	Al, Sc, Cr, V, Mn, Ni, Zn
Sobeck et al. (2006)	Mn
Cayrel et al. (2004)	Si, Zn
Stephens & Boesgaard (2002)	Si, Ni
Nissen et al. (2007)	Ni